

DTIC FILE COPY

2

WRDC-TR-90-3023



SIMULANT GAS TEST TECHNIQUE FEASIBILITY

Mr. Richard M. Traci

Fluid Physics Ind
4265 Manchester Avenue
Encinitas, CA 92024

DTIC
ELECTE
AUG 6 1990
S D
Er D

May 1990

Final Report for Period December 1988 - January 1990

Approved for public release; distribution is unlimited

FLIGHT DYNAMICS LABORATORY
WRIGHT RESEARCH AND DEVELOPMENT CENTER
AIR FORCE SYSTEMS COMMAND
WRIGHT-PATTERSON AIR FORCE BASE, OHIO 45433-6553

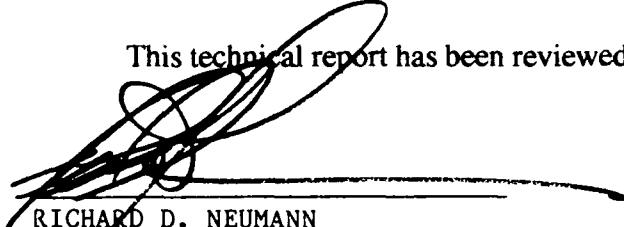
AD-A224 878

NOTICE


When Government drawings, specifications, or other data are used for any purpose other than in connection with a definitely Government-related procurement, the United States Government incurs no responsibility or any obligation whatsoever. The fact that the government may have formulated or in any way supplied the said drawings, specifications, or other data, is not to be regarded by implication, or otherwise in any manner construed, as licensing the holder, or any other person or corporation; or as conveying any rights or permission to manufacture, use, or sell any patented invention that may in any way be related thereto.

This report is releasable to the National Technical Information Service (NTIS). At NTIS, it will be available to the general public, including foreign nations.

This technical report has been reviewed and is approved for publication.

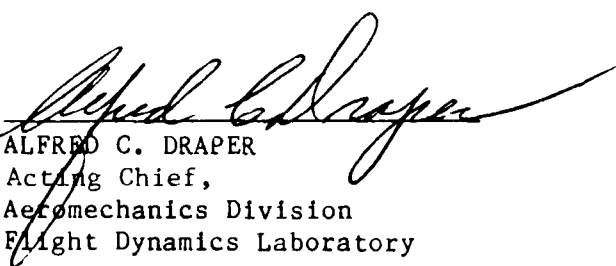


RICHARD D. NEUMANN
Project Engineer
High Speed Aero Performance Branch



VALENTINE DAHLEM
Chief
High Speed Aero Performance Branch

FOR THE COMMANDER



ALFRED C. DRAPER
Acting Chief,
Aeromechanics Division
Flight Dynamics Laboratory

If your address has changed, if you wish to be removed from our mailing list, or if the addressee is no longer employed by your organization please notify WRDC/FIMG, WPAFB, OH 45433-6553 to help us maintain a current mailing list.

Copies of this report should not be returned unless return is required by security considerations, contractual obligations, or notice on a specific document.

REPORT DOCUMENTATION PAGE

| | | | |
|--|--|---|---|
| 1a. REPORT SECURITY CLASSIFICATION Unclassified | | 1b. RESTRICTIVE MARKINGS None | |
| 2a. SECURITY CLASSIFICATION AUTHORITY WRDC/FIMG | | 3. DISTRIBUTION/AVAILABILITY OF REPORT Approved for Public Release; Distribution is Unlimited. | |
| 2b. DECLASSIFICATION/DOWNGRADING SCHEDULE | | | |
| 4. PERFORMING ORGANIZATION REPORT NUMBER(S) R90-09-03 | | 5. MONITORING ORGANIZATION REPORT NUMBER(S) WRDC TR 90-3023 | |
| 6a. NAME OF PERFORMING ORGANIZATION Fluid Physics Inc. | 6b. OFFICE SYMBOL (If applicable) | 7a. NAME OF MONITORING ORGANIZATION Wright Research and Development Center Flight Dynamics Laboratory (WRDC/FIMG) | |
| 6c. ADDRESS (City, State, and ZIP Code) 4265 Manchester Ave. Encinitas, CA 92024 | | 7b. ADDRESS (City, State, and ZIP Code) WPAFB OH 45433-6553 | |
| 8a. NAME OF FUNDING/SPONSORING ORGANIZATION | 8b. OFFICE SYMBOL (If applicable) | 9. PROCUREMENT INSTRUMENT IDENTIFICATION NUMBER Contract F33615-88-C-3011 | |
| 8c. ADDRESS (City, State, and ZIP Code) | | 10. SOURCE OF FUNDING NUMBERS | |
| | | PROGRAM ELEMENT NO. 61101F/ 62201F | PROJECT NO. 2404 ILIR |
| | | TASK NO. 07 ILIRFO | WORK UNIT ACCESSION NO. ILIRFO12 |
| 11. TITLE (Include Security Classification) Simulant Gas Test Technique Feasibility | | | |
| 12. PERSONAL AUTHOR(S) Mr. Richard M. Traci | | | |
| 13a. TYPE OF REPORT Final | 13b. TIME COVERED FROM Dec 88 TO Jan 90 | 14. DATE OF REPORT (Year, Month, Day) May 1990 | 15. PAGE COUNT 84 |
| 16. SUPPLEMENTARY NOTATION N/A | | | |
| 17. COSATI CODES | | | 18. SUBJECT TERMS (Continue on reverse if necessary and identify by block number) Hypersonic-test Air-chemistry Non-equilibrium-flow |
| FIELD | GROUP | SUB-GROUP | |
| | | | |
| | | | |
| 19. ABSTRACT (Continue on reverse if necessary and identify by block number) The uncertainty engendered by non-equilibrium air effects on hypersonic vehicle aerodynamics and heat transfer is compounded by the fact that such effects are difficult to validate in ground test facilities. Laboratory quality ground test data on air chemistry effects are clearly needed to investigate the rich parametric effects of scale, complex geometry, turbulence coupling, and altitude/Mach number flight regime. Moreover, data is needed for numerical model validation purposes. A proposed concept for such a test, referred to as the "Simulant Gas" shock tunnel test, is investigated in the present report. The approach is based on the use of simulant gas mixtures in a shock tunnel operating in the nonreflected shock mode. Simulant gases are sought which react at lower temperatures than oxygen and which have a relatively well defined "ignition" temperature. They thereby provide the possibility of remaining unreacted in the freestream of the expanded shock tunnel flow while reacting at representative and controllable rates in the shock layer of a test model. The test concept, if feasible, would provide a laboratory quality experimental simulation (Continued on reverse) | | | |
| 20. DISTRIBUTION/AVAILABILITY OF ABSTRACT <input checked="" type="checkbox"/> UNCLASSIFIED/UNLIMITED <input type="checkbox"/> SAME AS RPT. <input type="checkbox"/> DTIC USERS | | 21. ABSTRACT SECURITY CLASSIFICATION Unclassified | |
| 22a. NAME OF RESPONSIBLE INDIVIDUAL Richard D. Neumann | | 22b. TELEPHONE (Include Area Code) 513 255-5419 | 22c. OFFICE SYMBOL WRDC/FIMG |

technique which possesses reactive flow similitude relative to oxygen dissociation at hypersonic flight conditions.

The feasibility of the simulant gas test concept was evaluated by performing reactive flow scaling and reactive streamline flow analyses for a limited range of combustible gas mixtures. The method is illustrated for air by defining flight regimes and baseline shock tunnel test regimes for which nonequilibrium oxygen dissociation is operative in the vehicle/model shock layer. Corresponding operating regimes are defined for various candidate simulant gases using results of analyses of both the shock tunnel flowfield and test model stagnation region flow. Carbon monoxide, peroxide and hydrogen gas mixtures in air, over a range of stoichiometries and additive combinations, were examined for operation in a large scale shock tunnel such as the Calspan 48" hypersonic shock tunnel. The results principally indicate that the method is not generally feasible because of the difficulty of achieving an unreacted supply gas at conditions for which the test model flowfield is in the nonequilibrium reactive flow regime. Subsidiary results include: i) a carbon monoxide-air mixture with a small amount of peroxide can achieve a reactive model shock layer with an unreacted supply gas but may not be practical due to the small domain of permissible operating conditions, ii) lean carbon monoxide-air mixtures can induce oxygen dissociation at reduced supply gas intensities but with only marginal improvements over pure air, and iii) conditions are described for a nonequilibrium oxygen dissociation test in air which minimizes freestream dissociation and maximizes test time.

FOREWORD

This report was prepared by Fluid Physics Ind (FPI) Encinitas, CA as part of a research study sponsored by the Flight Dynamics Laboratory, Wright Research and Development Center, Aeronautical Systems Div. (AFSC), United States Air Force Wright-Patterson AFB, Ohio 45433-6553. The report describes research performed under Contract No. F33615-88-C-3011 and is intended to satisfy the final reporting requirements of that contract. Richard Neumann (WRDC/FIMG) provided technical guidance to the project and his interest in and guidance of the project is gratefully acknowledged by the author.

Richard M. Traci of Fluid Physics Ind. was Principal Investigator for the program and he was supported by consultants C.W. Wilson, in the area of chemical kinetics definition, by F.Y. Su in fluids modeling, and by Tom Searfus in computer programming.



| | |
|--------------------|--------------------------|
| Approved For | |
| DTIC GRA&I | ↓ |
| DTIC TAB | <input type="checkbox"/> |
| Unannounced | <input type="checkbox"/> |
| Justification | |
| By | |
| Distribution/ | |
| Availability Codes | |
| Dist | Availability or Special |
| A-1 | |

This page intentionally left blank.

TABLE OF CONTENTS

| | <u>Page</u> |
|--|-------------|
| 1. INTRODUCTION | 1 |
| 2. BACKGROUND AND APPROACH | 4 |
| 2.1 Reactive Shock Layer Flow Analysis | 4 |
| 2.2 Nonequilibrium Air Flight Regime Definition | 11 |
| 2.3 "Simulant Gas" Shock Tunnel Test Summary | 16 |
| 3. BASELINE SHOCK TUNNEL TEST WITH AIR | 19 |
| 4. CARBON-MONOXIDE-AIR SIMULANT GAS SHOCK TUNNEL TEST ANALYSIS | 33 |
| 5. PEROXIDE-AIR SIMULANT GAS MIXTURE ANALYSIS | 43 |
| 6. HYDROGEN-AIR SIMULANT GAS MIXTURE ANALYSIS | 49 |
| 7. CARBON MONOXIDE-AIR SENSITIVITY STUDIES | 55 |
| 8. CONCLUSIONS AND RECOMMENDATIONS | 62 |
| REFERENCES | 64 |
| Appendix A REACTIVE FLOW ANALYSIS ALONG BLUNTED CONE FLOW STREAMSLINE | 65 |
| Appendix B "SIMULANT" GAS REACTIVE MIXTURE CHEMISTRY ANALYSIS | 73 |

This page intentionally left blank.

LIST OF ILLUSTRATIONS

| <u>Figure</u> | <u>Page</u> |
|--|-------------|
| 1 Schematic of Shock Layer Reactive Streamline Analysis | 5 |
| 2 Oxygen Distribution Through Stagnation Region | |
| 1. Inch Nose Diameter Shape at Mach Number = 14 | 6 |
| 3 Schematic of Air Chemistry Effects | 8 |
| 4 Temperature Distribution in Stagnation Region | |
| 1. Inch Nose Diameter at Mach Number = 14 | 9 |
| 5 Gamma Distribution in Stagnation Region | |
| 1. Inch Nose Diameter at Mach Number = 14 | 10 |
| 6 Nonequilibrium Oxygen Reaction Flight Regimes | |
| 1 Inch Nose Diameter Sphere-Cone | 13 |
| 7 Nonequilibrium Oxygen Reaction Ballistic Range Test Regimes | |
| .15 Inch Nose Diameter Sphere-Cone | 14 |
| 8 Oxygen Distribution on Stagnation Streamline | 15 |
| 9 Schematic of Shock Tunnel Test | 17 |
| 10 Oxygen Distribution Through Stagnation Region | |
| Near Frozen through Near Equilibrium Conditions | |
| Shock Mach Number = 9.5 | |
| 1. Inch Nose Dia. Test Model, Test Section $M_\infty \approx 5.3$ | 19 |
| 11 Oxygen Dissociation in Air: Shock Tunnel Test Regimes | |
| 1. Inch Nose Diameter Test Model at $M_\infty \approx 5.3$ | 25 |
| 12 Oxygen Dissociation in Air: Shock Tunnel Test Regimes | |
| 12. Inch Nose Diameter Test Model at $M_\infty \approx 5.3$ | 26 |
| 13 Dissociation in Pure Oxygen: Shock Tunnel Test Regimes | |
| 12. Inch Nose Diameter Test Model at $M_\infty \approx 5.3$ | 27 |
| 14 Oxygen Dissociation in Air: Shock Tunnel Test Conditions | |
| 1. Inch Nose Diameter Test Model at $M_\infty \approx 5.3$ | 28 |
| 15 Oxygen Distribution Under Near Frozen Test Conditions | |
| Initial Pressure = .02 psi, Shock Mach Number = 9.5 | |
| Test Section Mach No. ≈ 5.3 , density altitude ≈ 200 Kft | 29 |
| 16 Oxygen Distribution Under Nonequilibrium Test Conditions | |
| Initial Pressure = .3 psi, Shock Mach Number = 9.5 | |
| Test Section Mach No. ≈ 5.3 , density altitude ≈ 150 Kft | 30 |
| 17 Oxygen Distribution Under Near Equilibrium Test Conditions | |
| Initial Pressure = 2. psi, Shock Mach Number = 9.5 | |
| Test Section Mach No. ≈ 5.3 , density altitude ≈ 110 Kft | 31 |
| 18 Oxygen Distribution Under Nonequilibrium Test Conditions | |
| Effect of Supply Gas Dissociation on Shock Layer | |
| Initial Pressure = .3 psi, Shock Mach Number = 9.5 | |
| Test Section Mach No. ≈ 5.3 , density altitude ≈ 150 Kft | 32 |
| 19 CO/Air Reactive Species Distribution Through Stagnation Region | |
| Stoichiometric CO/Air, $D_N = 12$ Inch, Initial Pressure = 1 psi | |
| Test Section Mach No. ≈ 5.3 , density altitude ≈ 125 Kft | 37 |
| 20 Carbon Monoxide-Air Reactive Flow Shock Tunnel Test Regimes | |
| Stoichiometric CO/Air, 1. Inch Nose Diameter Test Model | |
| Test Section Mach No. ≈ 5.3 | 39 |
| 21 Carbon Monoxide-Air Reactive Flow Shock Tunnel Test Regimes | |
| Stoichiometric CO/Air, 12. Inch Nose Diameter Test Model | |
| Test Section Mach No. ≈ 5.3 | 40 |

LIST OF ILLUSTRATIONS (Continued)

| <u>Figure</u> | <u>Page</u> |
|---------------|--|
| 22 | CO/Air Reactive Species Distribution Through Supply Tube Stoichiometric CO/Air, Initial Pressure = 1 psi, Tube Length = 70 Ft 41 |
| 23 | Carbon Monoxide-Air Shock Tunnel Supply Tube Reactivity Stoichiometric CO/Air; 12. Inch Nose Diameter Test Model Supply Tube Length = 70. Ft 42 |
| 24 | H ₂ O ₂ /Air Reactive Species Distribution Through Stagnation Region 20% H ₂ O ₂ in Air, D _N = 12 Inch, Initial Pressure = 1 psi Test Section M _∞ ≈ 4.8, density altitude ≈ 125 Kft 45 |
| 25 | Peroxide-Air Reactive Flow Shock Tunnel Test Regimes 20% H ₂ O ₂ in Air; 12. Inch Nose Diameter Test Model Test Section Mach Number ≈ 4.8 47 |
| 26 | Peroxide-Air Shock Tunnel Supply Tube Reactivity 20% H ₂ O ₂ in Air; 12. Inch Nose Diameter Test Model Test Section Mach Number ≈ 4.8 48 |
| 27 | H ₂ /Air Reactive Species Distribution Through Stagnation Region Stoichiometric H ₂ /Air, D _N = 12 Inch, Initial Pressure = 1 psi Test Section M _∞ ≈ 5.3, density altitude ≈ 125 Kft 51 |
| 28 | Hydrogen-Air Reactive Flow Shock Tunnel Test Regimes Stoichiometric H ₂ /Air; 12. Inch Nose Diameter Test Model Test Section Mach Number ≈ 5.3 53 |
| 29 | Hydrogen-Air Reactive Flow Shock Tunnel Supply Tube Reactivity Stoichiometric H ₂ /Air; 12. Inch Nose Diameter Test Model Test Section Mach Number ≈ 5.3 54 |
| 30 | Effect of Stoichiometry on CO/Air Shock Tunnel Test Regimes Carbon-monoxide/Air Mixture at 1. psi Supply Tube Pressure 12. Inch Nose Dia. Test Model, Test Section Mach No. ≈ 5.3 56 |
| 31 | CO/Air Reactive Species Distribution at Near Frozen O ₂ Dissociation Conditions: CO/Air at Stoichiometry Ratio = .5 Initial Pressure = 1. psi, Shock Mach Number = 6.0 57 |
| 32 | CO/Air Reactive Species Distribution at Nonequilibrium O ₂ Dissociation Conditions: CO/Air at Stoichiometry Ratio = .5 Initial Pressure = 1. psi, Shock Mach Number = 7.0 58 |
| 33 | Effect of Peroxide on CO/Air Shock Tunnel Test Regimes Stoichiometric CO/Air at 1. psi Supply Tube Pressure 12. Inch Nose Dia. Test Model, Test Section Mach No. ≈ 5. 59 |
| 34 | CO/Air Reactive Species Distribution at Nonequilibrium CO Reaction Conditions: Stoichiometric CO/Air + 10 ⁻⁴ H ₂ O ₂ Initial Pressure = 1. psi, Shock Mach Number = 2.5 61 |
| A1 | Blunted Cone Flow Schematic 65 |

1. INTRODUCTION

A concept for an air chemistry effects test technique, referred to here as a "Simulant Gas" shock tunnel test, has been evaluated in an engineering feasibility study summarized in the present report. The approach is based on the use of simulant gas mixtures which react at lower temperatures than oxygen which, if feasible, could provide a much needed ground-based experimental simulation technique for nonequilibrium air chemistry studies. The goal of the program was to evaluate the feasibility of this potentially laboratory-quality experimental simulation technique relative to its ability to provide finite rate air chemistry similarity to oxygen dissociation at hypersonic flight conditions. The technical approach to achieve this goal involved the evaluation and definition of a simulant gas shock tunnel test technique. The feasibility study utilized chemical kinetic assessment studies, reactive flow estimation methods, shock tunnel flow analysis methods and general experiment assessment activities. The results of these investigations are described in the present report beginning with a discussion of air chemistry effects in hypersonic flows, which describes the reactive flow analysis techniques used in the study, and culminating in conclusions concerning the efficacy of the simulant gas approach.

The next generation of advanced hypersonic flight vehicles will require an improved understanding of nonequilibrium or finite rate air chemistry effects on the vehicle aerothermodynamic environment. The fact that air reacts, thereby changing its composition at various rates and in various ways, in the shock layer flowfield about hypersonic vehicles can, in turn, lead to modifications to the aerodynamic pressure and thermal heating distributions important to vehicle operation. Advanced vehicles, to varying degrees and in various flight regimes, will be affected by nonequilibrium air effects on aerodynamics, heat transfer, propulsion subsystems and wake observables. The successful design of such vehicles requires a reduction in uncertainty in these areas which is to be achieved by improved models and novel ground test simulation techniques. Both simulation methods are presently deficient. Advanced numerical models are available, but they are largely not validated for nonequilibrium air chemistry. Ground test facilities cannot achieve the combination of high stagnation conditions with undissociated freestream flow required to simulate realistic nonequilibrium real gas effects. The present study seeks to contribute to the resolution of this dilemma by evaluating the feasibility of a "Simulant Gas" test technique for simulating finite rate air chemistry effects.

The uncertainty engendered by such effects is compounded by the fact that they are difficult to validate in ground test facilities. Total temperature and corresponding Mach number limitations of hypersonic aerodynamic wind tunnels, for example, result in perfect gas flowfields since dissociation cannot be induced at the low achievable flow temperatures. Alternative test techniques are ballistic range tests, shock tunnel tests, and of course flight tests. In the ballistic range tests, simple and small scale models are flown at representative altitudes and Mach numbers but diagnostic data is limited to trajectory data, some surface radiance (temperature) data and occasionally post test recovery. The shock tunnel, operating in the shock reflection mode, can approximate some hypersonic flight parameters but provides only millisecond test times and produces highly dissociated freestream flows.

These needs are addressed by performing a feasibility analysis of a unique "simulant gas" shock tunnel test technique. The "simulant gas" approach has its basis in the belief that air-like gas mixtures can be devised which are unreacted in the freestream of an expanded shock tunnel flow but which react at representative and controllable rates in the shock layer of a model in the test section. Success of the approach depends upon the ability to devise gas mixtures which react at lower total temperature conditions than air and which react at representative rates in the model shock layer at achievable flow conditions. Achieving this success would provide a laboratory quality and flexible experimental simulation technique which possesses reactive flow similitude to the oxygen dissociation portion of the hypersonic flight regime.

The objective of the Phase I feasibility study was to evaluate the simulant gas test concept to the extent necessary to motivate a demonstration test of the method. This objective was pursued by performing a combination of analytical studies including reactive mixture evaluation analyses and facility flowfield definition analyses. The present study, has concentrated on an investigation of reacting gas mixtures including carbon-monoxide, hydrogen, water vapor and peroxide in air, which could be used in a conventional or nonreflected mode shock tunnel test facility to simulate reaction rate effects in the shock layer of a test model. To provide an improvement over standard operation with air, the gas mixture must be unreacted in the freestream flow while reacting at representative rates in the shock layer. The unreacted freestream flow quality as well as the shock layer reactivity similitude thus provide the principal criteria for evaluating the test concept. Shock layer scaling and reactive streamline analysis methods, are used to screen candidate mixtures, and refine test condition similitude according to the above test criteria.

The present report begins with a background discussion of non-equilibrium air chemistry effects in Section 2. The section includes an analysis of flight regimes in which nonequilibrium effects may predominate, for motivating the problem, and introduces the scaling and reactive streamline flow analyses. The degree to which nonequilibrium chemistry effects can be simulated in a typical shock tunnel test is described in Section 3. It includes an analysis of shock tunnel operation with air as the "baseline of comparison" for evaluating simulant gases. Reactive flow operating regimes are delineated in a shock tunnel "Operating Map" developed using the reactive shock layer streamline analysis model. Sections 4, 5 and 6 contain the corresponding results for the principal simulant gas mixtures evaluated in the study, namely carbon-monoxide/air combustion, peroxide decomposition in air and hydrogen/air combustion respectively. The carbon-monoxide/air simulant gas mixture is revisited in Section 7 to investigate the sensitivity of the results to mixture parameters such as stoichiometry and peroxide additive. Finally, conclusions reached in the study relative to the feasibility of the simulant gas test are summarized in Section 8 along with recommendations for making the best out of available shock tunnel test methods for nonequilibrium air chemistry simulation. Appendices A and B describe the reactive shock layer streamline flow analysis and its generalization to simulant gas mixtures.

2. BACKGROUND AND APPROACH

As introduced above, reactive flow analysis and scaling techniques are used in the present study to evaluate both the flight regime for nonequilibrium air effects as well as the corresponding shock tunnel operating regime for the simulant gas test technique. In this section, these methods are described, utilized to evaluate the flight regime for nonequilibrium oxygen dissociation effects and modified for use in the simulant gas shock tunnel test examination. In Section 2.1, the analysis method is summarized with liberal reference to the more detailed analysis contained in the appendices to provide the analytical background to the study. Also provided there is quantitative and conceptual description of air chemistry effects in the shock layer of a hypersonic vehicle. The scaling parameters which result from the reactive shock layer streamline analysis are used in Section 2.2 to define the flight regimes for which finite rate air chemistry effects are operative. The discussion contained in Section 2.3 highlights the modifications to the analysis for the present application and describes the simulant gas shock tunnel approach.

2.1 Reactive Shock Layer Flow Analysis

Air chemistry effects on high speed vehicles are related to the degree of molecular species dissociation and the rate at which this dissociation occurs in the high temperature stagnation region. Both of these quantities can be calculated based on rate expressions for the main dissociation reaction and upon conservation relations for flow conditions in the stagnation region. The degree of dissociation ($\Delta n/n_f$ where n is the molecular number density and subscript f denotes undissociated conditions) is essentially the fraction of molecules which have dissociated to atomic form. It provides a measure of the deviation of the real gas from the ideal or nondissociated gas conditions. In quantitative terms, it can be stated:

$$\frac{\Delta n}{n_f} \quad \left\{ \begin{array}{l} \ll 1 \rightarrow \text{no equilibrium real gas effect} \\ \approx 1 \rightarrow \text{potential real gas effect} \end{array} \right. \quad (1)$$

where $\Delta n/n_f$ is evaluated at representative flow conditions such as the shock layer stagnation conditions.

The other aspect of air chemistry effects, of primary interest to the present study, is the rate at which reactions occur relative to the rate at which the flowfield changes along a

flow streamline about a highspeed vehicle. It can be modeled using the species conservation equations driven by the chemical rate equations for transformations among species. For present purposes, the stagnation streamline between the standoff shock and the vehicle nose is considered. It is suggested along with appropriate terminology in Figure 1.

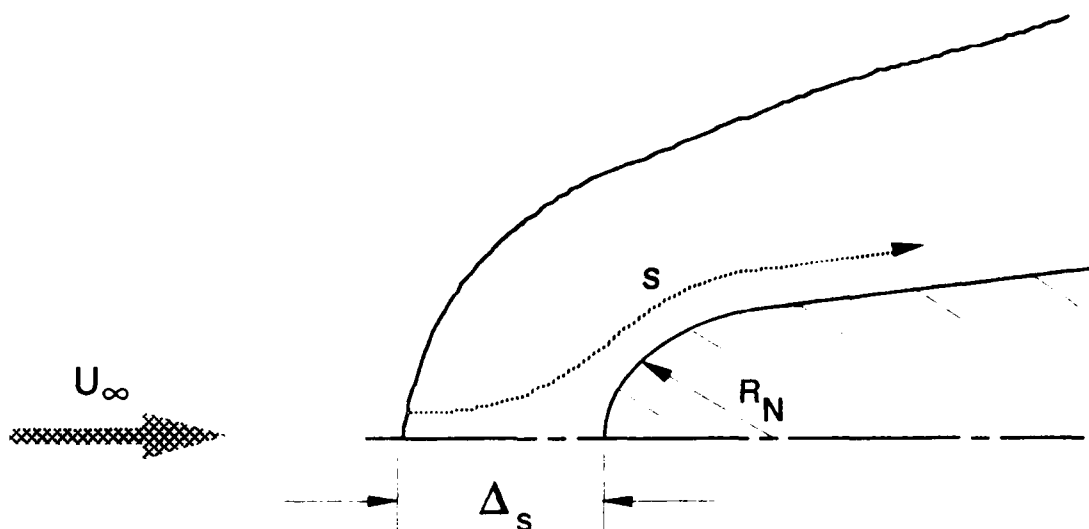


Figure 1. Schematic of Shock Layer Reactive Streamline Analysis

The detailed analysis, contained in Appendix A, for the species conservation along the stagnation streamline results in the following nondimensionalization of parameters and the governing equation for the oxygen concentration:

$$\bar{n} = \frac{n}{n_{as}}, \quad \bar{\rho} = \frac{\rho}{\rho_s}, \quad \bar{q} = \frac{q}{U_\infty}, \quad \bar{s} = \frac{s}{R_N}$$

$$\frac{d}{ds} \left(\frac{n_{O_2}}{\bar{\rho}} \right) = \frac{1}{\bar{\rho} \bar{q}} \sum_m \left(\Lambda_R^m \bar{n}_O^2 - \Lambda_D^m \bar{n}_{O_2} \right) n_m \quad m = O_2, N_2, O \quad (2)$$

$$\Lambda_R^m = \frac{R_N}{U_\infty} k_R^m n_{as}^2, \quad \Lambda_D^m = \frac{R_N}{U_\infty} k_D^m n_{as}$$

where the usual fluid notation is used; ρ denotes density, R_N is the vehicle nose radius, k is the dissociation rate due to collisions with O_2 or N_2 (superscript) and Λ_D^m are the nondimensional dissociation rates. The analysis summarized above, indicates that a good scaling parameter for such effects is the so-called Damköhler number, which is the right hand

side of Equation (2) evaluated at flow conditions just behind the shock. For O_2 dissociation it is given by:

$$\Lambda_{O_2} = \frac{\tau_{\text{FLOW}}}{\tau_{\text{REACTION}}} = \frac{0.21 \rho_2 R_n}{\rho_\infty U_\infty} [k_d^{O_2} n_{O_2} + k_d^{N_2} n_{N_2}] \quad (3)$$

A similar more complicated parameter can be written for nitrogen dissociation effects as well as for general simulant gas mixtures. The parameter can be used to define flight regimes for O_2 dissociation rate effects guided by the fact that $\Lambda \ll 1$ implies frozen ideal gas conditions, and $\Lambda \gg 1$ implies equilibrium real gas conditions. Nonequilibrium effects would be operative for $\Lambda \approx O(1)$.

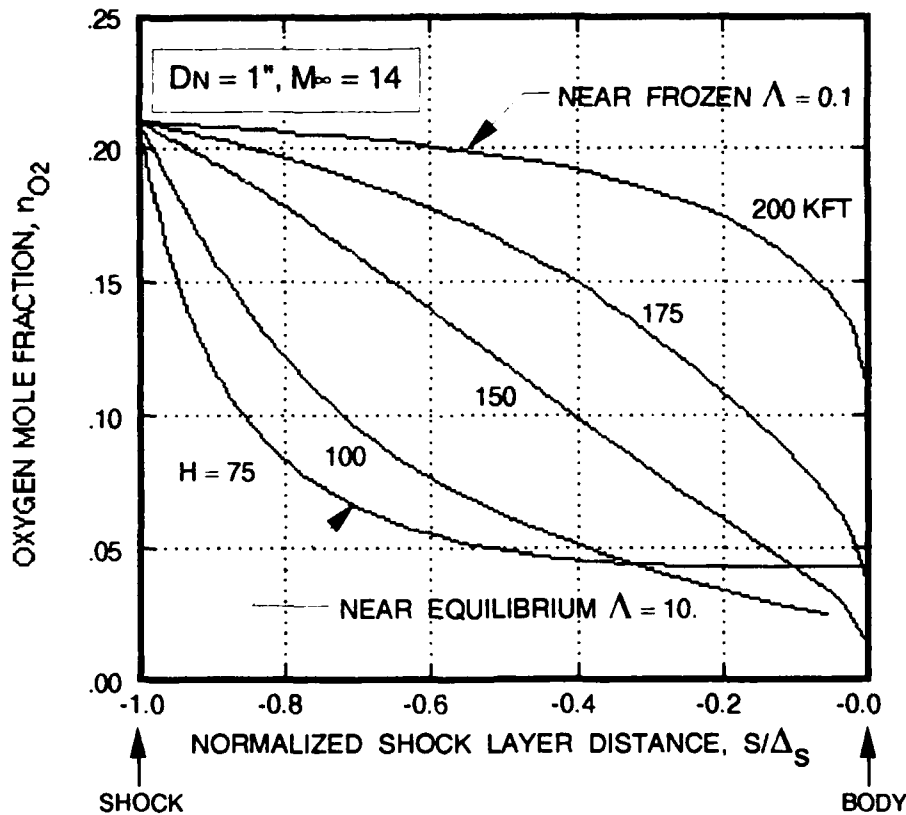


Figure 2. Oxygen Distribution Through Stagnation Region 1. Inch Nose Diameter Shape at Mach Number = 14.

A qualitative picture of air chemistry effects can be based on the Damköhler number delineation guided by the quantitative picture of the oxygen species concentration along a

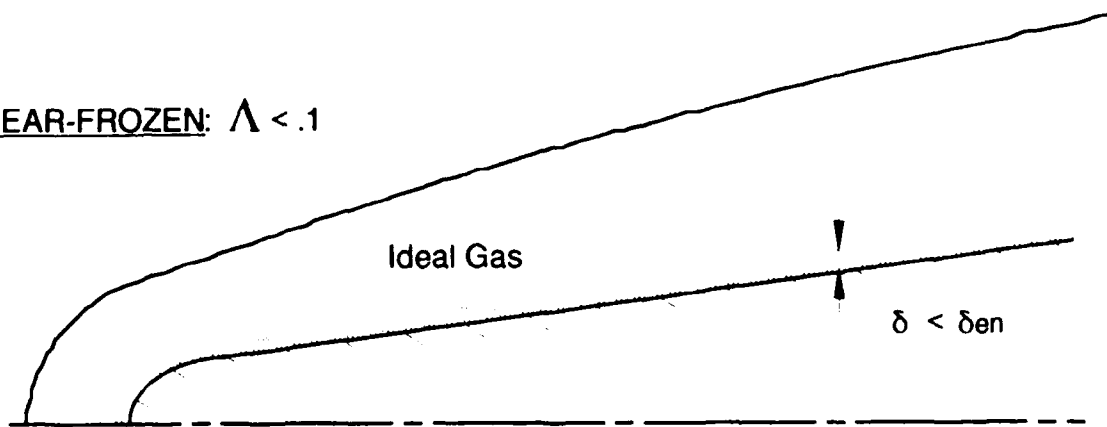
stagnation streamline presented in Figure 2. The figure shows the variation in molecular oxygen concentration along the stagnation streamline for various flight altitudes at a velocity of Mach 14. The results were developed using the STREAM code implementation of the reactive streamline flow model described in detail in Appendix A. Figure 2. shows the significant difference in gas composition on the stagnation streamline as flight altitude is varied from near equilibrium conditions at an altitude of 75.Kft to near frozen conditions at an altitude of 200. Kft.

A more qualitative, but illustrative, picture of air chemistry effects which emerges from the Damköhler number delineation and quantitative results such as just described, is indicated schematically in Figure 3. For near frozen flow conditions, $\Lambda < .1$, air may be treated as an ideal gas throughout much of the flow except for a thin layer near the surface in which the oxygen mole fraction takes on a value roughly equivalent to the mole fraction (f_{O_2}) at equilibrium stagnation conditions. The thickness of the layer is somewhat less than the entropy layer thickness and f_{O_2} varies rapidly to its frozen value just outside the layer. For such conditions, the vehicle aerodynamics would be expected to be frozen, since the stagnation region (see Figure 2) and entire shock layer are essentially frozen at the freestream composition. The effective γ throughout the flow is different than that for the freestream gas mixture since it is modified by thermal effects (vibrational effects are assumed to be in equilibrium) so that the shock shape and flow properties would be typical of an ideal gas flow at a modified gamma. The thin nonequilibrium layer is expected to have little effect on the pressure distribution, although its effect on heat transfer must be considered.

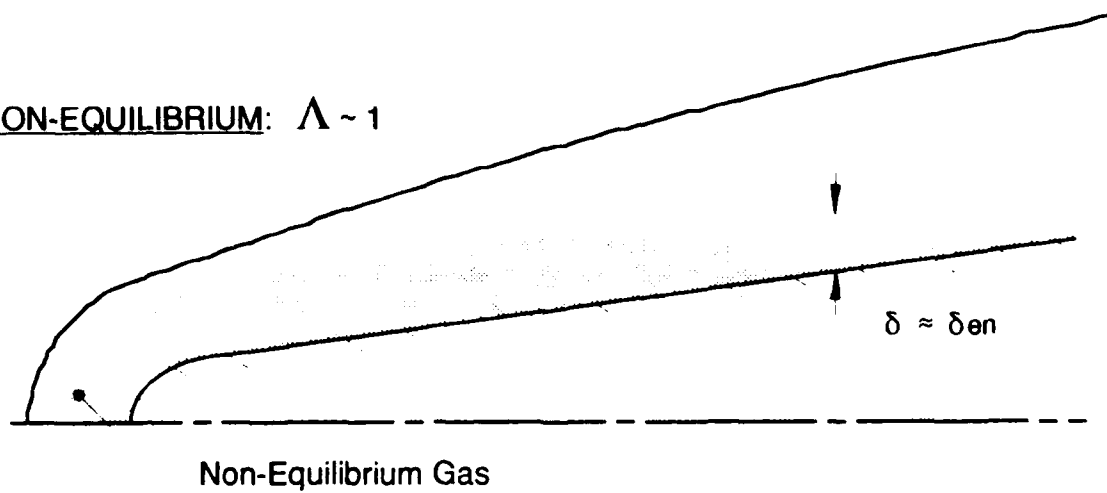
As the rate parameter Λ increases to $O(1)$, the thickness of this nonequilibrium layer grows until both the stagnation region and the entropy layer are in a nonequilibrium state. The oxygen mole fraction varies from its frozen state, at the shock and outside the entropy layer, to its equilibrium state, near the surface. The variation in nonequilibrium oxygen concentration from near equilibrium ($\Lambda > 10.$) conditions at an altitude of 75 Kft to near frozen ($\Lambda < .1$) conditions at 200 Kft is evident in Figure 2. Between these conditions the stagnation region shock layer is in a fully nonequilibrium state, as is the downstream entropy layer, and γ varies considerably between the shockfront and the surface within these layers. Thus the species distributions and pressure distribution over the surface may be very different than either the frozen gas or the equilibrium gas case.

As Λ increases beyond $O(1)$, the stagnation region approaches equilibrium although recombination of the flow to its ideal cone flow state occurs in a highly variable distance

NEAR-FROZEN: $\Lambda < .1$



NON-EQUILIBRIUM: $\Lambda \sim 1$



NEAR-EQUILIBRIUM: $\Lambda > 10$

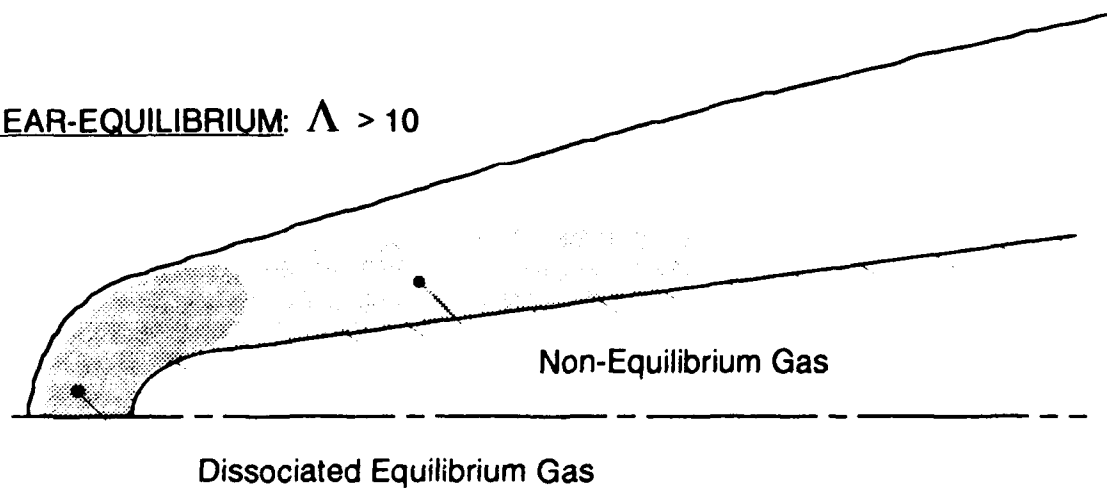


Figure 3. Schematic of Air Chemistry Effects
(exaggerated shock layer)

down the cone, depending on the recombination rate. Thus, for $\Lambda \approx 10$, the stagnation region is near equilibrium but there is a residual nonequilibrium effect in the entropy layer which is highly dependent on flight altitude. This nonequilibrium downstream region is believed to have little effect on the surface pressure since it is highly localized in the thin entropy layer and downstream pressure is dominated by shock shape and shock layer flow conditions near the cone junction.

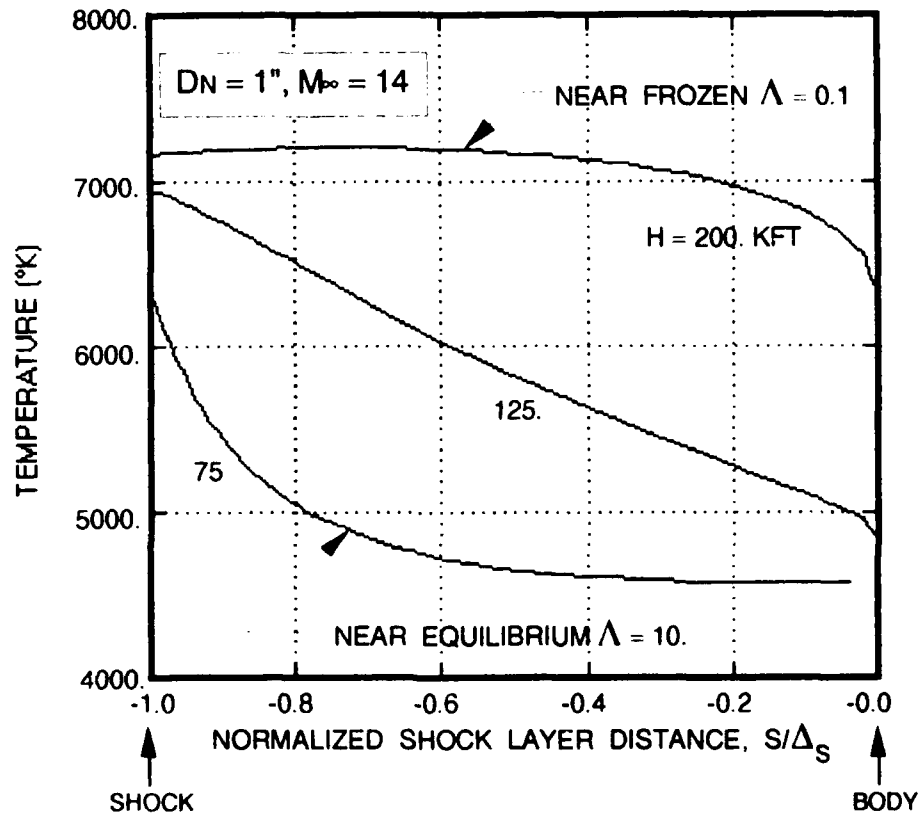


Figure 4. Temperature Distribution in Stagnation Region
1. Inch Nose Diameter at Mach Number = 14.

The shock layer gas composition would not be noteworthy from an aerothermodynamic standpoint, were it not for its effect on the thermodynamic state of the shock layer flow. The effect on two of the principal thermodynamic quantities, temperature and ratio of specific heats (γ), is presented in Figures 4 and 5 respectively. In each case, the variation from near frozen ($h=200$ Kft) through nonequilibrium ($h=125$ Kft) to near equilibrium ($h=75$ Kft) conditions is depicted for the 1 inch nose diameter and Mach number 14 flight condition. Figure 4 shows the significant difference in shock layer temperatures depending on the chemical state of the flow. The roughly 40% difference in average shock

layer temperature, from frozen to equilibrium conditions, translates into a corresponding difference in shock standoff distance since this distance is inversely proportional to the mean density in the stagnation region. Thus the effective nose bluntness is similarly affected which can modulate the overall shock shape, pressure distribution and ultimately the aerodynamics of the vehicle. The temperature differences could also affect the heat transfer to the vehicle depending upon the catalytic properties of the surface. Similar percentage differences are shown in Figure 5. for the effect of chemical nonequilibrium in the shock layer on the ratio of specific heats, γ , of the gas. These distributions suggest a potential effect on the nature of the flow expansion about the sphere-cone junction and hence on the pressure distribution in this crucial region.

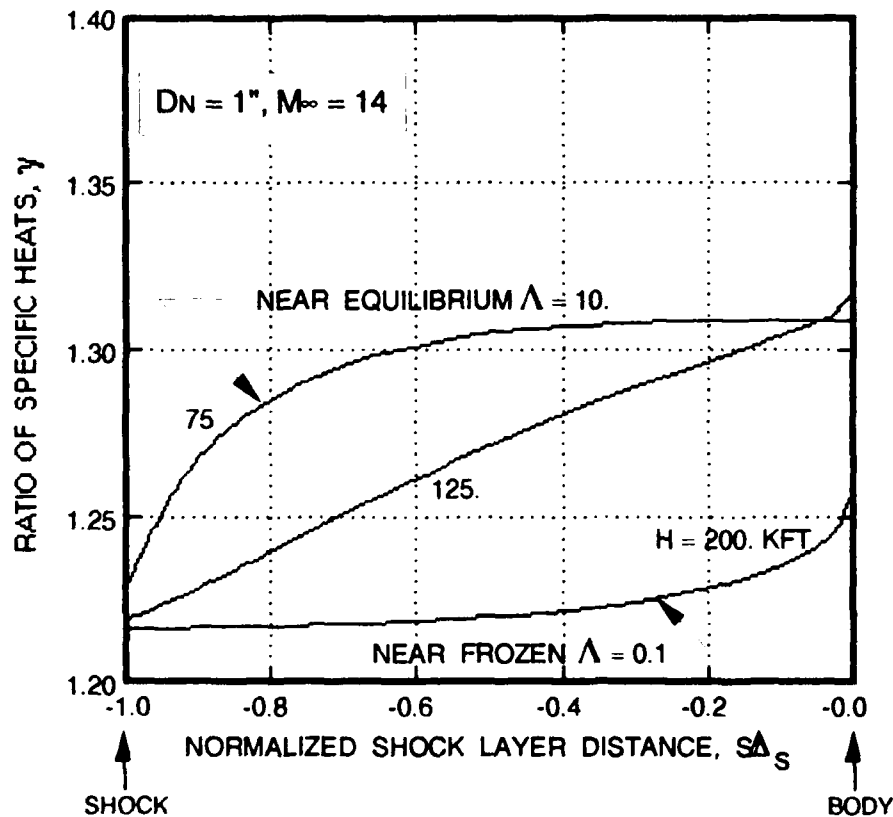


Figure 5. Gamma Distribution in Stagnation Region
1. Inch Nose Diameter at Mach Number = 14.

2.2 Nonequilibrium Air Flight Regime Definition

As suggested previously, the reactive shock layer flow analysis can be used to examine the operating conditions for which gas chemistry effects are operative. The degree of dissociation and rate parameters, in particular, can be used to define the various regimes in flight or ground test facilities in which gas chemistry effects are important. These "Operating Maps" are developed in this section for a typical flight vehicle and ballistic range model in Mach number/Altitude parameter space. Using this approach, Figures 6 and 7 define the approximate oxygen chemical state for atmospheric flight of a 1-inch nose diameter vehicle and for flight in a ballistic range of a .15 inch nose diameter model respectively.

The degree of dissociation contours shown on the figures (the dashed $\phi = .1, .9$ contours signify 10%, 90% dissociation) indicate that in flight, O_2 dissociation becomes important in the velocity range corresponding to Mach 8 to 10 and is essentially complete by Mach 12 to 15 for the 75 to 200 Kft altitude range of interest. Although not shown, a similar evaluation shows that N_2 dissociation is not important for Mach numbers less than about 20. The dissociation contours indicate that to the right of the $\phi = .9$ contour the shock layer would be fully dissociated, from equilibrium considerations, and thus subject to so-called real gas effects. It is however clear from the previous section that this "driving potential" may not be realized depending upon finite rate chemistry considerations.

A more complete picture is achieved by considering the Damköhler number reactive flow scaling. The rate parameter, Λ_{O_2} , for O_2 dissociation can be used to delineate flight and range test regimes for which air may be considered frozen, in equilibrium or in nonequilibrium. The detailed reactive flow analyses introduced above indicate that:

$$\Lambda_{O_2} < .1 \quad \Rightarrow \quad \text{Frozen Flow}$$

$$.1 < \Lambda_{O_2} < 10. \quad \Rightarrow \quad \text{Nonequilibrium Flow}$$

$$\Lambda_{O_2} > 10. \quad \Rightarrow \quad \text{Equilibrium Flow}$$

Contours of $\Lambda_{O_2} = .1$ and 10 are shown on Figures 6 which indicate that, for this flight regime, there is a broad band of flight conditions (the cross-hatched region delineated by the $\Lambda_{O_2} = .1$ contour on the left and the $\Lambda_{O_2} = 10$ contour on the right) in which nonequilibrium

flow effects may be important. To the right and below the crosshatched band equilibrium air chemistry is in effect, and to the left and above the band the flow may be considered frozen at the freestream gas composition.

Smaller vehicle sizes, such as ballistic range test models ($D_N = .15$ inch), cause a broadening and bending over of the nonequilibrium band as shown in the ballistic range test operating map presented in Figure 7. Due to the smaller scale shock layer (proportional to D_N) it takes a higher flight Mach number, resulting in a higher temperature (higher dissociation rate), to achieve the same degree of shock layer reactivity as the flight scale vehicle. Thus, due to this scale effect, nonequilibrium effects are potentially more important in the necessarily small scale ballistic range tests than in flight. So that finite rate air chemistry scaling considerations discussed here must be considered to ensure similitude between range test and flight conditions. Oxygen concentration profiles along the shock layer stagnation streamline are presented in Figure 8.a and 8.b for the range model and flight vehicle respectively. These indicate that, with the exception of slightly different equilibrium dissociation levels at the stagnation point, the concentration profiles for both cases are similar for the same Damköhler number value (see Lam in figures). This verifies the reactive flow similitude described above.

The discussion serves to illustrate the nonequilibrium air effects of interest and to define the methods to be used in the scaling analysis and reactive shock layer analysis which are used to evaluate alternative reactive gas mixtures. Of most interest to the present approach, is the Damköhler number scaling which defines the flow and chemical parameters controlling similitude relative to finite rate chemistry effects. Most importantly it indicates the potential for manipulating the chemical rate parameter using alternate gas mixtures to achieve nonequilibrium shocklayer flows at lower total temperatures.

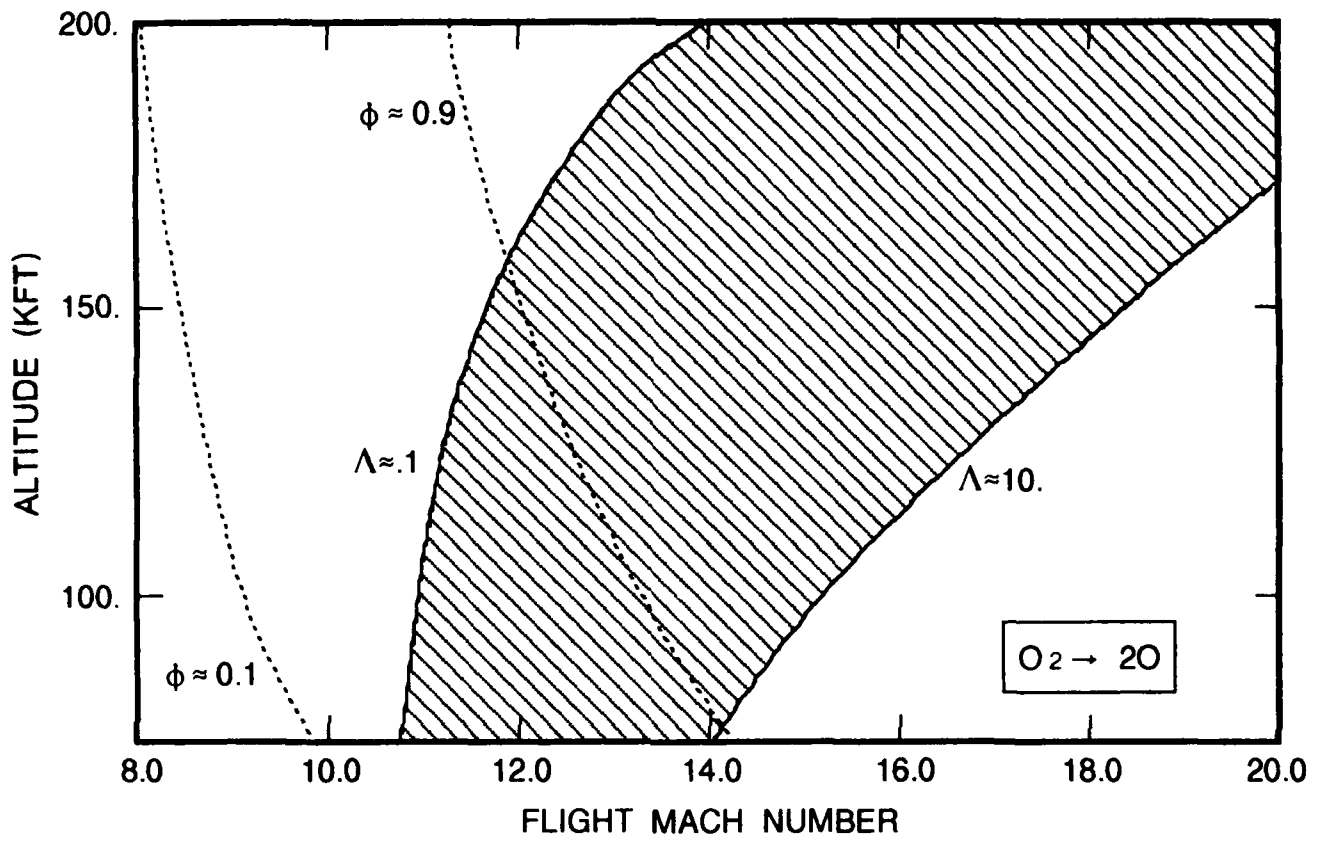


Figure 6. Nonequilibrium Oxygen Reaction Flight Regimes
1 Inch Nose Diameter Sphere-Cone

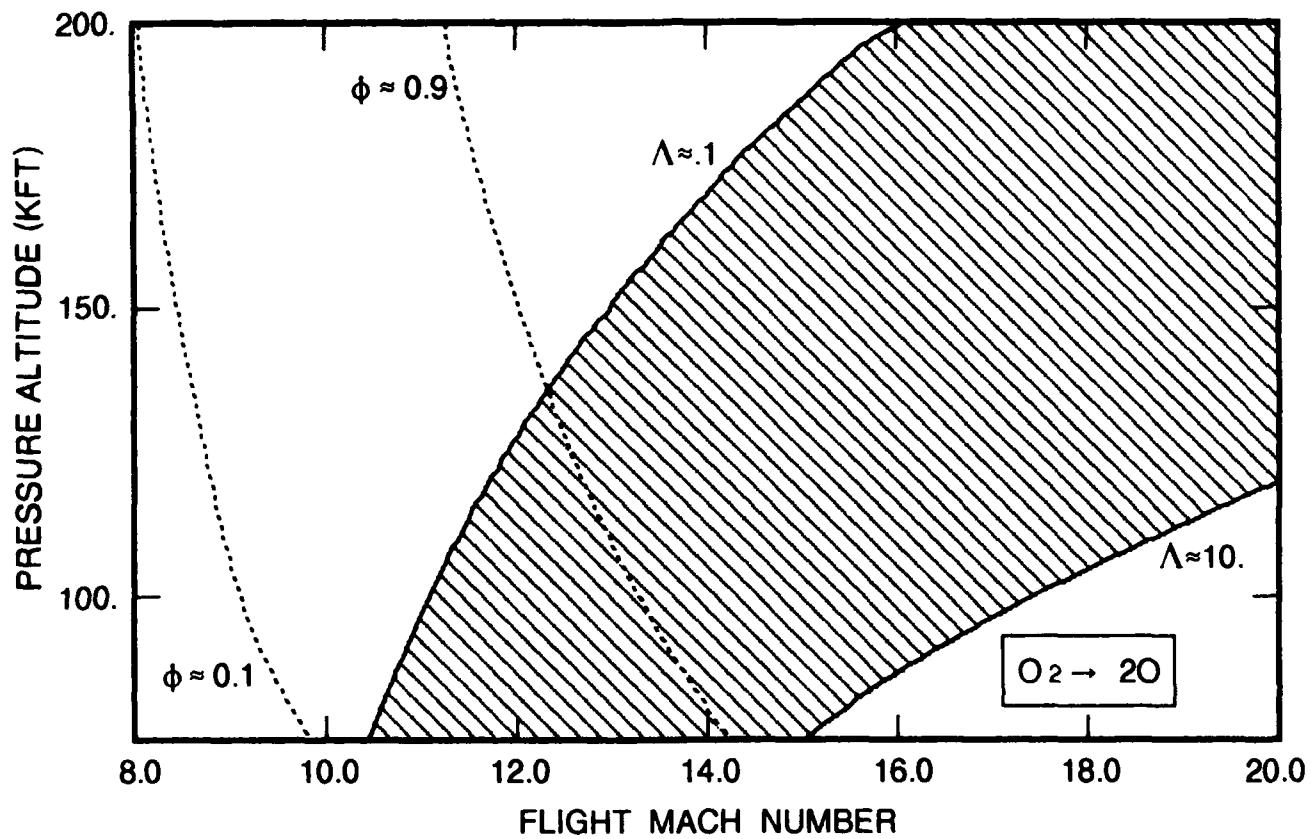
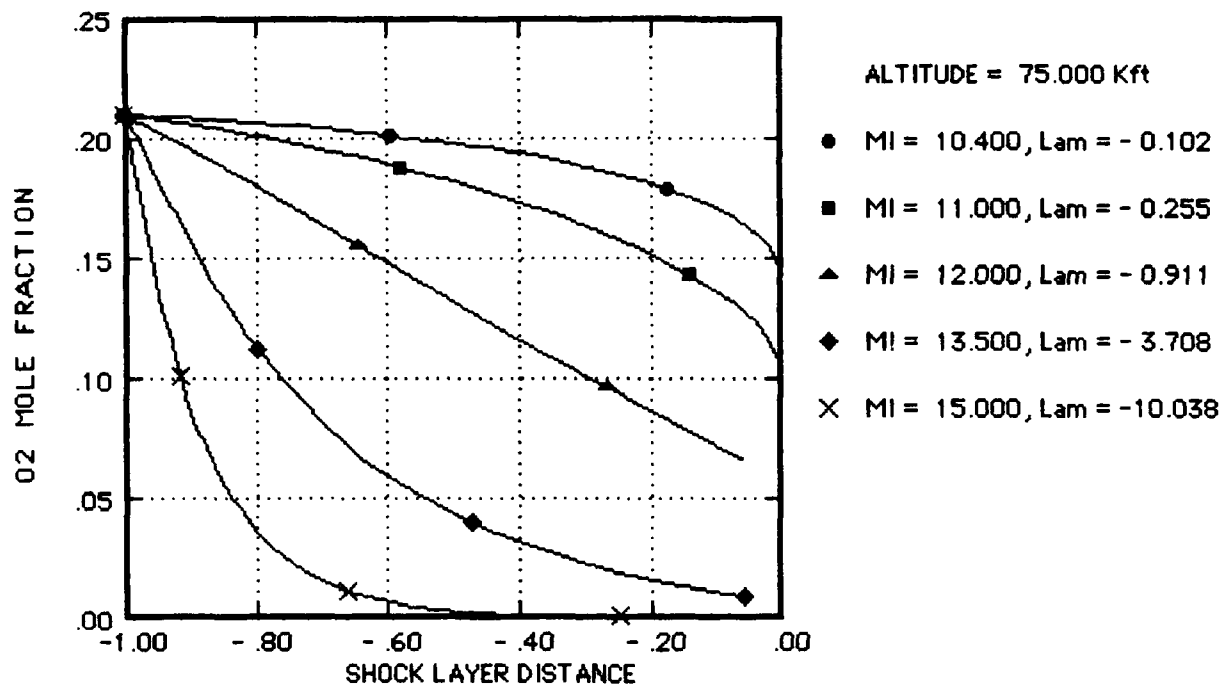
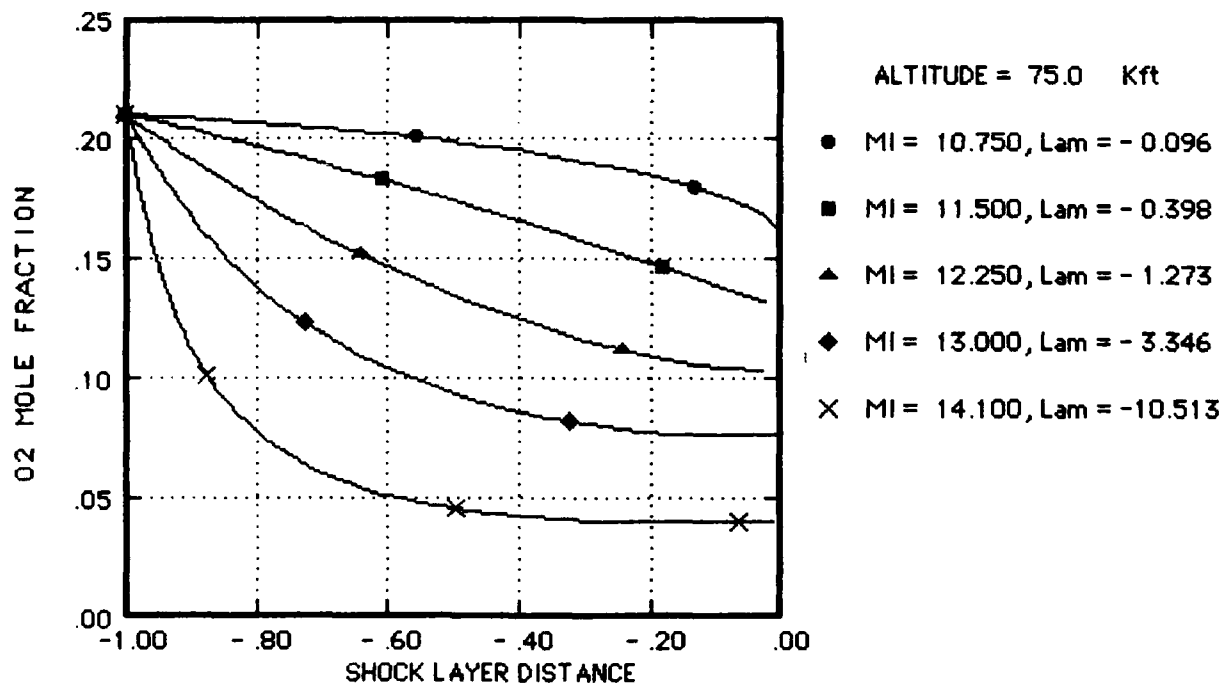


Figure 7. Nonequilibrium Oxygen Reaction Ballistic Range Test Regimes
 .15 Inch Nose Diameter Sphere-Cone



a) Ballistic Range, $D_N = .15$ inch



b) Flight, $D_N = 1$ inch

Figure 8. Oxygen Distribution on Stagnation Streamline

2.3 "Simulant Gas" Shock Tunnel Test Summary

The present feasibility study uses the reactive flow analyses described above to study the potential for using "simulant gases" in existing ground test facilities as a test for finite rate chemistry effects. The concept involves using a reacting gas mixture in a shock tunnel test facility to simulate reaction rate effects in the shock layer of a model. The reactive flow scaling analysis suggests designing a gas mixture and test conditions which match the Damköhler number of atmospheric flight conditions. The mixture would have to react faster at lower total temperatures than oxygen dissociation, for example, but remain unreacted in the supply gas of the shock tunnel. Such a test design would be very useful for numerical model validation, if not directly for evaluating air chemistry effects. The exact nature of the reaction is not very important so long as the mixture reacts in the model shock layer at a rate corresponding to unit Damköhler number. Satisfying this criteria requires the initial screening and subsequent evaluation of a multiplicity of potential reactive mixtures.

The evaluation of simulant gas mixtures involved the screening of "air-like" mixtures with binary reaction systems according to the following criteria: "air-like" shock/expansion behavior, rapid reaction at 1000 to 1500°K, simple and well-documented reaction step, low toxicity and explosiveness, and low liquefaction temperature. A survey of potential gas mixtures and reactive systems, described in Appendix B, was performed early on in the study which identified mixtures of carbon monoxide, CO, peroxide, H₂O₂, hydrogen, H₂, and water vapor, H₂O, in air as being promising simulant gas candidates. The evaluation study reported on here thus concentrated on these gas mixtures.

Two types of analyses were performed: approximate shock layer scaling and flow streamline analyses, to define a simulant gas flow regime map; as well as to describe simulant gas shock layer behavior at selected test points. The methods have been used to define shock tunnel "Operating Maps", paralleling the flight regime maps presented in the previous subsection. These maps have been developed for oxygen dissociation in air, to provide a baseline for comparison (described in Section 3), and for the principal gas systems considered in this study, namely: carbon monoxide-air combustion (Section 4), peroxide decomposition (Section 5), and hydrogen-air combustion (Section 6). The sensitivity of the operating regime results to various promising admixtures within the CO-H₂-H₂O₂-H₂O-Air chemical system (Section 7) has also been examined.

The methods and models used in the flight regime analysis presented in the previous subsection (and Appendix A) have been modified to treat the flow of a relatively general (O_2 , N_2 , H_2O , CO , H_2O_2 , H_2 , O , H , OH , OOH , CO_2) gas mixture in a shock tunnel. Instead of velocity/altitude as the defining flow parameters, in this case, the initial supply tube pressure/shock Mach number, along with the expansion nozzle area ratio define the test section flow properties which the model experiences. The salient results of the analysis are presented as a tunnel "Operating Map" which defines the reactive flow regimes relative to the operating parameters. This identically parallels the flight regime analysis and highlights the test conditions for reactive flow similitude—the objective of the test definition study.

For analysis purposes, the shock tunnel test set-up illustrated in Figure 9 is utilized. The schematic indicates the operation of the shock tunnel in the nonreflected shock mode which merely expands the supply gas, processed by the incident shock (with Mach No. M_i), to a test section condition (M_∞ , ρ_∞). The test section flow conditions, to which the model is exposed, are determined by M_i and the initial supply gas conditions, P_i , T_i , along with the nozzle expansion ratio (A_{ts}/A_s). The reactive shock layer analysis code was modified to define the model shock layer flow conditions based on these specified tunnel operating conditions (M_i , P_i , T_i). The assumption is made here that the facility dependent driver tube properties can be selected to initiate a shock of appropriate Mach number, M_i , into the driven (supply) tube. Furthermore, the shock tunnel is assumed to be completely defined by the supply tube length, L , which controls the test time, and the nozzle area ratio which controls the test section Mach number. In all of the investigations performed in this study, the initial supply temperature was taken as normal room temperature, $T_i = 530.^\circ R$, so that, given the

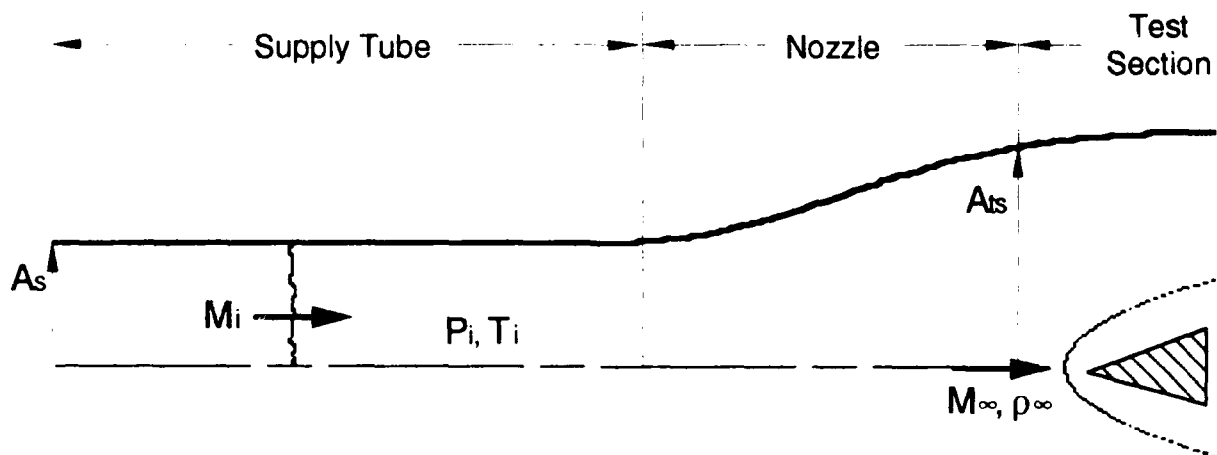


Figure 9. Schematic of Shock Tunnel Test

simplified tunnel geometry, the tunnel operating conditions are completely defined by the shock Mach number and initial supply tube pressure. Thus the shock tunnel test operating maps will be evaluated and presented relative to these parameters.

The analysis thus accounts for the incident shock jump conditions and steady adiabatic expansion of the trailing flow to an arbitrary test section area for, in this case, an ideal gas mixture. The shock jump conditions determine the supply gas properties (P_s , T_s) which are used to determine the reactivity of the supply gas relative to its residence time, Δt_{test} , in the supply tube. The analysis solves the basic shock conservation equations for a mixture of ideal gases assuming a post shock pressure given by a real gas modification (based on a fit to Hanson, 1957) to the constant γ shock pressure. The test time is evaluated conservatively from the difference in arrival times at the expansion nozzle between the incident shock and the trailing contact surface. A modified version of the STREAM code solves the reactive flow equations for a fluid parcel traveling at the uniform supply gas conditions for a time interval given by Δt_{test} . This model is used in each of the sections below to determine the supply gas reactivity relative to the shock layer reactivity.

The test section freestream flow properties, as mentioned above, are determined by considering an adiabatic expansion of the supply gas over the supply tube/test section area ratio. This is accomplished by implicitly solving the Mach number/area ratio relation for a constant γ . The value of γ at the supply gas conditions is used in this expression and a rapidly convergent Newton-Raphson iteration method is used to determine the test section Mach number given the specified area ratio. All other test section flow properties follow from the one dimensional flow property/Mach number relations with assumed constant γ and from the gas mixture equation of state.

In all of the calculations in the present report, the geometry of the Calspan shock tunnel with 48 inch nozzle (8 inch supply tube and 48 inch test section diameter; 70 ft supply tube length) was used and this results in a relatively constant test section Mach No. of ≈ 5.3 for all of the test conditions examined. Also, a simple sphere-cone model with 1 inch and 12 inch nose diameter was utilized as a representative test model sizes which can be accommodated in the Calspan tunnel. According to the reactive flow scaling described above, larger models would also provide a tendency to shock layer flow equilibrium—all other conditions being equal—and, as will be shown below, improve the potential performance of the simulant gas method.

3. BASELINE SHOCK TUNNEL TEST WITH AIR

Air is of course the normal working fluid in shock tunnel testing of either the reflected or nonreflected shock mode, and it is essential to investigate its behavior under the conditions investigated in the present study. In this way, the "standard-for-comparison" is set for evaluation of the simulant gas mixtures. The methods and models described above are thus used in this section to develop results for shock tunnel operation in this baseline operational mode.

Figure 10 presents the predicted O_2 mole fractions along the stagnation streamline between the shock and the model surface for shock tunnel operation at a shock Mach number of 9.5 and initial pressures between 2. and .02 psi. Curves are presented which range from near frozen ($\Lambda = .1$) through the nonequilibrium range ($\Lambda \approx 1$) to near equilibrium ($\Lambda = 10$) conditions. The variation in shock layer reactivity is achieved by varying the initial supply tube pressure (P_i) over the range indicated in the legend of the figure. For example, at this shock Mach number the the model shock layer is in an equilibrium state for tunnel pressures

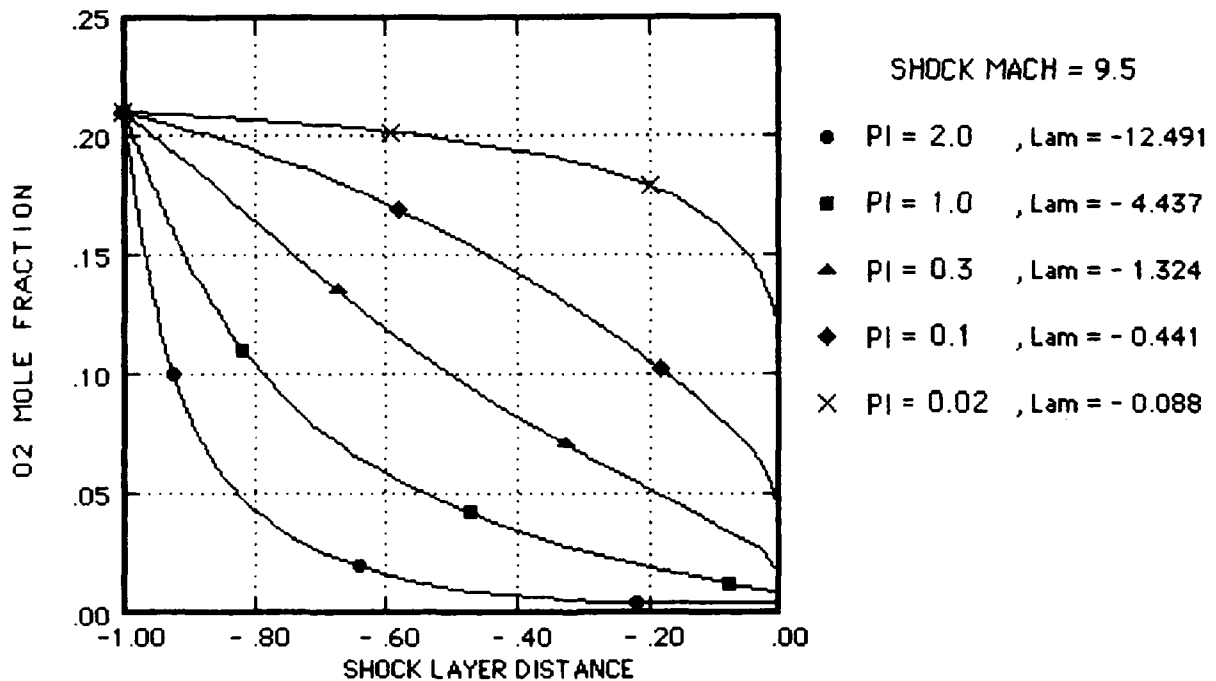


Figure 10. Oxygen Distribution Through Stagnation Region
Near Frozen through Near Equilibrium Conditions
Shock Mach Number = 9.5
1. Inch Nose Dia. Test Model, Test Section $M_\infty \approx 5.3$

above 2. psi. For lower pressures, the shock layer is in the nonequilibrium regime until it reaches near frozen conditions at $P_i \approx .02$ psi. Over this range of operating conditions, the test section Mach No. is relatively constant at $M_\infty \approx 5.3$ (for expansion in the 48 inch Calspan nozzle) and the test section density altitude varies with the initial pressure: ≈ 110 . Kft at 2 psi to ≈ 200 . Kft at .02 psi Thus the more tenuous gas at lower initial shock tunnel pressures requires a higher intensity flow (higher total temperature) to achieve reactive conditions than provided by a shock Mach number of 9.5 .

The results of a number of simulations such as those just described were combined to define shock tunnel "Operating Maps" for oxygen dissociation and the results are presented in Figures 11 through 13 below. The figures parallel the flight regime results of Figure 6 except that here the principal shock tunnel operating parameters of incident shock Mach number (M_i) and initial supply tube pressure (P_i) are used to define the shock tunnel test regimes which, according to the previous analysis, provide reactive flow similitude to the corresponding flight regime. As before the shaded region in each figure denotes the nonequilibrium oxygen dissociation regime which defines test conditions for finite rate air chemistry testing.

The results presented in Figure 11, taken first, are developed for a 1 inch nose diameter test model. As previously, the nonequilibrium oxygen regime is delineated by the Damköhler number scaling with Λ between .1 and 10. It is recalled that the Damköhler number is evaluated at frozen flow conditions (undissociated) just behind the shock in the model shock layer. For oxygen dissociation, this turns out to be the maximum reaction rate along the stagnation streamline. Also shown in Figure 11 are the contours of oxygen degree-of-dissociation, ϕ , which denote conditions for slight, $\phi = .1$, and significant, $\phi = .9$, dissociation of O_2 at equilibrium stagnation conditions. The band of nonequilibrium test conditions parallels the nonequilibrium flight regime in that it indicates the tendency to increasing nonequilibrium effects as initial pressure or altitude decreases. Also in concert with flight are the degree of dissociation contours which exhibit a relatively small effect of pressure or altitude (nearly vertical lines). Almost regardless of initial pressure, the same Mach number provides the same potential for ultimate degree of dissociation

The equilibrium and nonequilibrium results on Figure 11 clearly indicate that, for example, in the region of $P_i < 1$ psi and $M_i > 9$ (upper right hand corner) the actual reactivity of the model shock layer is considerably less than the equilibrium expectation. That is, for $P_i < 1$ psi, equilibrium real air considerations would predict a highly dissociated shock layer for

$M_i > 9$, whereas finite rate chemistry effects result in considerably less dissociation. Thus testing in this regime of test conditions could explore the effects of oxygen dissociation from frozen to equilibrium conditions.

It is pointed out, however, that the $\phi = .9$ curve on Figure 11 roughly corresponds to a 20% degree-of-dissociation in the shocked supply gas. Thus, testing at conditions in the large interesting region of nonequilibrium effects would result in a deteriorated test section flow. That is, over 20% of the O_2 would be reacted to O atoms before the flow reached the test section. This of course is the genesis of the shock tunnel test simulation problem.

It is instructive to investigate the manner in which model scale and "Air" composition modify the test regimes since the 48 inch shock tunnel can accommodate significantly larger models than 1 inch and it is an easy matter to change the initial gas composition. In addition both of these test parameters can lead to improvements over testing at the 1 inch scale in air. The effects of these test design parameters on the test regimes are presented in Figure 12, which utilizes a 12 inch nose diameter test model, and Figure 13 which applies for a pure oxygen test gas.

According to the reactive flow scaling analysis (refer to Equation (3)), the effect of model scale is to linearly expand the shock layer, which for the same flow conditions linearly increases the "flow timescale" or the time for the reaction to proceed. Thus as expected, and shown in the regime map of Figure 12, the 12 inch test model shifts the nonequilibrium regime to the left, to lower shock Mach numbers, and up, to lower initial pressures, relative to the smaller scale model (compare to Figure 11). The figure also shows the dotted equilibrium degree-of-dissociation contours which are not dependent on model scale and therefore are the same in both Figures 11 and 12. Comparing the figures shows that for the same P_i , the 12 inch model can achieve the same degree of shock layer reactivity as the 1 inch model at a lower M_i : lower by 1. at $P_i = 10$. psi and by 2. at $P_i < .1$ psi. This could have some advantages for minimizing the degree of dissociation in the freestream flow, which as described below increases with increasing shock Mach number. However, the shift to lower initial pressures shown in Figure 12 indicates that nonequilibrium testing would correspond to higher effective altitudes (200 to 250 Kft) in which rarefied gas effects could begin to further complicate the test. Otherwise, testing could proceed at lower altitudes and Mach numbers, say Mach number = 8 with density altitude between ≈ 100 to ≈ 200 Kft but the ultimate degree of dissociation in the shock layer would be less by about half. Thus the

differences between frozen and equilibrium results would be less and the case for a definitive finite rate chemistry effect clouded.

The test regime map for pure oxygen and a 12 inch nose diameter test model is presented in Figure 13 for comparison to the corresponding case for air just described in Figure 12. Again both the nonequilibrium regime is shown along with contours of flow conditions for constant equilibrium degree of dissociation ($\phi = .1$ to $.4$). Comparing the figures indicates that the nonequilibrium flow regimes are surprisingly almost identical for both air, Figure 12 and pure oxygen, Figure 13; the differences are clearly within the order of accuracy of the present analysis. This indicates that for the present model nitrogen and oxygen molecules are about equally efficient dissociation partners for oxygen. More noteworthy, however, are the degree of dissociation contours, which indicate that the equilibrium level of molecular dissociation is considerably lower in pure oxygen than air. The curves are nearly vertical, i.e. little altitude effect, as were the corresponding contours for air, however the $\phi = .3$ contour for oxygen occurs at the same Mach number ($M_i \approx 10$) as the $\phi = .9$ contour for air. Thus for testing in pure oxygen it seems that the ultimate difference between frozen and equilibrium condition is reduced compared to air, perhaps leading to a less definitive test.

This section on oxygen dissociation is closed by outlining a test for finite rate chemistry effects based on the analysis and results given to this point. The test would use air as the working gas in a Calspan scale shock tunnel operating in the nonreflected shock mode. The test seeks to isolate the nonequilibrium effect, maximize the observable difference due to this effect and minimize features that obscure the effect thereby providing a baseline for comparing the qualities of the general simulant gas test. The suite of test conditions, along with expected shock layer results, are presented in Figures 14 through 18 below to define the degree which the objectives are achieved.

Figure 14 repeats the operating map for oxygen dissociation in air for the 1 inch nose diameter test model (Figure 11) along with some additions. The additions, define the suggested test trajectory depicted by the solid line at $M_i = 9.5$ connecting the crossed circles between $P_i = 2.$ and $P_i = .02$ psi. Also added to the curve are the cross-hatched lines which denote the freestream degree of dissociation, $\phi_s = .2, .3,$ and $.4$ which provides a measure of this feature of the freestream flow which is an undesired characteristic of shock tunnel tests. Referring back to the oxygen concentration distributions in Figure 10, it is noted that a sequence of tests at $M_i = 9.5$ for initial supply tube pressures between $P_i = 2.$ to $.02,$ would

examine shock layer behavior from near equilibrium conditions, through highly nonequilibrium conditions to frozen flow conditions. From equilibrium considerations alone, the shock layer would be expected to be highly dissociated ($\phi > .9$) for all test conditions along the test line so that the "driving force" and hence the differences, equilibrium : frozen, are maximized. The freestream flow is estimated to be between 20 to 35% dissociated depending upon the initial supply tube pressure; relatively large but about the best that could be done with air.

Figures 15, 16, and 17 present results for oxygen distribution in the supply tube and model shock layer for the most interesting test conditions, namely: frozen flow at $P_i = .02$, fully nonequilibrium flow at $P_i = .3$, and equilibrium flow at $P_i = 2$ psi respectively. These are calculated with the STREAM code applied in a sequential calculation of oxygen dissociation at constant supply tube conditions followed by a calculation along the stagnation streamline of the test model. The supply tube calculation, as described in Section 2.3, follows a fluid particle from the time the shock arrives at the end of the tube (beginning of the nozzle) until the contact surface arrives at the same location. The test time is estimated, by this approximation, to be $\approx .75$ msec for the present conditions.

The oxygen mole fraction shown in Figures 15.a, 16.a, 17.a thus represent an approximation to the variation in oxygen composition which arrives at the test section at various times during the total test time. The supply tube oxygen distribution for near frozen conditions, presented in Figure 15.a, for example, shows the reduction of the oxygen mole fraction from its undissociated value of .21 early in the test (supply tube distance = -1.) to about .15 late in the test (0.). The variation in molecular oxygen concentration with respect to the supply tube distance indicates that the dissociation rates are relatively slow at these conditions. The corresponding results for the nonequilibrium condition, Figure 16.a, and the near equilibrium condition, Figure 17.a show that the oxygen dissociation rates in the supply become progressively higher as the initial pressure increases but the ultimate degree of dissociation is about the same for each test condition; .2 to $\approx .35$. By these estimates, the time dependent variation in oxygen concentration which arrives at the test section should be significant at the near frozen flow condition but small at the other test conditions.

Figures 15.b, 16.b, and 17.b illustrate the predicted oxygen distributions within the model shock layer for the three test conditions: near frozen, nonequilibrium, and near equilibrium respectively. These results parallel the ideal results (i.e. assuming no freestream dissociation) presented earlier in Figure 10 except that in the present cases the oxygen mole

fraction just downstream of the model bow shock is the value calculated from the supply tube rather than the undissociated oxygen mole fraction of .21. For near frozen conditions, Figure 15.b shows that little further oxygen dissociation takes place in the model shock layer except very close to the stagnation point. For fully nonequilibrium conditions, Figure 16.b, however, the oxygen distribution varies in an almost linear manner from its freestream value at the shock to nearly 0. at the stagnation point. Finally, Figure 17.b shows that the model shock layer is almost entirely fully dissociated for the near equilibrium case.

The fact that the freestream flow that the model experiences is partially dissociated is the principal defect of shock tunnel test similitude relative to oxygen dissociation at flight conditions. Of course other deficiencies such as the relatively short test time ($\approx .75$ msec) and the formation of significant amounts of nitrous oxide (NO)—not considered in the present analysis—are also present but these are not believed to be significant impediments to a useful test. To illustrate the degree of the freestream dissociation effect at the important nonequilibrium test condition, Figure 18 compares the oxygen distribution in the model shock layer for the ideal freestream flow to the distribution for the reactive supply tube case. The distributions enter the shock layer at about 30% different levels but approach the same value near the stagnation point, so that the change in shock layer properties due to oxygen state would be expected to differ by, on average, by about 15%. It is believed that the near equilibrium case would differ significantly less from its corresponding ideal freestream case since in each case the oxygen distributions approach the same equilibrium condition close to the shock front. On the other hand, the shock layer in the near frozen case is dominated by oxygen concentration in the freestream so it would be $\approx 30\%$ different than its ideal counterpart throughout the shock layer.

Taking these deficiencies in total, it is believed that such a test as described here, although not ideal, could provide a useful measure of nonequilibrium oxygen dissociation effects especially in relation to the numerical model validation needs cited above.

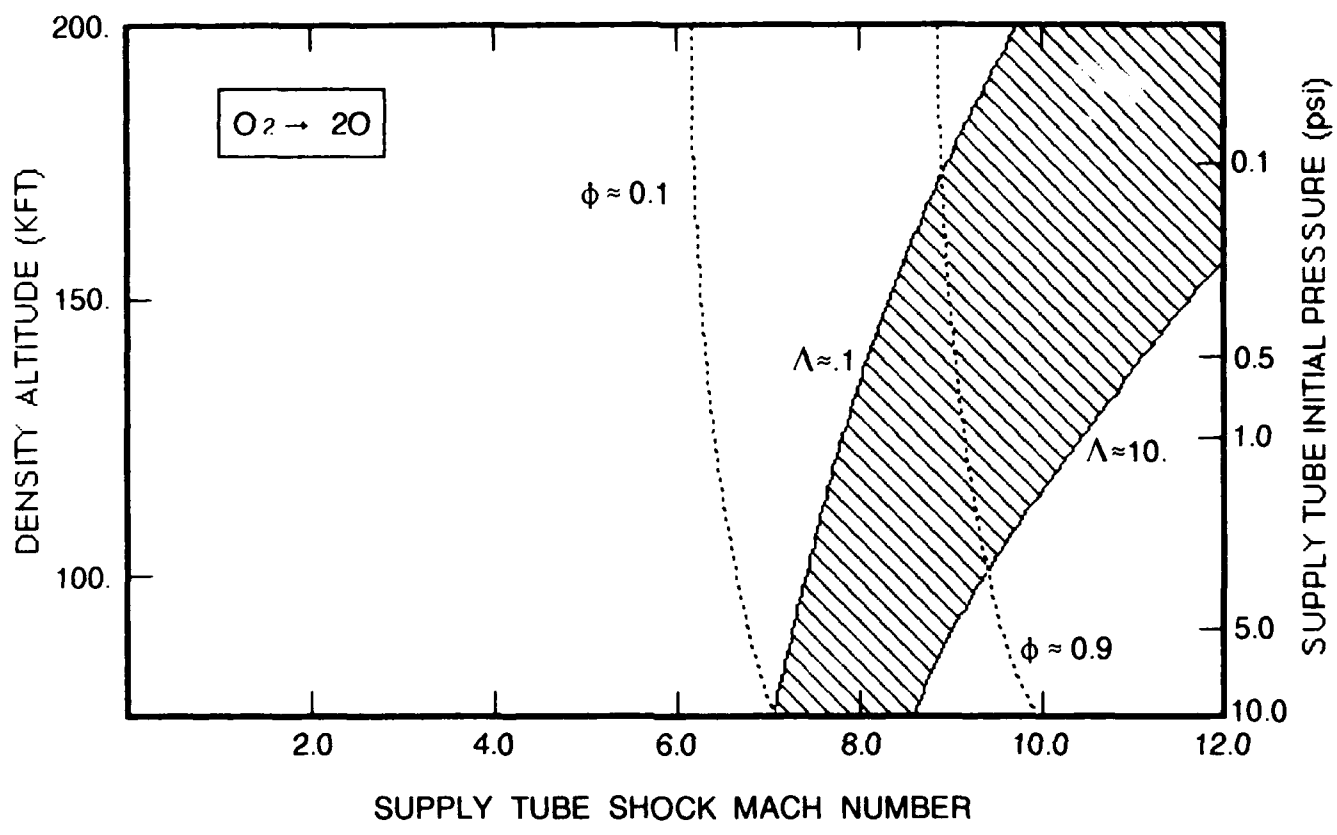


Figure 11. Oxygen Dissociation in Air: Shock Tunnel Test Regimes
 1. Inch Nose Diameter Test Model at $M_\infty \approx 5.3$

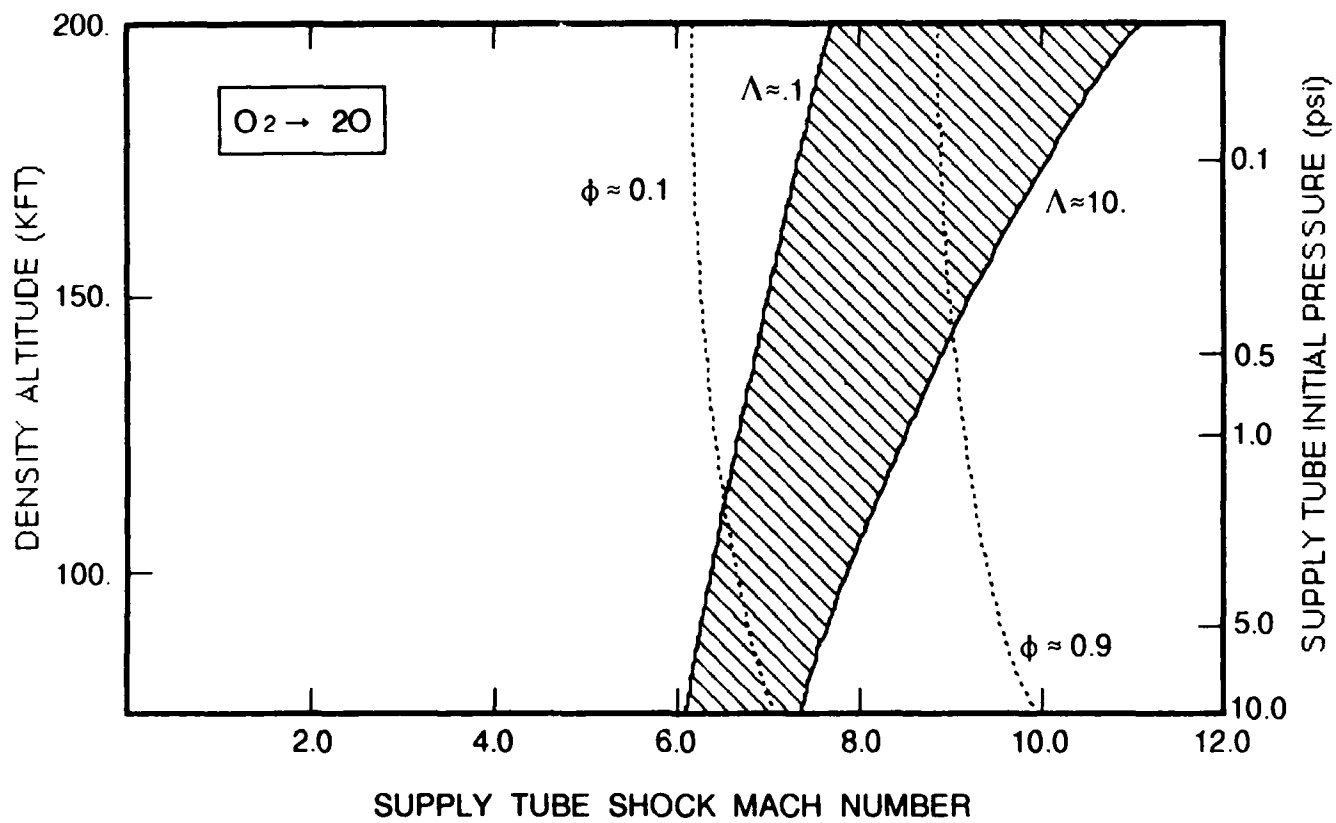


Figure 12. Oxygen Dissociation in Air: Shock Tunnel Test Regimes
 12. Inch Nose Diameter Test Model at $M_\infty \approx 5.3$

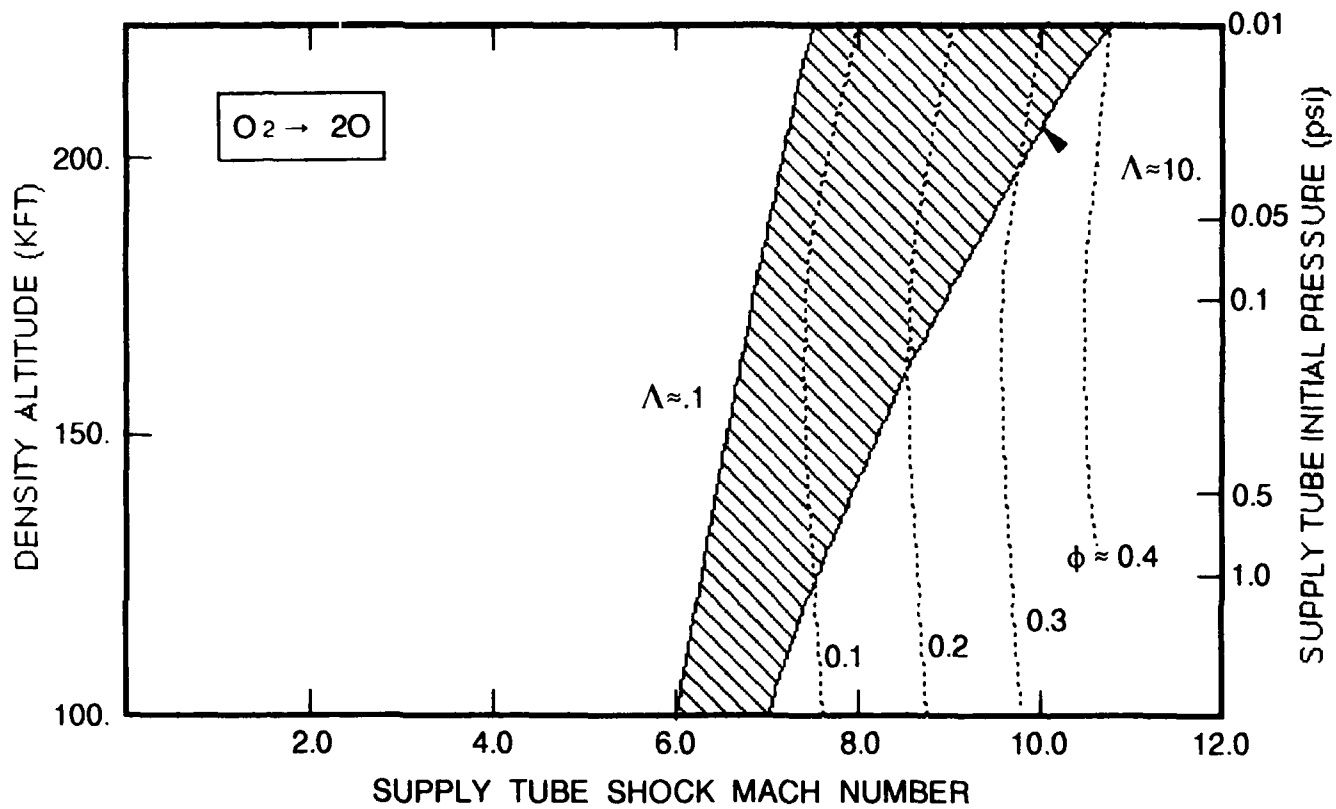


Figure 13. Dissociation in Pure Oxygen: Shock Tunnel Test Regimes
 12. Inch Nose Diameter Test Model at $M_{\infty} \approx 5.3$

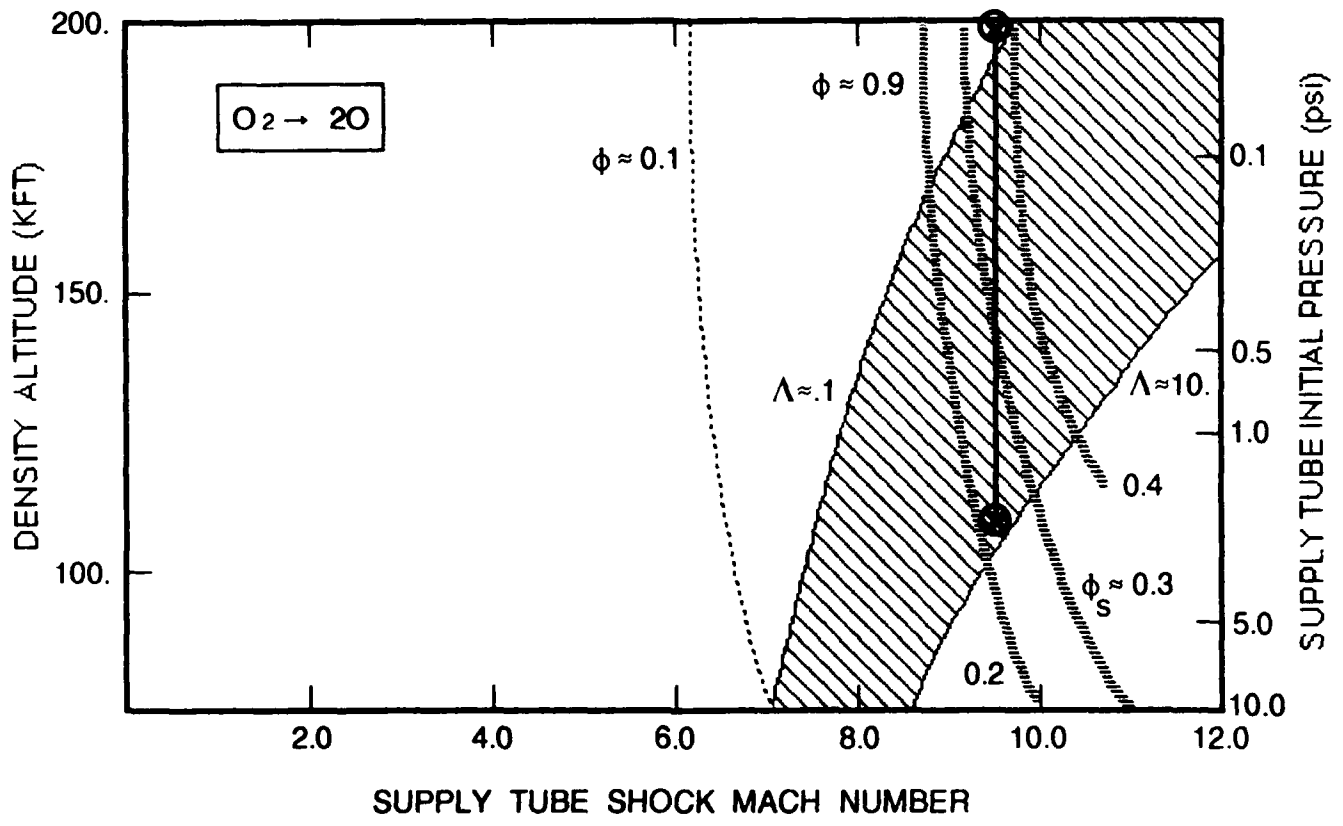
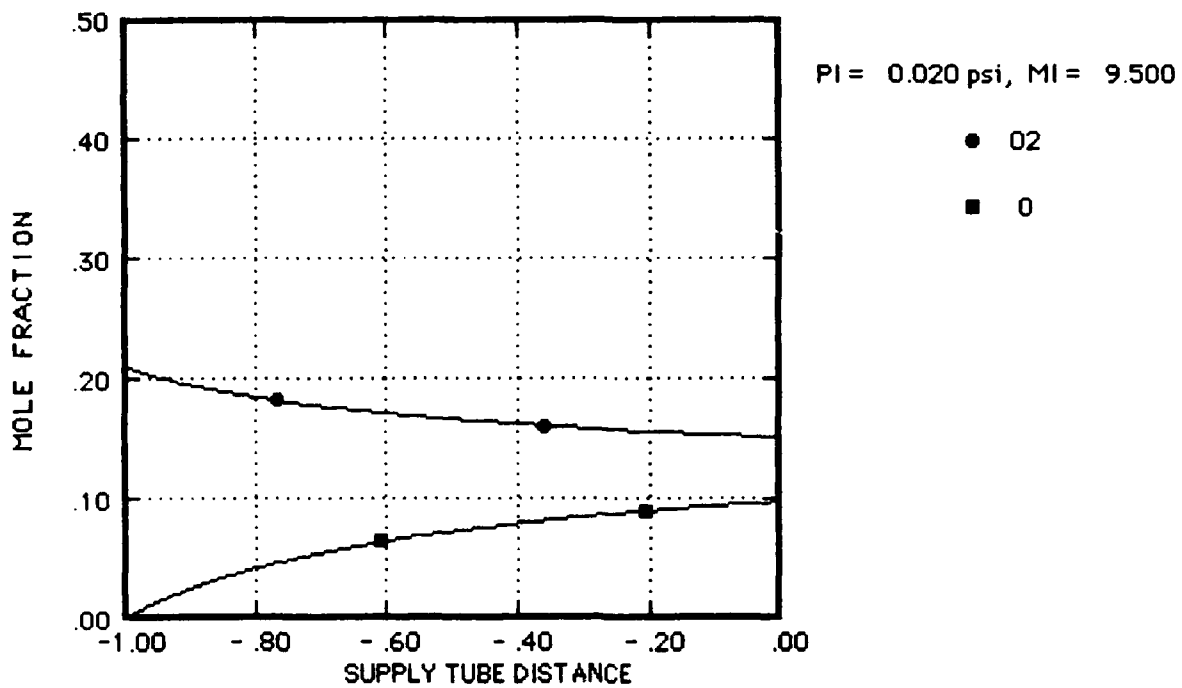
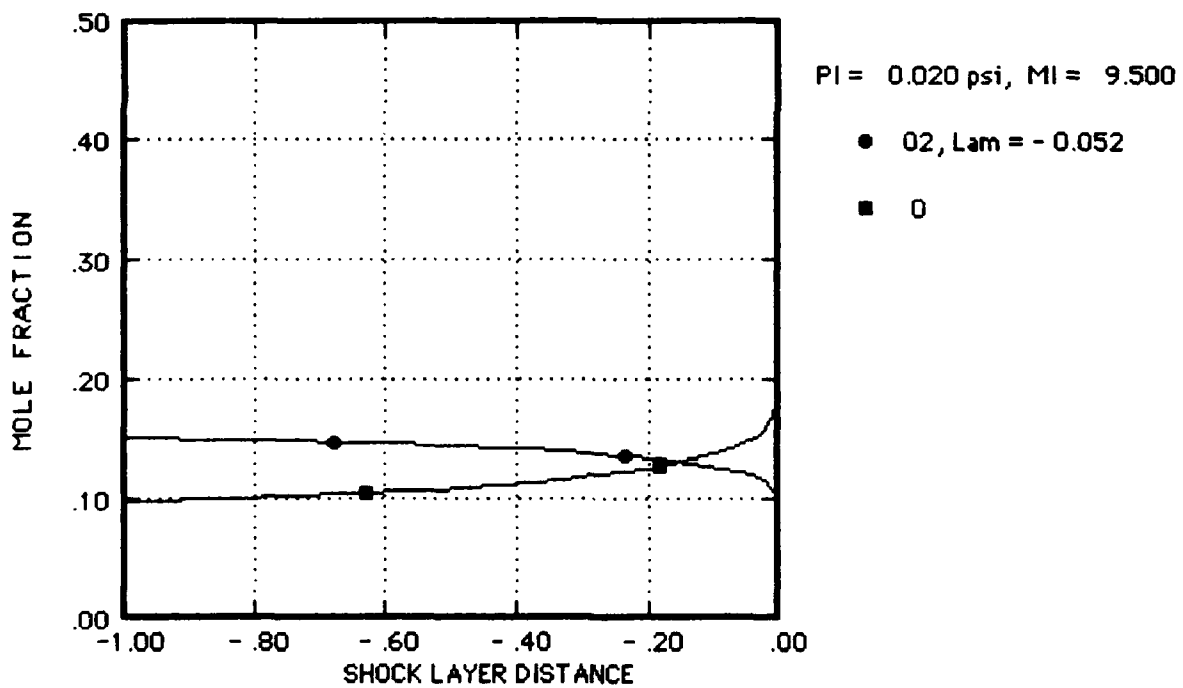


Figure 14. Oxygen Dissociation in Air: Shock Tunnel Test Conditions
 1. Inch Nose Diameter Test Model at $M_{\infty} \approx 5.3$



a) Supply Tube, L = 70 ft



b) Model Shock Layer, D_N = 1 inch

Figure 15. Oxygen Distribution Under Near Frozen Test Conditions
 Initial Pressure = .02 psi, Shock Mach Number = 9.5
 Test Section Mach No. \approx 5.3, density altitude \approx 200 Kft

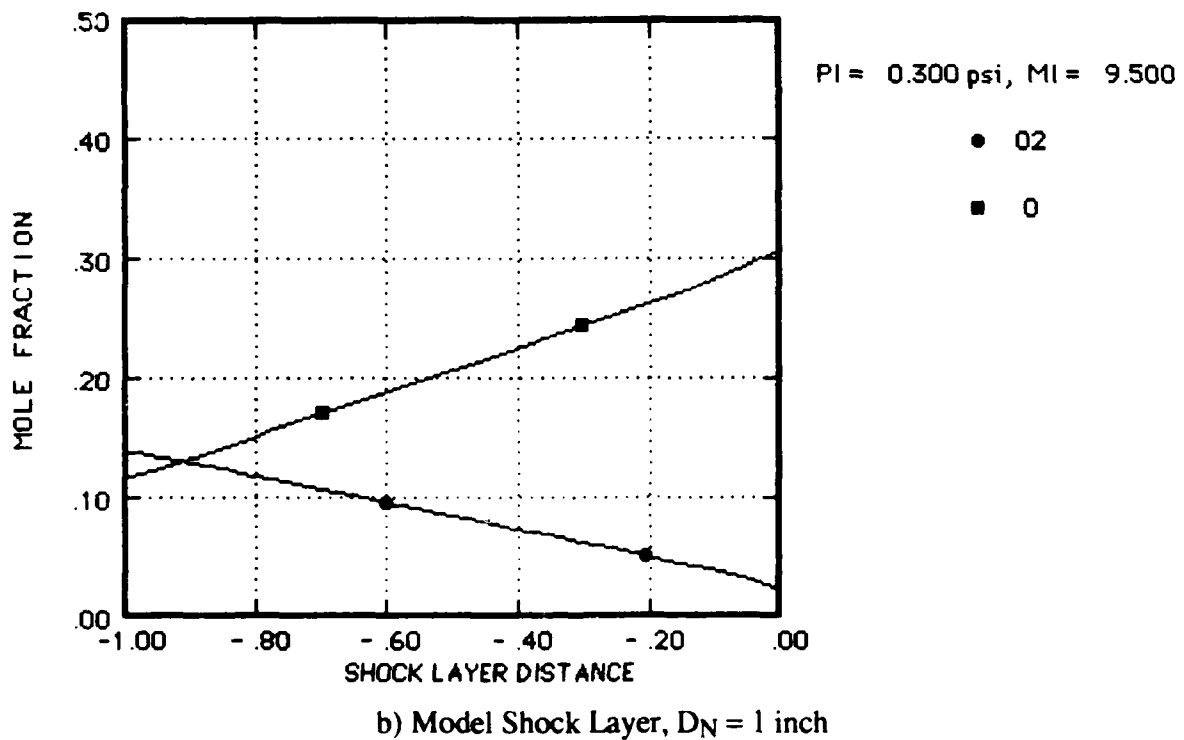
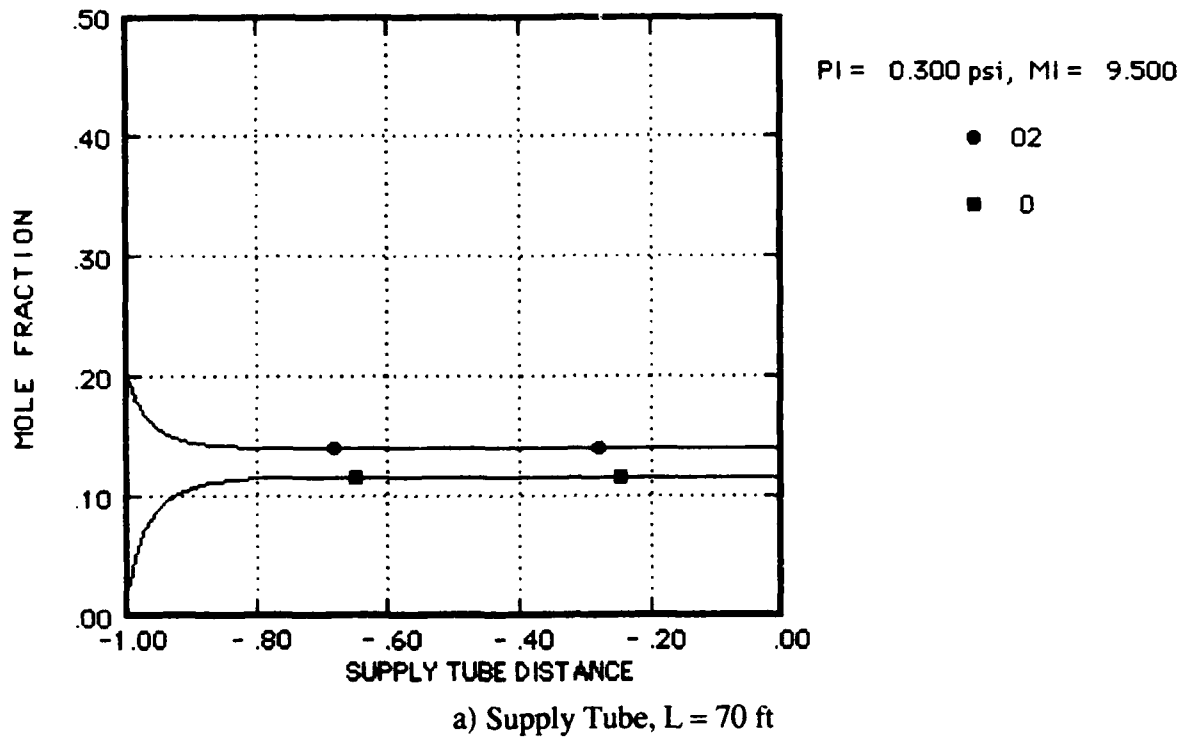
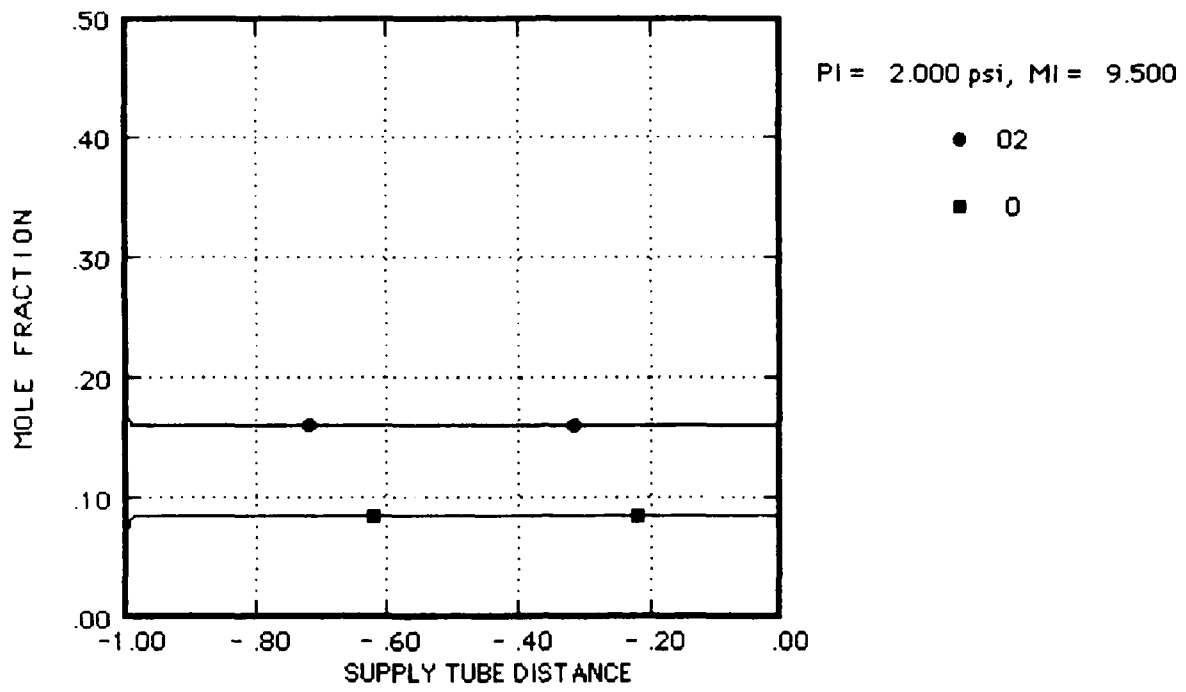
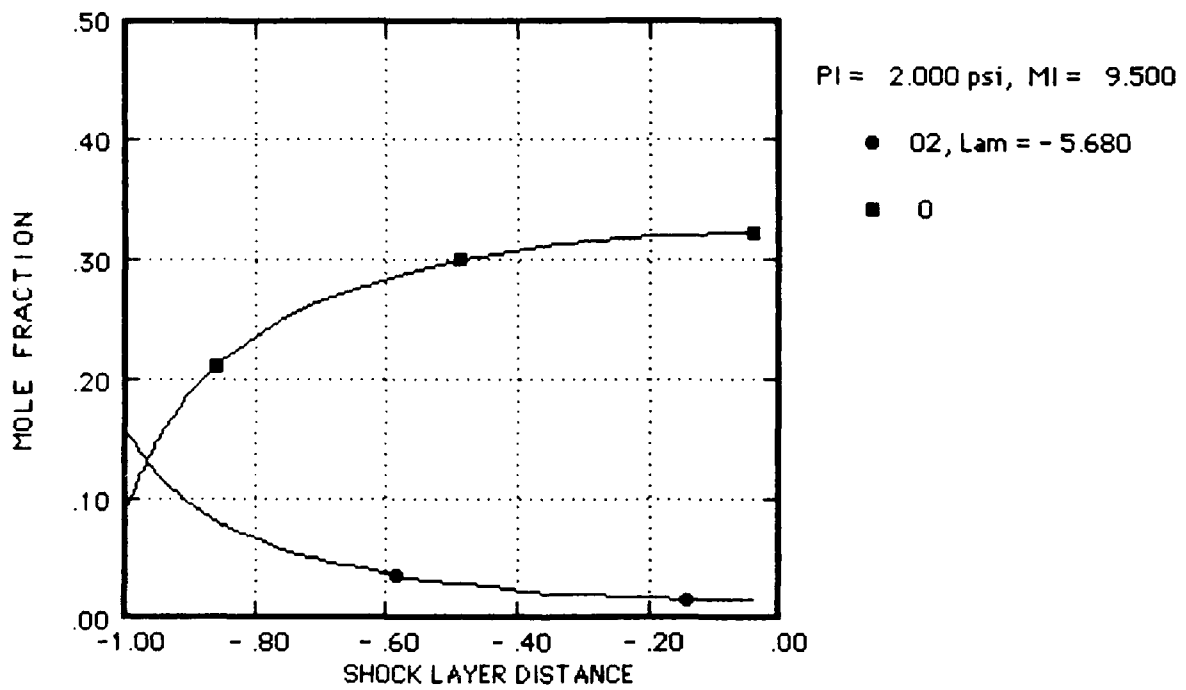


Figure 16. Oxygen Distribution Under Nonequilibrium Test Conditions
 Initial Pressure = .3 psi, Shock Mach Number = 9.5
 Test Section Mach No. \approx 5.3, density altitude \approx 150 Kft



a) Supply Tube, L = 70 ft



b) Model Shock Layer, D_N = 1 inch

Figure 17. Oxygen Distribution Under Near Equilibrium Test Conditions
 Initial Pressure = 2. psi, Shock Mach Number = 9.5
 Test Section Mach No. \approx 5.3, density altitude \approx 110 Kft

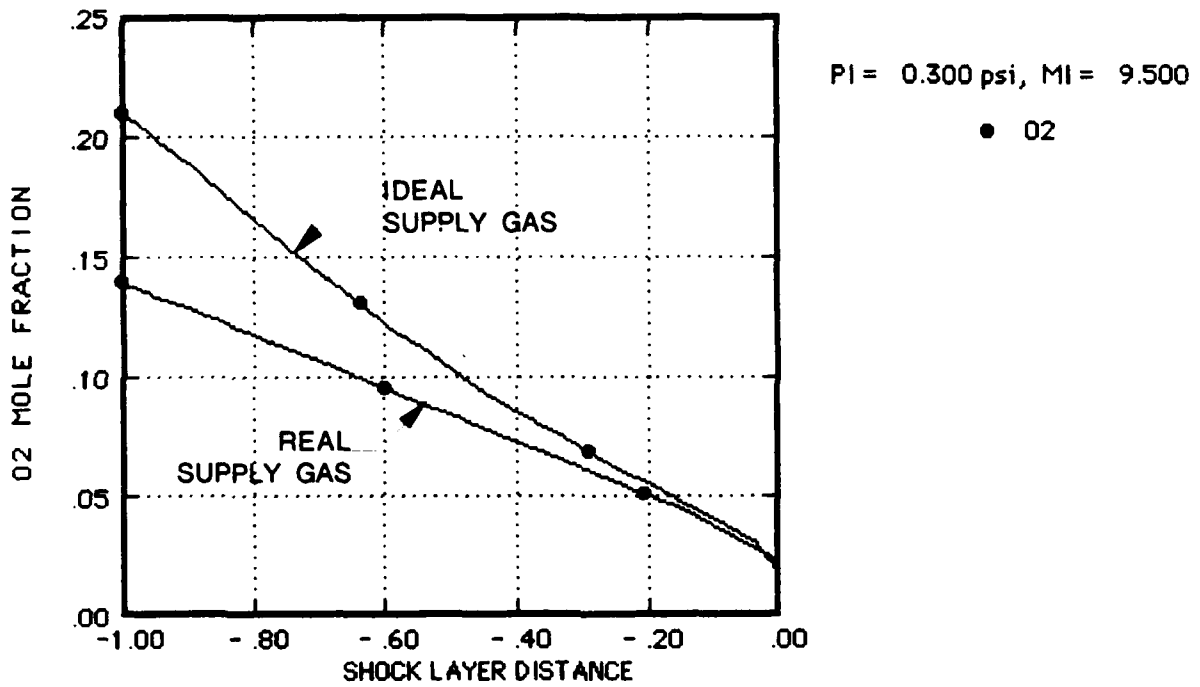


Figure 18. Oxygen Distribution Under Nonequilibrium Test Conditions
 Effect of Supply Gas Dissociation on Shock Layer
 Initial Pressure = .3 psi, Shock Mach Number = 9.5
 Test Section Mach No. ≈ 5.3 , density altitude ≈ 150 Kft

4. CARBON-MONOXIDE-AIR SIMULANT GAS SHOCK TUNNEL TEST ANALYSIS

Shock tunnel flow simulations with simulant gas mixtures have been performed to resolve the deficiencies of shock tunnel tests with air. As pointed out in the previous section two principal deficiencies of high enthalpy hypersonic shock tunnel testing are the short test times and the highly dissociated expanded flows which they typically produce. Both deficiencies arise in large part due to the high supply temperatures needed for air operation which result in high wavespeeds and a high degree of reactivity in the air supply. Both problems are ameliorated by gas mixtures which react at lower temperatures and which react at a defined "ignition temperature" such as combustible gases. Such mixtures can be shocked to lower static temperatures than air to result in reduced wavespeeds, hence longer test times, and decreased supply gas reactivity leading to unreacted test section flows. Determining the degree to which these benefits can be realized provides the main objective of the shock tunnel flowfield analyses. Initial studies have centered on a potential demonstration test which utilizes a "strawman" gas mixture consisting of carbon-monoxide in air and the results of this investigation are described in this section.

The CO/Air reactive mixture has the distinct advantage of very air-like properties so that facility operational experience with air should carry over to tests with this gas with little modification. The test would utilize driver and driven gas properties which would result in a gas supply in the driven tube which would remain unreacted as it expands to the test section but react in the model shock layer. Depending on shock Mach number, a range of flow and total temperatures can be achieved for controlling freestream and model shock layer reactions. From approximate considerations of mixture ignition temperature at shock heating conditions, $M_1 \approx 3$ to 4 would provide a promising combination of low supply tube temperature—hence low reactivity and wavespeed—and high total temperature for reaction in the model shock layer. These estimates have been refined using the reactive shock layer streamline model recently developed for shock tunnel operation of general gas mixtures of Air-CO-H₂-H₂O-H₂O₂ (see Appendices A and B).

Initial estimates motivated a single test condition using the carbon-monoxide/air mixture for which nonequilibrium effects should be operative in the model shock layer. The reactive flow analyses have been utilized to define a range of reactive flow operating conditions leading to the definition of a shock tunnel test "operating map." Reactive streamline flow results which define the nonequilibrium operating regime for a stoichiometric

carbon-monoxide/air mixture are presented in this section in Figure 19 leading to the CO/Air "Operating Maps" presented in Figure 20 and 21. In all of these current studies the Calspan 48 inch shock tunnel configuration is utilized as described above.

For comparison purposes, the presentation follows the oxygen dissociation results of the previous section. Figure 19.a, b, and c present stagnation streamline distributions of specie mole fractions (see legend) at a near frozen flow condition, fully nonequilibrium and near equilibrium condition respectively for a representative 1. psi initial supply tube pressure. The figures illustrate the variation in shock layer reactivity as the incident shock Mach number is varied from 3.95 to 4.8. Over this range of conditions the simulated test section conditions vary little from $M_\infty \approx 5.3$ and density altitude ≈ 125 Kft. The specie distributions in Figure 19 show the variation of the principal reactive components for CO-Air combustion, namely: the rapid conversion of CO and O₂ to CO₂ in the reaction zone. Not evident in these plots are the relatively slower buildup of the radical species (OH, OOH, H) to small ($O(10^{-5})$) but important levels upstream of and in preparation for the main oxidation reaction. The small radical concentrations in fact control the ultimate combustion of CO.

The results of Figures 19.a, b, c can be compared to the oxygen mole fraction distributions in Figures 15.b, 16.b, and 17b. In contradistinction to the distributed reaction characteristic of O₂ dissociation, the CO/Air reaction results in a more concentrated reaction zone which is very close to the model surface for the frozen flow case (Figure 19.a), is about midway through the shock layer for the nonequilibrium case (Figure 19.b), and is close to the shock for the near equilibrium case (Figure 19.c). In the former case it would be expected that little of the shock layer flow is reacted and in the latter case all of the blunt body portion of the shock layer would be reacted. This would thus mimic O₂ dissociation from frozen to equilibrium flow respectively.

This "flameliike" behavior of the CO-Air reaction is characteristic of a combustible mixture in which a rapid combustion reaction follows a relatively slow radical buildup step. The effective time duration of the overall combustion is determined by an induction period which is controlled by radical (OH, OOH, H) specie generation (see Appendix B). This characteristic is the origin of the "ignition temperature" concept which was used for the initial screening of potential simulant gas mixtures. It is also the origin of a problem with the simulant gas concept insofar as combustible gases are concerned as will be discussed below.

As in the previous cases, the results of numerous calculations such as the above can be combined to develop an "Operating Map" for shock layer reactivity in shock tunnel parameter space (M_i , P_i). This presentation of the multiplicity of results is included in Figures 20 and 21 to define the nonequilibrium reaction regime for shock tunnel operation with a stoichiometric CO/Air gas mixture using test models with nose diameters of 1 inch and 12 inches respectively. The shaded region in the figure delineates this regime and is compared to the corresponding region for the baseline O_2 dissociation reaction at the same model scale. It can be seen that the CO/Air "Simulant Gas" can achieve nonequilibrium reaction conditions at reduced shock Mach numbers compared to air. The benefits become less as initial supply tube pressure is decreased below ≈ 2 psi, but are significant at effective test section density altitudes up to 150 Kft or more depending on the model size. The results for the 12 inch model in Figure 21 exhibit less variation with respect to altitude than the smaller 1 inch diameter case and provide a reduced shock Mach number benefit relative to oxygen dissociation up to a density altitude of 200 Kft or more. Also important to note is the shift of the nonequilibrium regime to lower Mach numbers due to the longer flow time for reaction provided by the larger model and shock layer scale.

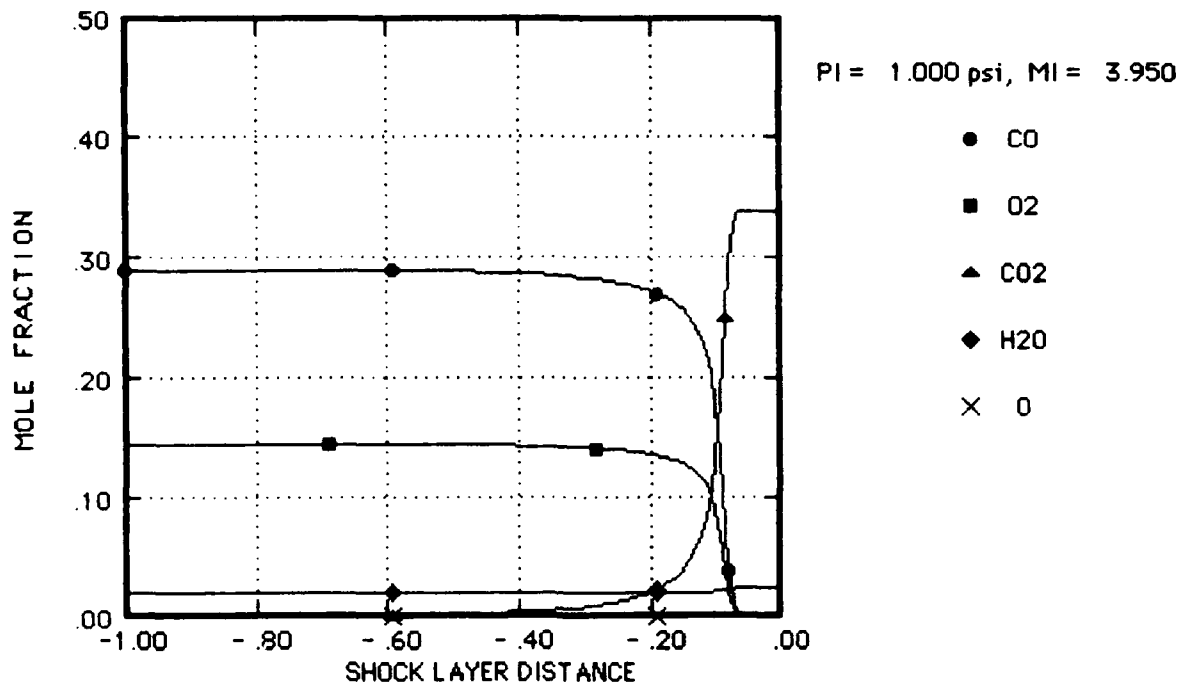
Based on these results, a nonequilibrium chemistry test could be designed to parallel the oxygen dissociation test described in Section 3. Referring to Figure 4 for the 12 inch model, a sequence of test points with shock Mach number, $M_i = 4.0$, and initial supply tube pressures from 10. psi to ≈ 1 . psi would simulate a reactive shock layer test from near equilibrium to near frozen flow conditions. It would thus mimic the oxygen dissociation test at $M_i = 9.5$. In the present case, however, the test times would be in the range of 2. to 5. msec, depending on test condition; much larger than the submillisecond test times of the test in air. In addition, the test section flow Mach number would be very close to 5.3 for all relevant test conditions. Although seemingly promising, the definition of such a test with CO-Air is however jumping the gun since the supply tube reactivity has not as yet been examined.

Unfortunately, the concept of the "ignition temperature" which would keep the supply gas unreacted while providing for rapid reaction rates in the model shock layer is misleading. In fact, simulations using the STREAM code applied to the CO-Air mixture in the supply tube show that the supply gas would react before it ever reached the test model for test conditions defined above. Thus the CO-Air simulant gas test as outlined above will not work as advertised.

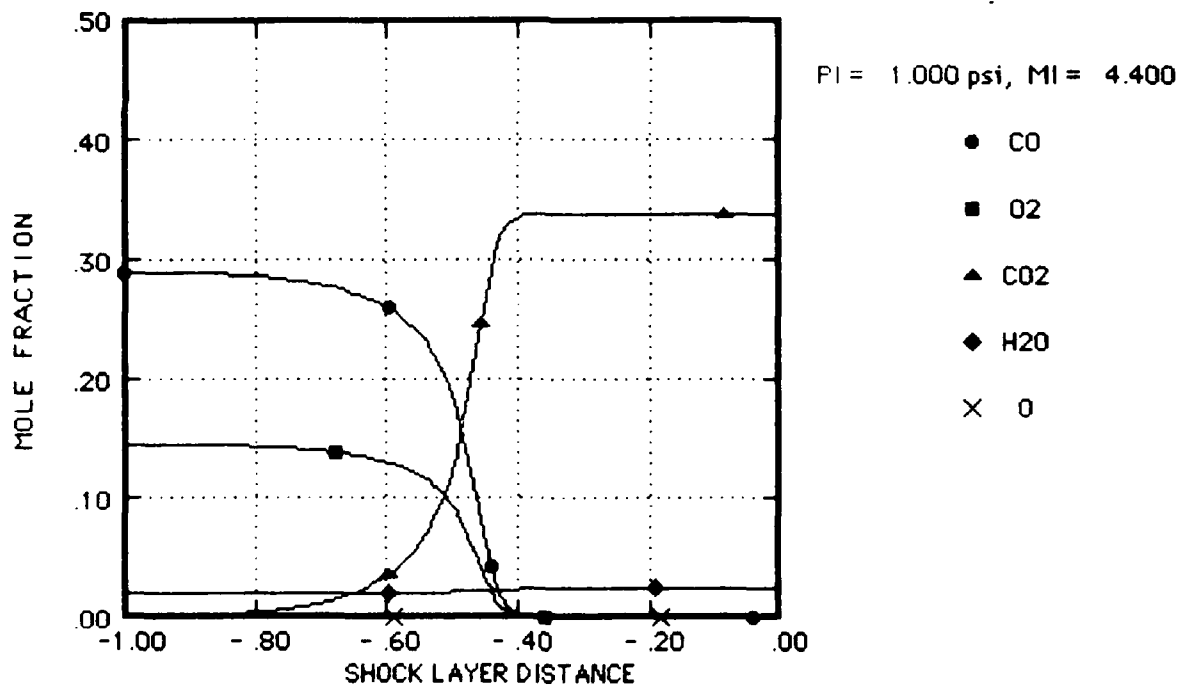
This rather discouraging result is evidenced by the results presented in Figures 22 and 23 below. Figure 22.a and b present the reactive species distributions in the supply tube for $P_i = 1$ psi and $M_i = 3.6$ and 3.8 respectively. These apply to a reactive fluid particle in the supply tube in the same manner as described for oxygen dissociation in Section 3. The results show that the longest lived fluid particle in the supply tube is just beginning to react at the very last instant of its travel in the tube for a shock Mach number of 3.6 (Figure 22.a). At a shock Mach number of 3.8 the supply gas is fully reacted during the last 20% of the supply. For illustration purposes the $M_i = 3.6$ condition is defined as the incipient supply tube reactivity condition.

This parameter was mapped out for a range of conditions relative to the CO-Air operating map and the results are presented in Figure 23 which repeats the $D_N = 12$ inch operating map of Figure 21 with the addition of the supply tube reactivity curve. Figure 23 shows that for all test conditions to the right of the "supply tube reactivity" curve the supply gas would be reacted and to the left it would be unreacted, as suggested on the figure. Thus for test conditions throughout the interesting nonequilibrium shock layer region, the supply gas would be fully reacted for at least a portion of the test duration. That is, early on in the test the gas mixture reaching the test section would be unreacted but later in the test the gas mixture would be the fully reacted products of combustion. As M_i is increased to the right of the incipient reactivity curve, the test section gas mixture would be unreacted for a smaller fraction of the total test time. Since the test time is relatively long compared to the test in air, a reduced duration test could be salvaged in part. However, additional calculations indicate that only a small portion of the nonequilibrium CO-Air regime would provide a possible test at reduced test time conditions. Thus, although feasible, it would not be a very robust nonequilibrium chemistry test.

It has already been noted that increased test model size shifts the nonequilibrium reaction regime to lower shock Mach numbers (compare Figure 21 for $D_N = 12$ inch vs Figure 20 for $D_N = 1$ inch) and thus to less reactive supply tube conditions. However, a model bigger than 12 inch can probably not be accommodated in the Calspan 48 inch shock tunnel. Other test parameters also tend to shift the test regime to the left (lower test section Mach number) or the reactivity curve to the right (shorter supply tube) and these have also been investigated, but they provide only marginal improvements in the feasibility of the test. Chemical mixture parameters such as stoichiometry of the CO-Air mixture and the use of additives are more promising and their effects are investigated in some detail in Section 7.

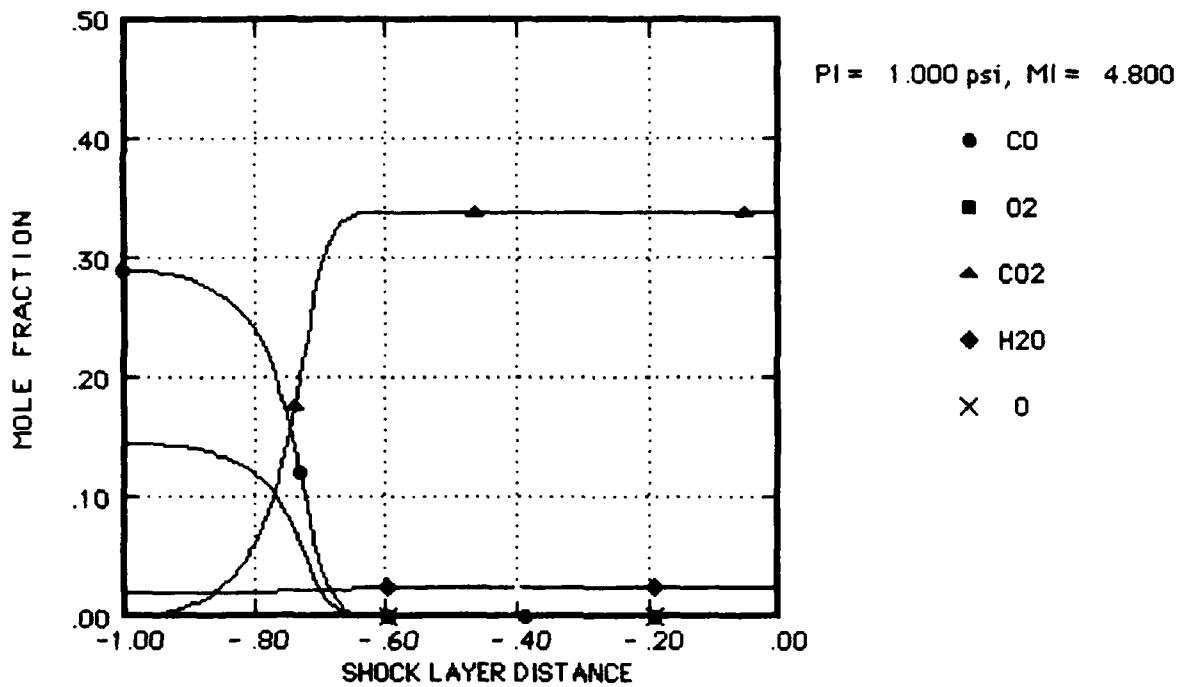


a) Near Frozen, $M_1 = 3.95$



b) Nonequilibrium, $M_1 = 4.4$

Figure 19. CO/Air Reactive Species Distribution Through Stagnation Region
 Stoichiometric CO/Air, $D_N = 12$ Inch, Initial Pressure = 1 psi
 Test Section $M_\infty \approx 5.3$, density altitude ≈ 125 Kft



c) Near Equilibrium, $M_i = 4.8$

Figure 19. CO/Air Reactive Species Distribution Through Stagnation Region
 (Cont'd) Stoichiometric CO/Air, $D_N = 12$ Inch, Initial Pressure = 1 psi
 Test Section $M_\infty \approx 5.3$, density altitude ≈ 125 Kft

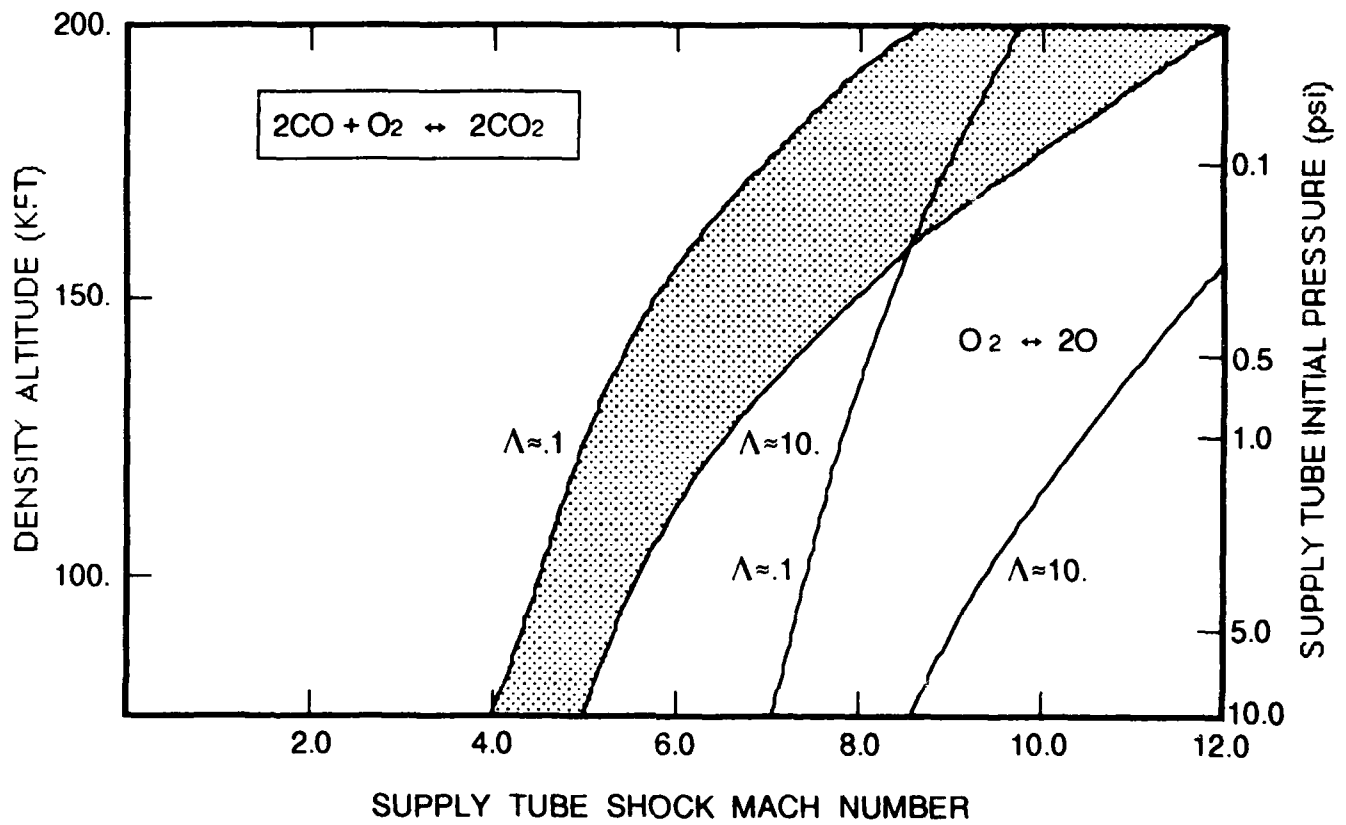


Figure 20. Carbon Monoxide-Air Reactive Flow Shock Tunnel Test Regimes
 Stoichiometric CO/Air; 1. Inch Nose Diameter Test Model
 Test Section Mach Number ≈ 5.3

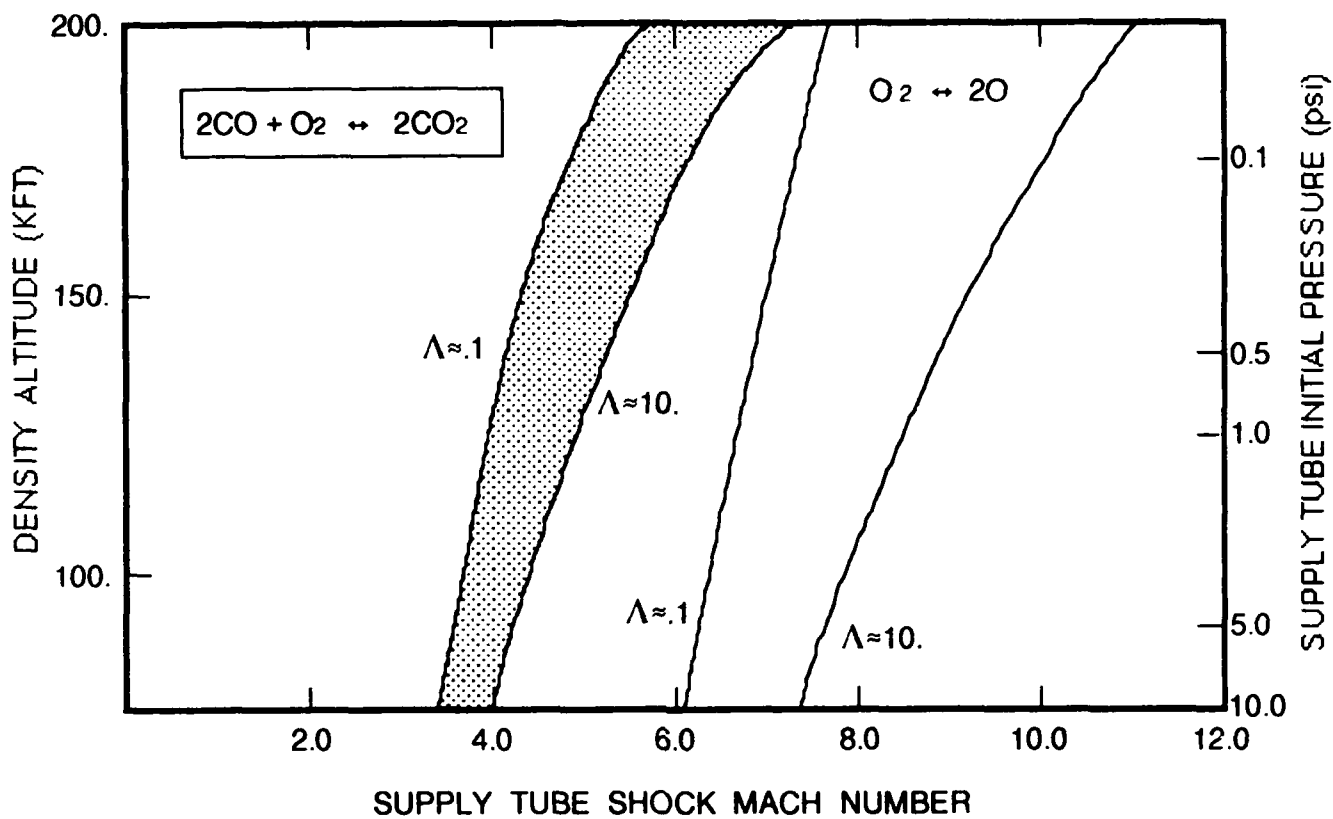
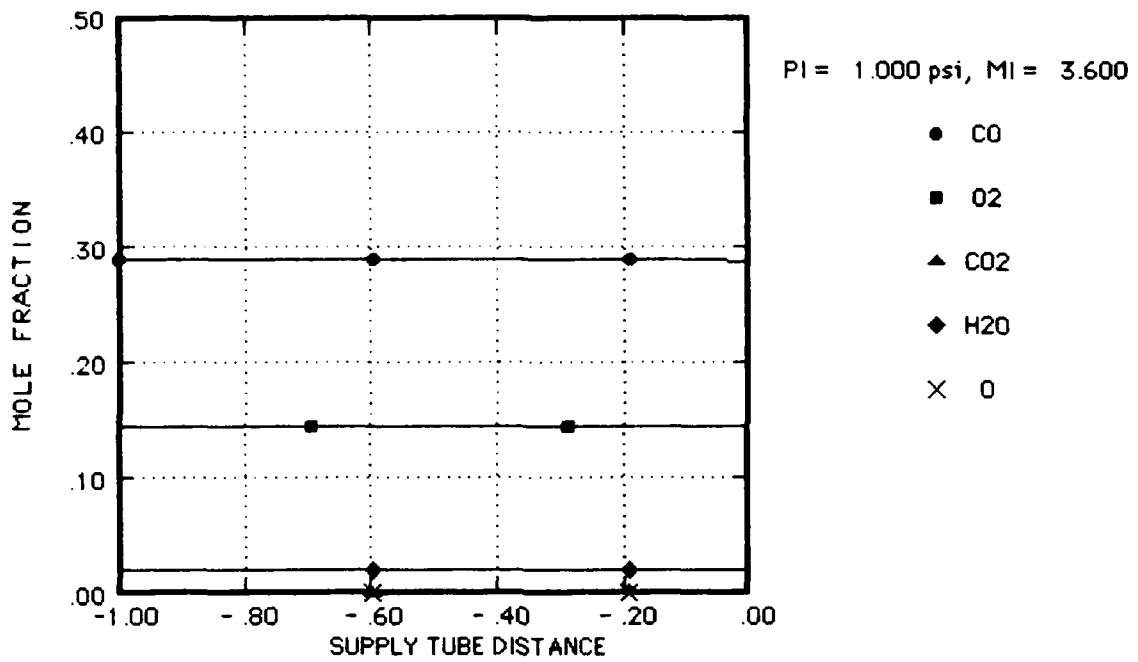
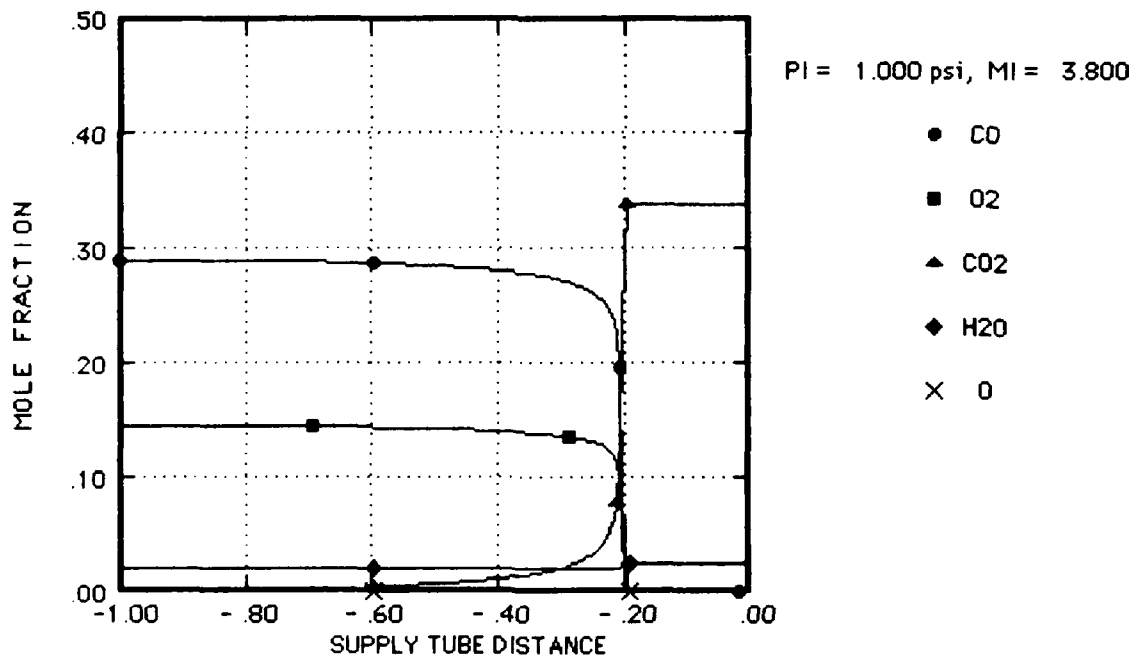


Figure 21. Carbon Monoxide-Air Reactive Flow Shock Tunnel Test Regimes
 Stoichiometric CO/Air; 12. Inch Nose Diameter Test Model
 Test Section Mach Number ≈ 5.3



a) Unreacted, $M_i = 3.6$



b) Reacted, $M_i = 3.8$

Figure 22. CO/Air Reactive Species Distribution Through Supply Tube
Stoichiometric CO/Air, Initial Pressure = 1 psi, Tube Length = 70 Ft

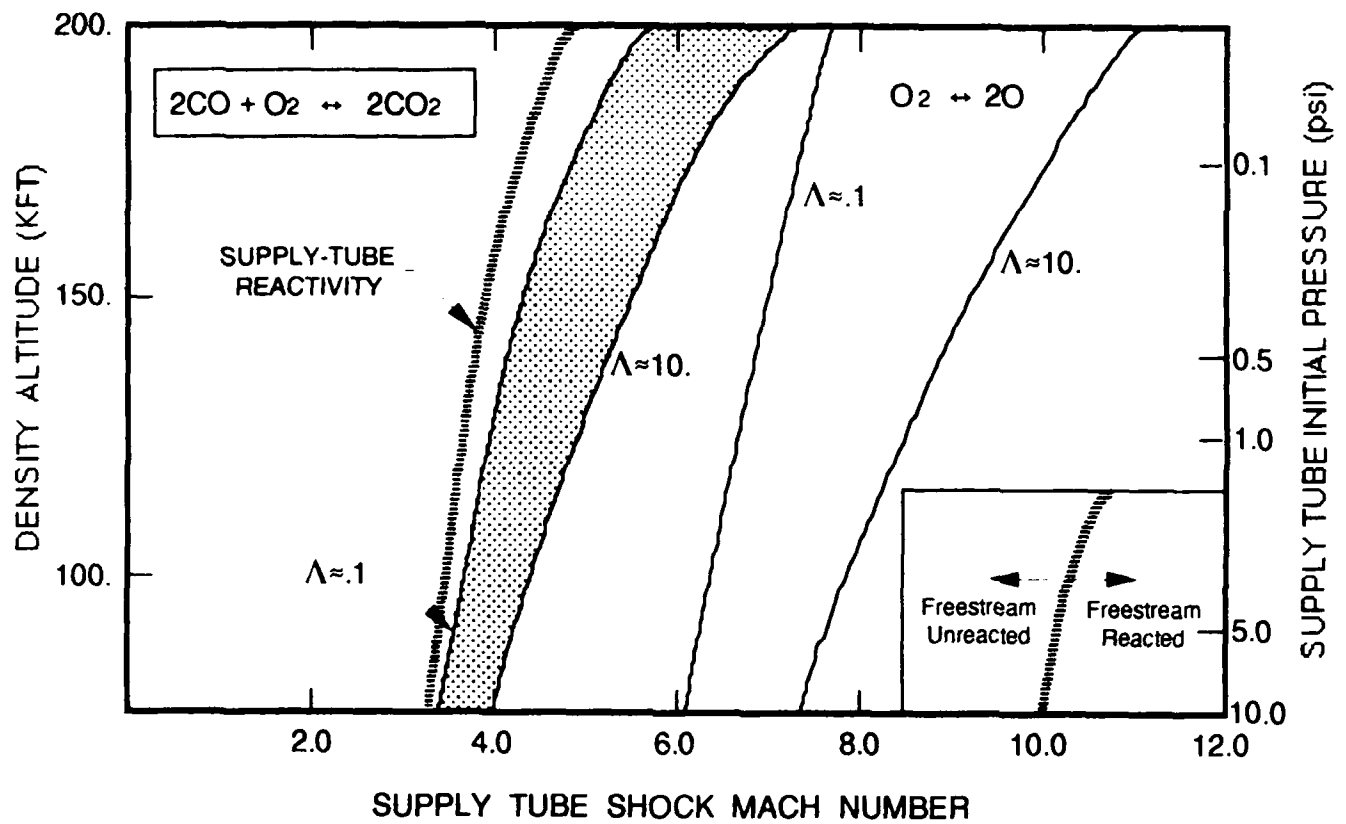


Figure 23. Carbon Monoxide-Air Shock Tunnel Supply Tube Reactivity
 Stoichiometric CO/Air; 12. Inch Nose Diameter Test Model
 Supply Tube Length = 70. Ft

5. PEROXIDE-AIR SIMULANT GAS MIXTURE ANALYSIS

The rapidity of the peroxide decomposition reaction, determined in the gas mixture screening studies, suggests its use as a simulant gas to further reduce shock intensity required to reach nonequilibrium shock layer conditions. Initial estimates indicate that such conditions can be achieved with a shock Mach No. of only 2.3 at one atmosphere initial pressure. This reduction in shock speed results in a significant improvement in test time over the CO-Air mixture for example. Should the supply tube gas remain unreacted—a big if—peroxide would provide a useful simulant gas test medium. The practical possibilities for these speculations are explored in this section.

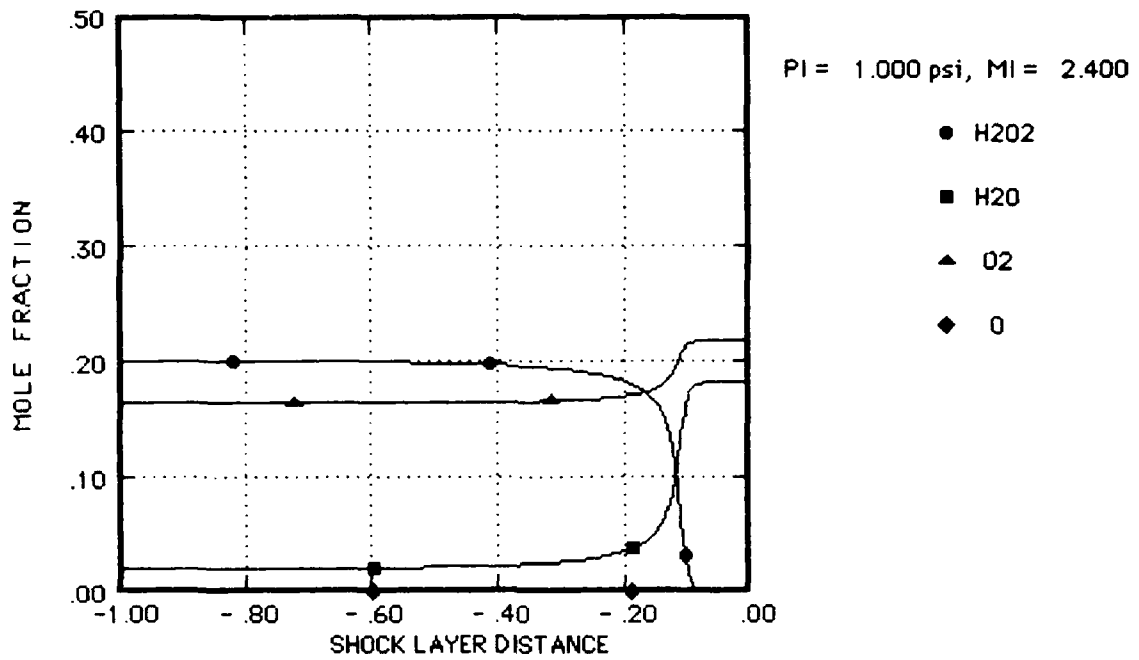
Reactive shock layer streamline and resulting operating map results are presented for peroxide decomposition in Figures 24 through 26 which parallel the CO-Air presentation given above. All results apply for a 20% peroxide-air mixture in the Calspan 48" shock tunnel and a test model scale of 12 Inches. The reactive species distributions along the stagnation streamline, presented in Figure 24, illustrate the shock layer composition for a typical case with 1. psi initial supply tube pressure at near frozen ($M_i = 2.4$, Figure 24.a), nonequilibrium ($M_i = 2.6$, Figure 24.b), and near equilibrium ($M_i = 2.8$, Figure 24.c) conditions. In each case, the relatively narrow reaction zone in which H_2O_2 is converted to O_2 and H_2O is evident. This is reflective of the rapid decomposition reaction which was preceded by the radical specie production during the induction period.

The combination of a number of such calculations into a peroxide simulant gas test operating map is shown in Figure 25 along with the contrasting results for carbon monoxide combustion and oxygen dissociation. As before the shaded region defines the nonequilibrium shock layer reaction regime for the H_2O_2 -Air mixture. The significant reduction in supply tube shock intensity required to achieve nonequilibrium conditions in peroxide relative to carbon monoxide and air respectively is immediately evident from the figure. For the range of supply tube pressures, or effective density altitudes considered, shock Mach numbers of only 2 to 3 are sufficient whereas carbon monoxide requires Mach numbers of 4 to 6 and oxygen dissociation 6 to 10. Should these test conditions be achievable, estimates indicate that test times would be in the whopping 6. to 10. msec range, depending on initial pressure, due to the relatively slow wave speeds. Figure 25 also indicates that the H_2O_2 -Air system has a relatively narrow transition region, i.e. a relatively sudden transition from unreacted or frozen conditions to fully reacted or equilibrium conditions, as M_i is increased in this range. It covers less than a .5 shock Mach number range at $P_i = 10$. psi and a Mach number

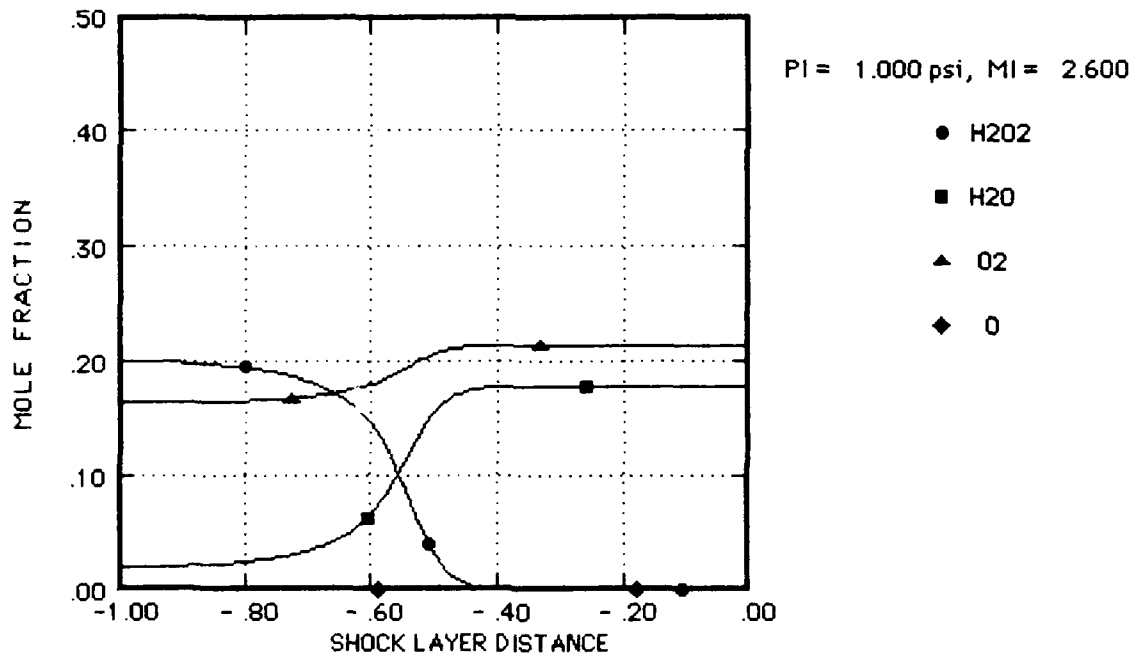
difference of about 1. at .02 psi, the lowest pressure considered. Thus testing in the nonequilibrium reaction regime would be difficult and subject to experimental variability.

These speculations become moot however upon investigating the reactivity of the supply tube for peroxide mixtures. As with the CO-Air mixture, the peroxide-Air mixture considered here is found to react in the supply tube before reaching the test section for the nonequilibrium conditions of interest. Results of supply tube reactive streamline calculations are presented in Figure 26 as the supply tube reactivity line which, as before, denotes conditions for which peroxide will react in the supply gas; to the right of the crosshatched curve the supply gas will be reacted and to the left it will remain unreacted throughout the test time. Figure 26 indicates that this incipient supply gas reaction condition follows the near frozen flow ($\Lambda = .1$) boundary of the nonequilibrium test regime very closely. For pressures below about .1 psi it in fact extends into the test regime but not much more than shown in Figure 26. to the lowest pressures investigated ($P_i = .01$ psi).

Thus a marginal simulant gas test would be feasible for peroxide. Allowing for a fully reacted supply gas late in the test, nonequilibrium simulant gas test conditions could be devised near the frozen flow boundary but a full suite of test conditions from frozen to equilibrium shock layer conditions is not possible. As a result of these studies, it is more likely that peroxide will be useful as an additive to control other reactive systems such as CO-Air and that possibility is investigated in Section 7.

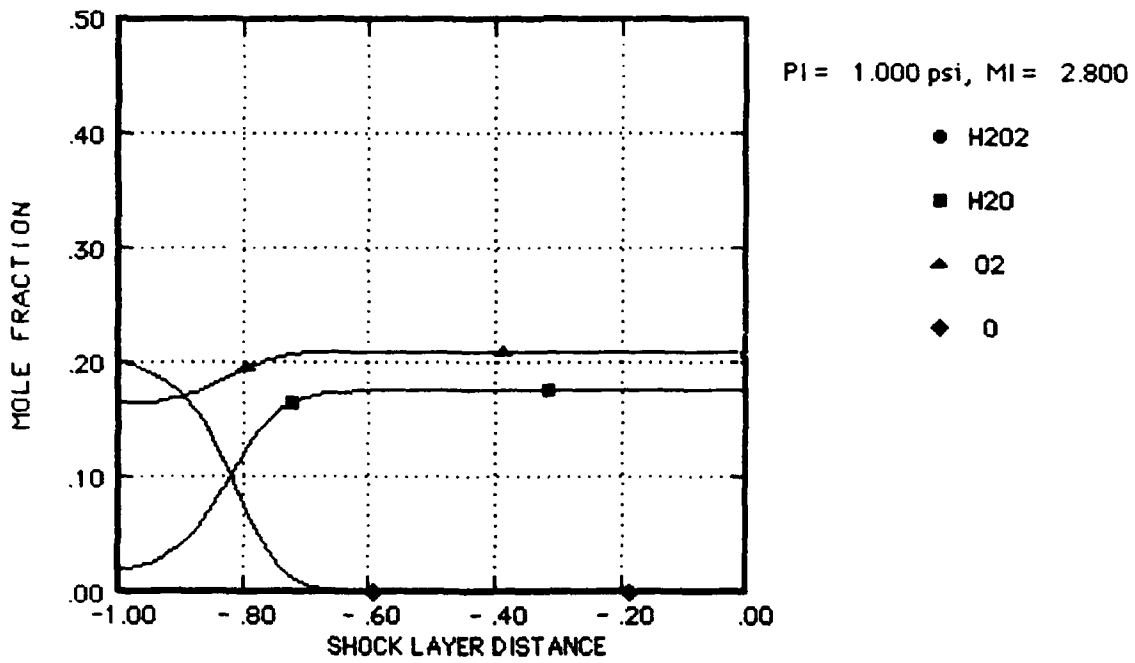


a) Near Frozen, $M_i = 2.4$



b) Nonequilibrium, $M_i = 2.6$

Figure 24. H_2O_2 /Air Reactive Species Distribution Through Stagnation Region
 20% H_2O_2 in Air, $D_N = 12$ Inch, Initial Pressure = 1 psi
 Test Section $M_\infty \approx 4.8$, density altitude ≈ 125 Kft



c) Near Equilibrium, $M_i = 2.8$

Figure 24. H_2O_2 /Air Reactive Species Distribution Through Stagnation Region
 (Cont'd) 20% H_2O_2 in Air, $D_N = 12$ Inch, Initial Pressure = 1 psi
 Test Section $M_\infty \approx 4.8$, density altitude ≈ 125 Kft

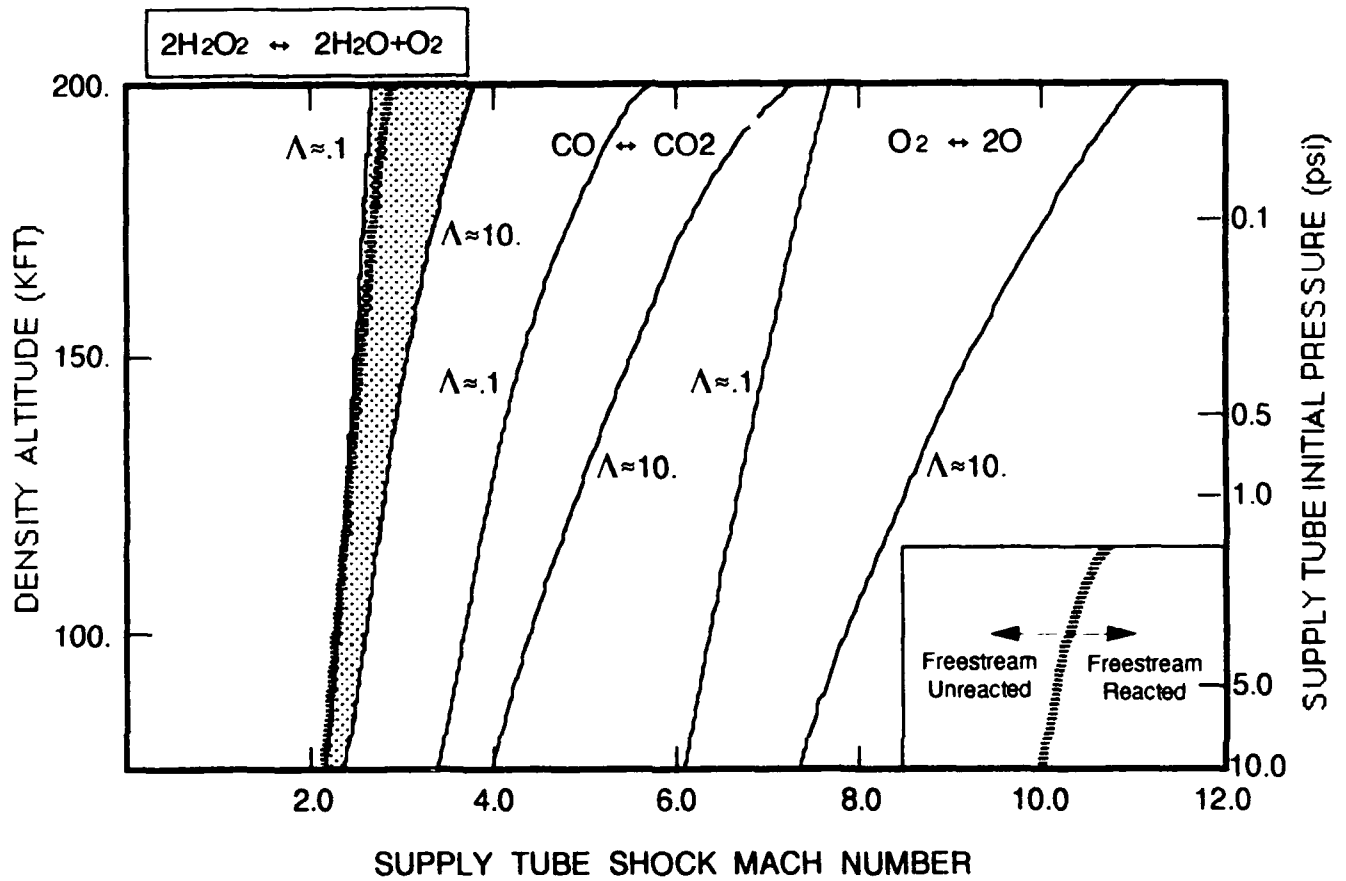


Figure 26. Peroxide-Air Shock Tunnel Supply Tube Reactivity
 20% H₂O₂ in Air; 12. Inch Nose Diameter Test Model
 Test Section Mach Number ≈ 4.8

6. HYDROGEN-AIR SIMULANT GAS MIXTURE ANALYSIS

Hydrogen combustion represents a well documented reactive system with a relatively simple reaction mechanism. Both of these desirable properties motivate its use as a candidate simulant gas since they provide for accurate analyses needed to set test conditions as well as potential experimental results which can be unambiguously compared to numerical model predictions. Estimates indicate that hydrogen requires a shock Mach No. similar to carbon-monoxide to reach the nonequilibrium reaction regime so that benefits similar to the CO-Air test would accrue relative to shock tunnel operation with air. These estimates are refined in this section using the reactive streamline model with the hydrogen reactive system described in Appendix B.

The presentation of results again parallels the CO-Air presentation of Section 4. and includes plots of the hydrogen reactive species distributions along the stagnation streamline in Figure 27 which are used to define the operating regime map presented in Figure 28 and the supply gas reactivity map in Figure 29. All of the results were developed using parameters characteristic of a Calspan scale shock tunnel (48 inch nozzle, 70 ft supply tube, model scale with $D_N = 12$ inch) and a stoichiometric hydrogen-air mixture.

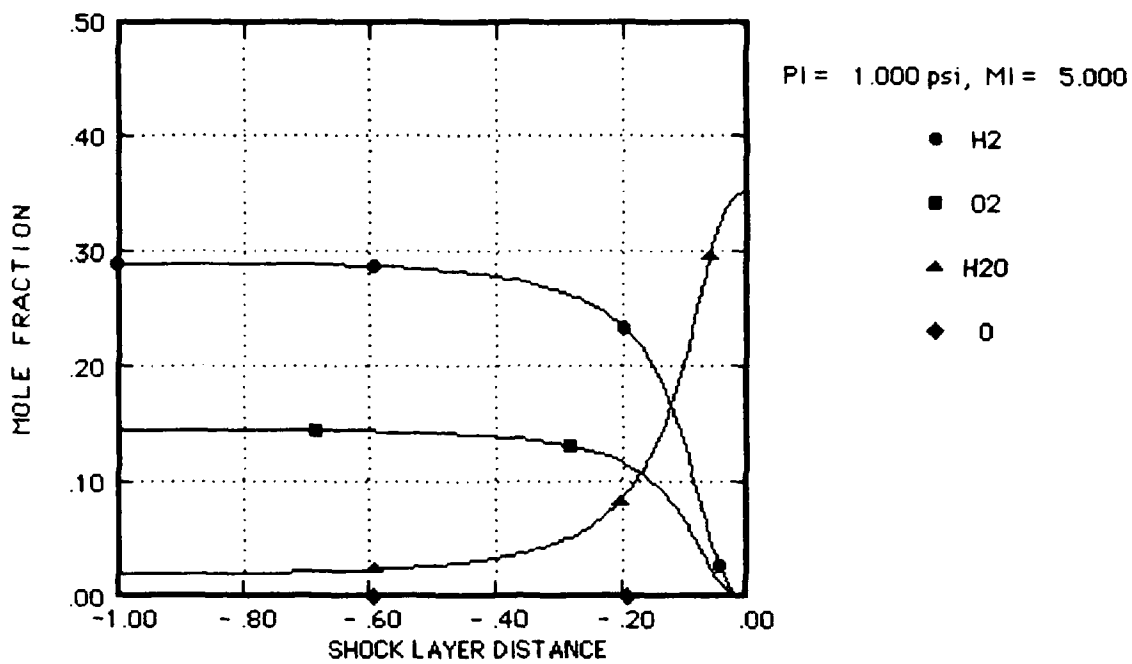
Figure 27 presents the principal reactant specie distributions for hydrogen combustion along the stagnation streamline of a 12 inch nose diameter model at typical 1. psi initial supply tube pressure conditions. The distributions extend from the case classified as near frozen reaction conditions (for $M_i = 5.$) in Figure 27.a, through nonequilibrium conditions (for $M_i = 6.$) in Figure 27.b to near equilibrium conditions (for $M_i = 7.$) in Figure 27.c. The figures show the combustion of H_2 and O_2 to H_2O in the combustion zone ignoring the trace quantities of radicals in the important induction zone upstream of the "flamezone". The reaction zone is seen to be wider for hydrogen than carbon-monoxide (see Figure 19) and peroxide (Figure 24) reflecting the generally lower reaction rates. At the highest shock Mach number conditions, $M_i = 6.$ and $M_i = 7.$, Figure 27.b and c, show that some of the oxygen is dissociated before it can fully react with hydrogen. This suggests the possibility of utilizing lean mixtures of fuel-air to induce oxygen dissociation at lower shock Mach numbers than air and this concept will be investigated in Section 7. for carbon-monoxide-air mixtures.

The shock layer results were combined to map out conditions for a nonequilibrium test regime and the results are presented in the shock tunnel operating map contained in Figure 28. The figure presents the nonequilibrium hydrogen reaction regime as the shaded

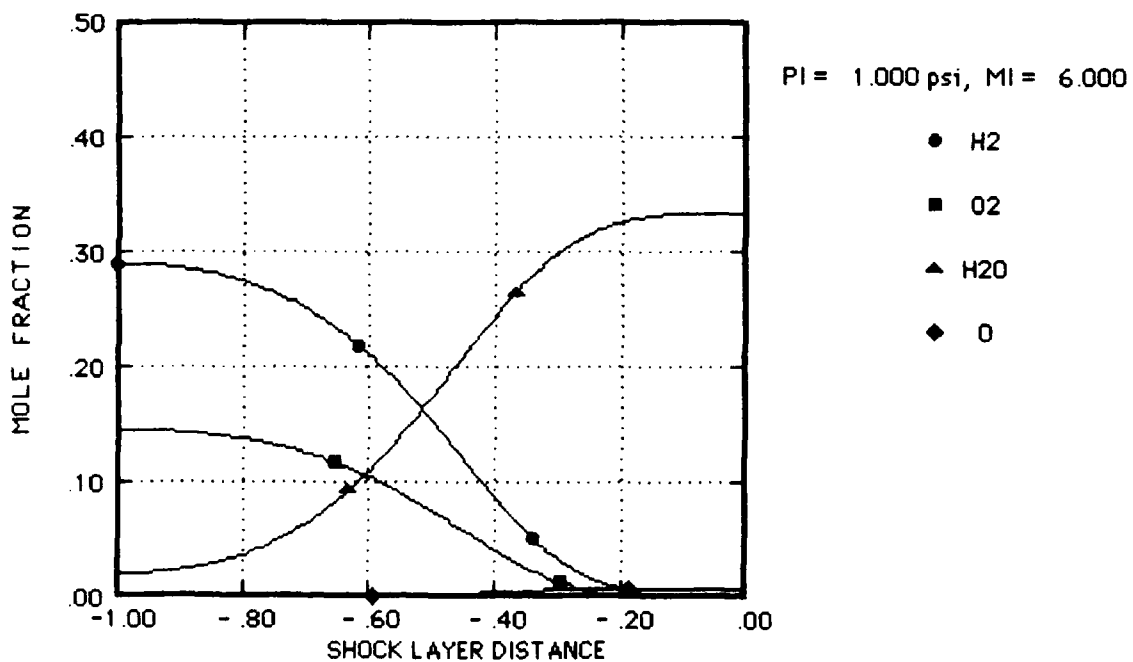
region between the near frozen, $\Lambda = .1$, and near equilibrium, $\Lambda=10$. lines and compares it to the corresponding regime for the CO-Air reaction and O_2 dissociation. The results show that hydrogen straddles the test regimes for the other mixtures and overlaps at the lowest pressures considered. For hydrogen, the nonequilibrium regime extends from $M_i = 4$ to 5 at $P_i = 10$. psi and expands to $6. < M_i < 11$. at about $P_i = .02$ psi. Figure 28 shows that hydrogen is less reactive than carbon-monoxide for this application and under the low pressure conditions does not have much of an advantage over oxygen dissociation in air.

Examination of the supply tube reactivity for hydrogen shows that it is susceptible to the same problem as carbon-monoxide and peroxide only more so. Figure 29 presents the supply tube reactivity curve for stoichiometric hydrogen air and compares it to the corresponding shock layer reaction regime just discussed. As is evident, the supply gas is likely to be fully reacted at shock Mach numbers less than those needed to attain reactions in the shock layer of the 12 inch test model. In the present case, the results suggest that the incipient reactivity curve may extend into the nonequilibrium regime at supply pressures greater than atmospheric. The benefits are likely to be marginal however and higher pressures were not investigated further.

The present results indicate that the use of hydrogen as a simulant gas does not seem feasible for the same reason that the other combustible gas mixtures result in marginal simulant gas tests. It seems likely that hydrogen will be more useful as an additive to replace undesirable water vapor in the carbon-monoxide-air mixture rather than as an H_2 -air simulant gas system.

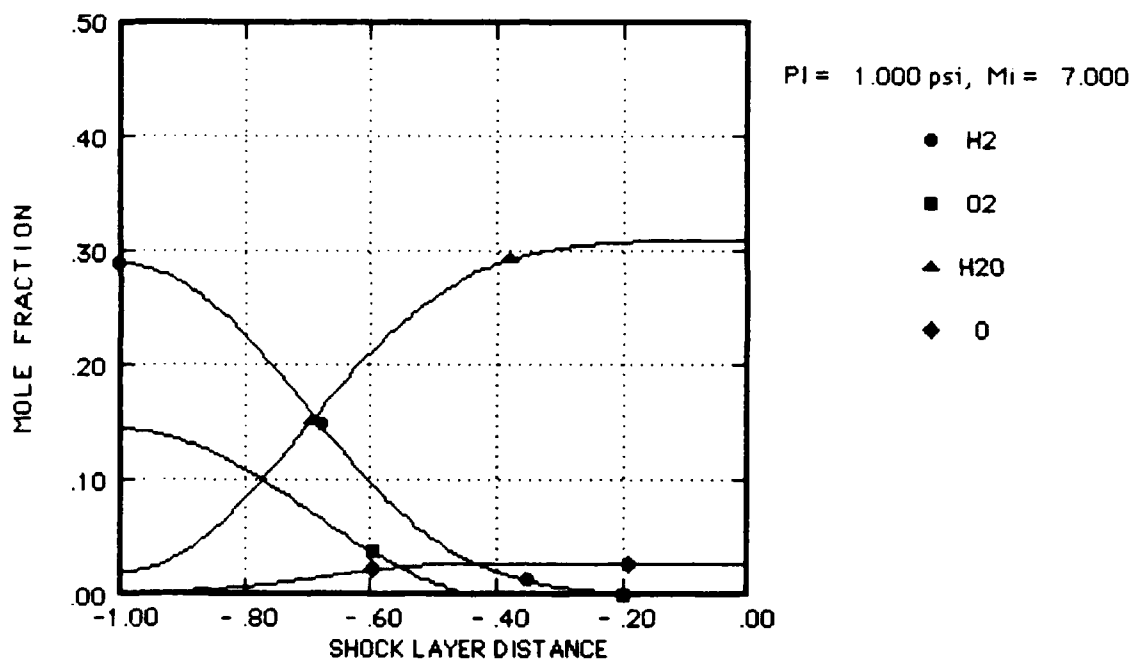


a) Near Frozen, $M_i = 5.0$



b) Nonequilibrium, $M_i = 6.0$

Figure 27. H_2 /Air Reactive Species Distribution Through Stagnation Region
 Stoichiometric H_2 /Air, $D_N = 12$ Inch, Initial Pressure = 1 psi
 Test Section $M_\infty \approx 5.3$, density altitude ≈ 125 Kft



c) Near Equilibrium, $M_i = 7.0$

Figure 27. H_2 /Air Reactive Species Distribution Through Stagnation Region
 (Cont'd) Stoichiometric H_2 /Air, $D_N = 12$ Inch, Initial Pressure = 1 psi
 Test Section $M_\infty \approx 5.3$, density altitude ≈ 125 Kft

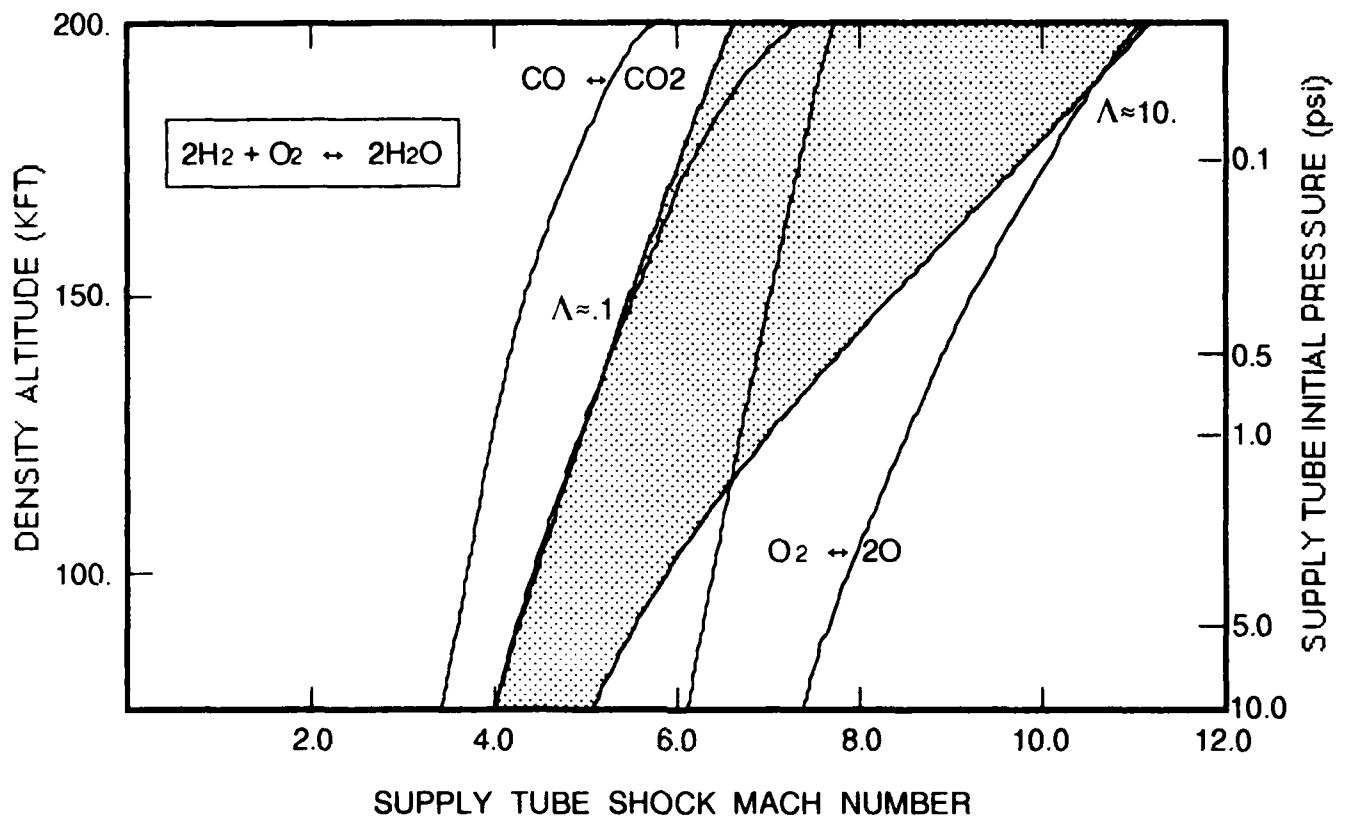


Figure 28. Hydrogen-Air Reactive Flow Shock Tunnel Test Regimes
 Stoichiometric H₂/Air; 12. Inch Nose Diameter Test Model
 Test Section Mach Number ≈ 5.3

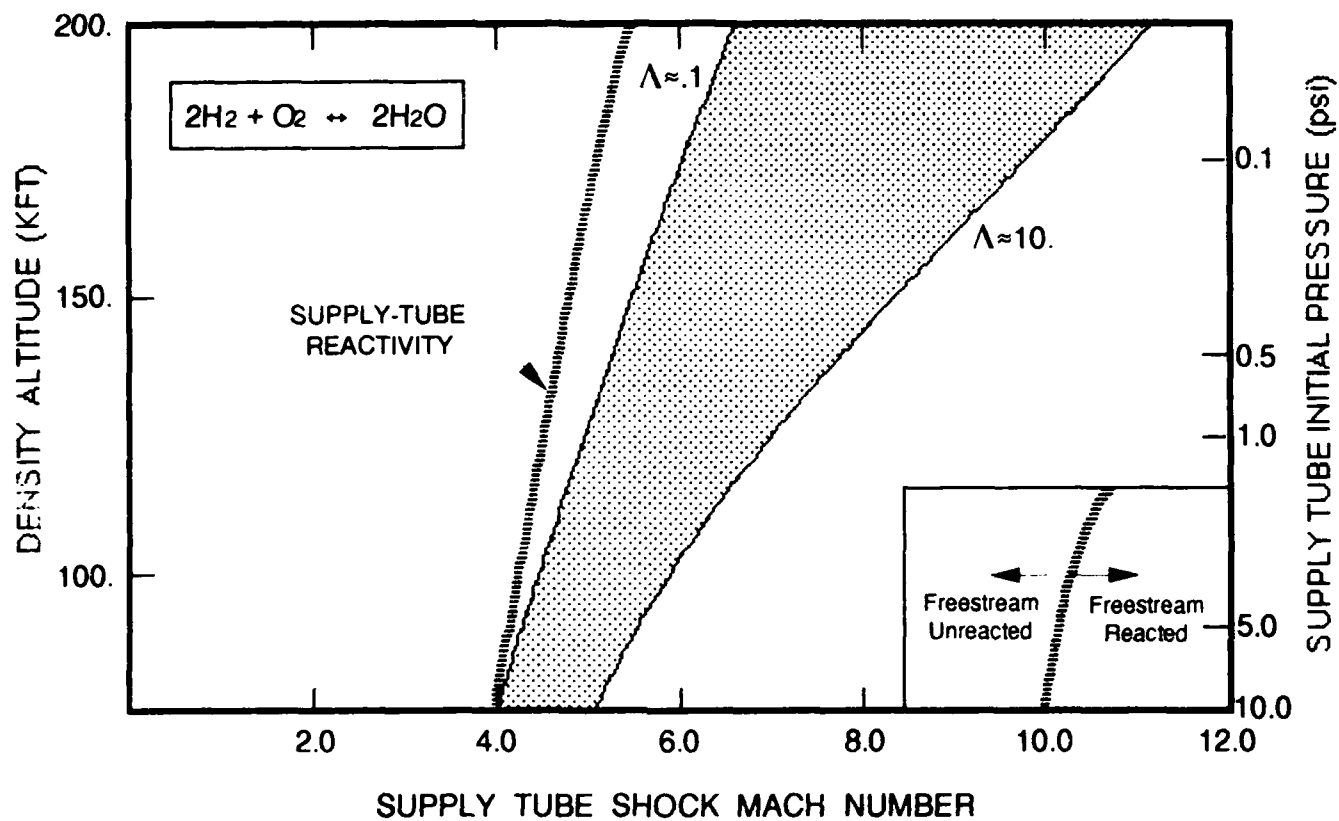


Figure 29. Hydrogen-Air Reactive Flow Shock Tunnel Supply Tube Reactivity
 Stoichiometric H₂/Air; 12. Inch Nose Diameter Test Model
 Test Section Mach Number ≈ 5.3

7. CARBON MONOXIDE-AIR SENSITIVITY STUDIES

The simulant gas results to this point are somewhat disappointing due to the inability to achieve an unreacted freestream flow at reactive shock layer test conditions; ironically the same problem that the simulant gas technique is designed to remedy. However the technique remains intriguing since under some conditions it is borderline possible. This is especially true of the carbon-monoxide and peroxide mixtures so that two features of these mixtures are explored further in this section: CO/Air stoichiometry and the use of H₂O₂ additive in a CO/Air mixture.

Stoichiometry or mixture ratio (Φ is the ratio of the actual moles of reactant to the moles of reactant for an ideal reaction) has the effect of diluting the reactant system thus lowering the shock layer temperature and lowering overall reaction rates while providing a more air-like distributed reaction zone. Since the global reaction rate for the mixtures considered here is dominated by the radical specie generation rate, Φ should have a minor effect on the operating parameters defining the nonequilibrium regime. However, in the interest of completeness, the potential for a nonlinear effect which could improve the shock layer vs supply tube reactivity is worth investigating and results of such a study are presented in Figure 30.

The results shown in Figure 30 apply for the representative case of CO/Air at an initial supply tube pressure of 1. psi and a model scale of 12 inches. The curves in the figure show the effect of stoichiometry on the shock Mach number for i) incipient supply tube reaction, ii) the beginning of the nonequilibrium shock layer regime ($\Lambda = .1$) and iii) the achievement of near equilibrium shock layer conditions ($\Lambda = 10.$). The results for $\Phi = 1.$ are the same as those presented in Section 4. The results for lean mixtures ($\Phi < 1.$) and rich mixtures ($\Phi > 1.$) verify the speculation above that off stoichiometric mixtures are less reactive and hence require a more intense shock to initiate reactions. Also the rather small variation in all curves over the range of $0. < \Phi < 1.5$ indicates the dominance of the radical generation rate in the overall reactivity of the mixture. The conditions between $\Lambda = .1$ and $\Lambda = 10.$ define the nonequilibrium regime and it is clear from Figure 30 that the incipient supply tube reactivity curve parallels and remains below the conditions for shock layer reaction for all stoichiometries considered. Thus the stoichiometric ratio of the CO-Air mixture does not improve the possibilities for a successful simulant gas test. It is likely that a similar conclusion would apply to the peroxide and hydrogen reactive systems.

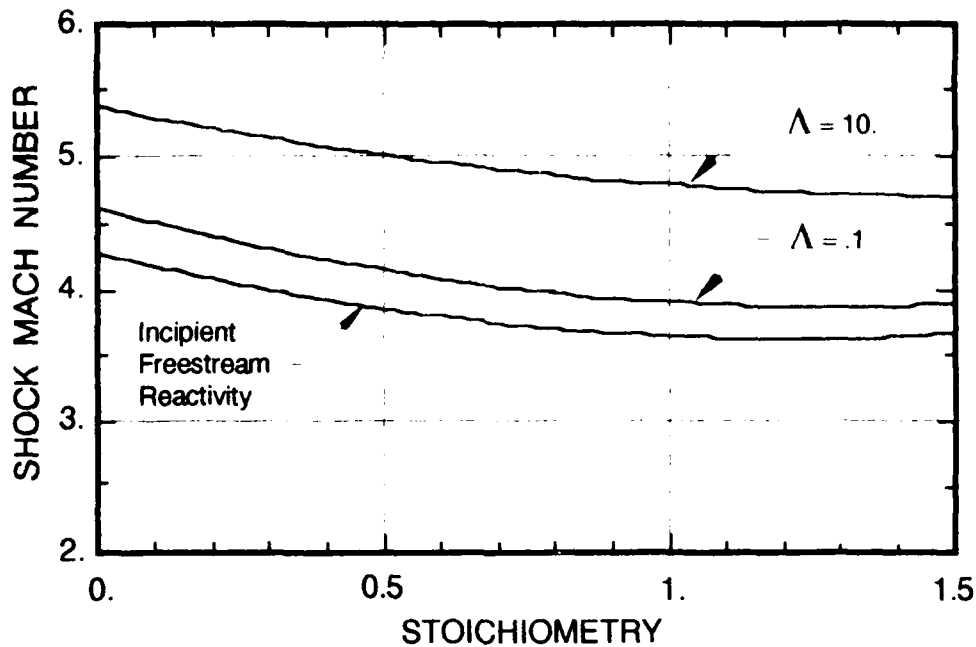
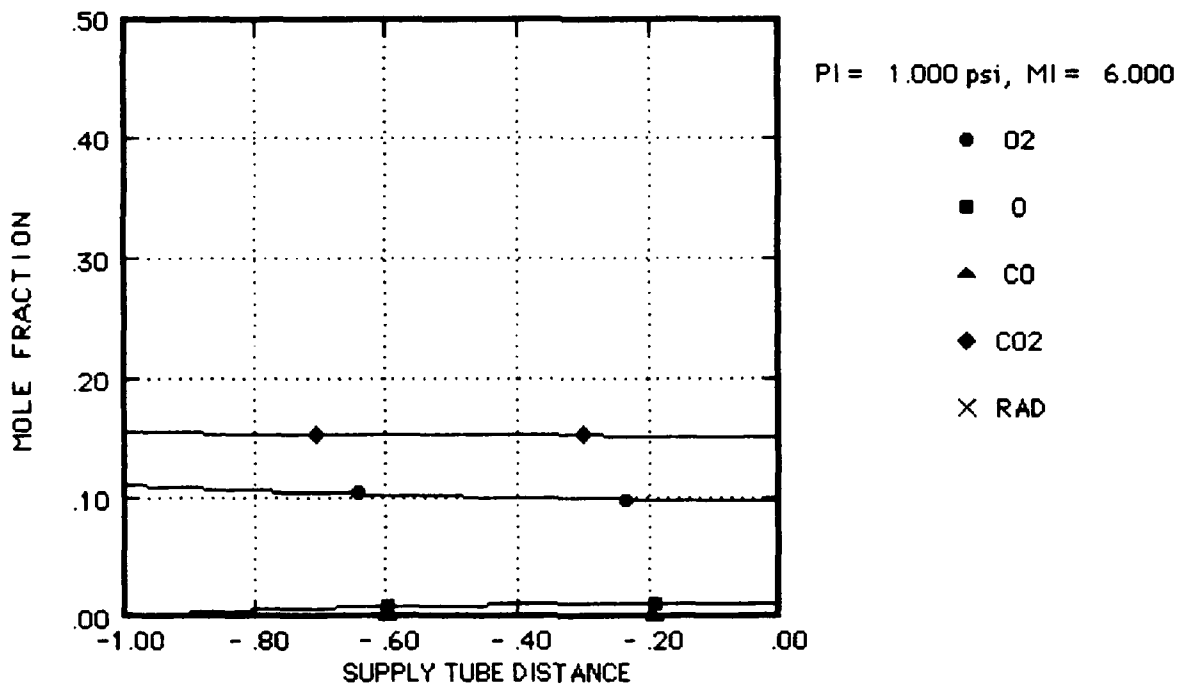
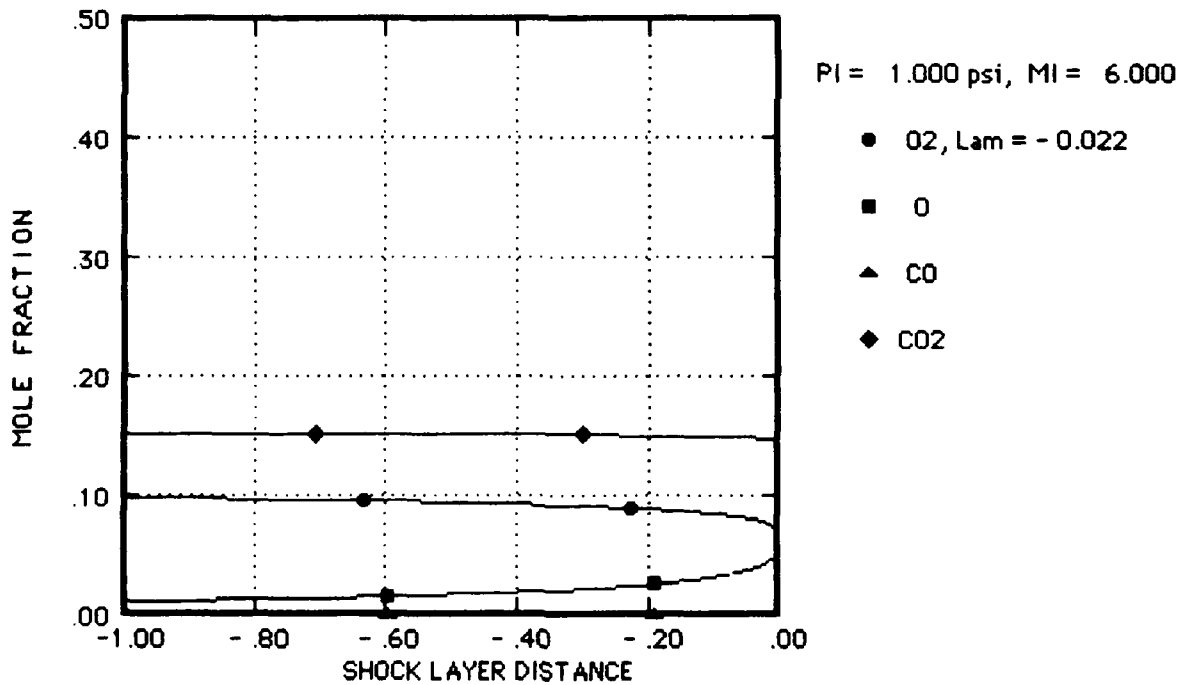


Figure 30. Effect of Stoichiometry on CO/Air Shock Tunnel Test Regimes Carbon-monoxide/Air Mixture at 1. psi Supply Tube Pressure 12. Inch Nose Dia. Test Model, Test Section Mach No. ≈ 5.3

Although unsuccessful, the stoichiometry results present the possibility of another test method. That is to use lean combustible mixtures, CO/Air for example, which react completely in the supply tube but raise the subsequent shock layer temperatures enough to induce oxygen dissociation at lower shock Mach numbers than pure air. Results for such an approach are presented in Figures 31 and 32 for a CO/Air mixture with $\Phi = .5$, $D_N = 12$. inch and $P_i = 1$. psi. Figure 31 presents species distributions in the supply tube (Figure 31.a) and shock layer (Figure 31.b) for an initial shock Mach number, $M_i = 6$.; Figure 32 provides corresponding results for $M_i = 7$. Figure 31.a shows that the CO reacts very fast at the supply tube conditions leaving about 11% residual oxygen which proceeds to dissociate slightly (by about 10%) as it passes through the supply tube. Upon reaching the model shock layer, Figure 31.b shows that the oxygen dissociates only very near the stagnation point, and represents a near frozen shock layer flow condition. At a somewhat higher shock Mach number, $M_i = 7$ presented in Figure 32, the residual oxygen dissociates somewhat more ($\approx 20\%$) in the supply tube and achieves a nonequilibrium oxygen dissociation condition in the model shock layer. These results represent only a marginal improvement over oxygen dissociation in air (see Section 3.) in terms of a slightly decreased freestream flow degree of dissociation and a slightly increased test time.



a) Supply Tube, L = 70 ft



b) Model Shock Layer, $D_N = 12$ inch

Figure 31. CO/Air Reactive Species Distribution at Near Frozen O₂ Dissociation Conditions: CO/Air at Stoichiometry Ratio = .5 Initial Pressure = 1. psi, Shock Mach Number = 6.0

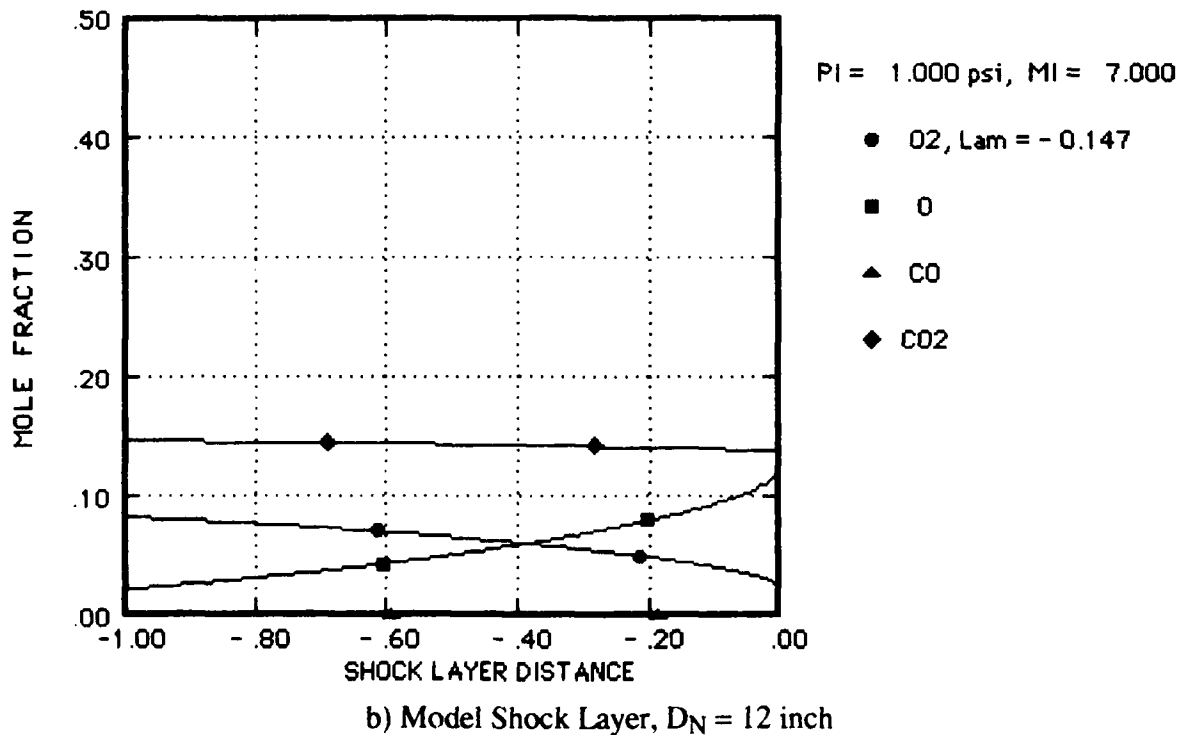
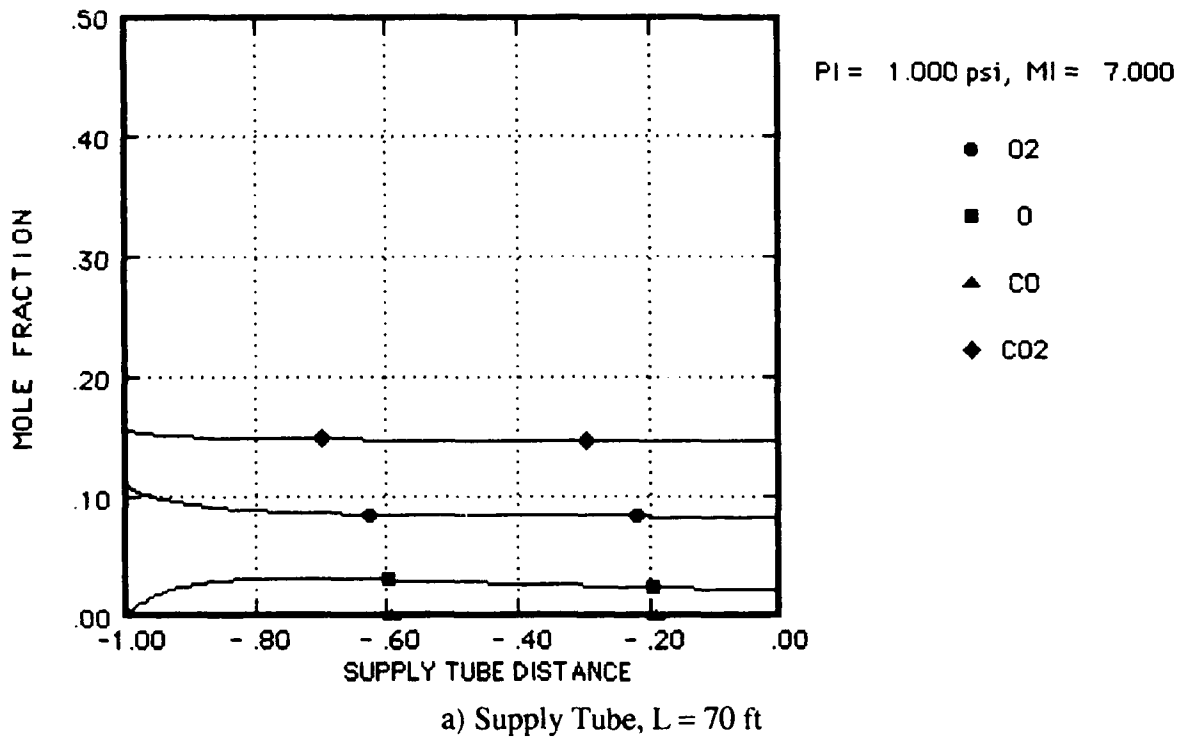


Figure 32. CO/Air Reactive Species Distribution at Nonequilibrium O₂ Dissociation Conditions: CO/Air at Stoichiometry Ratio = .5 Initial Pressure = 1. psi, Shock Mach Number = 7.0

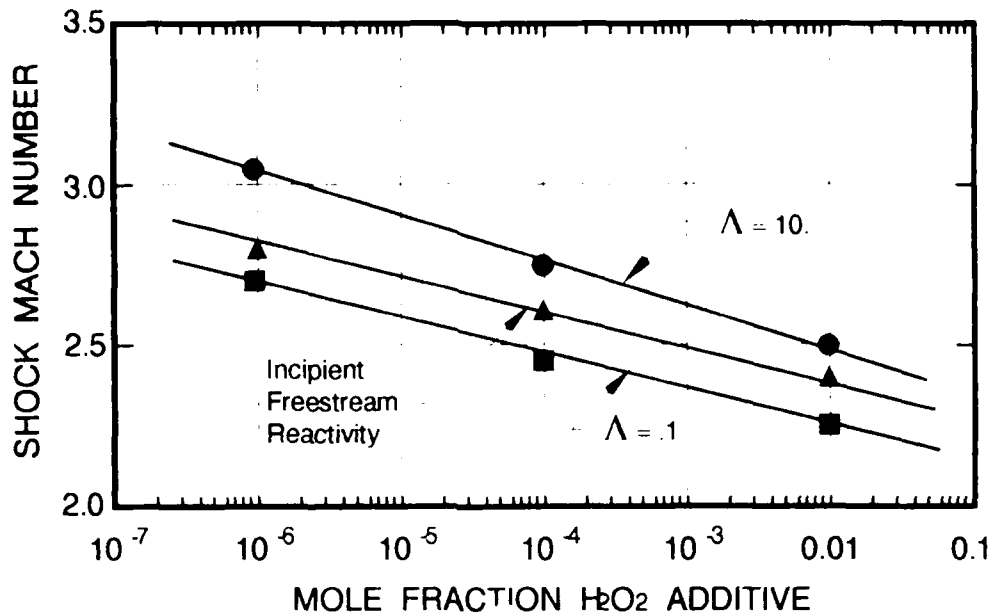


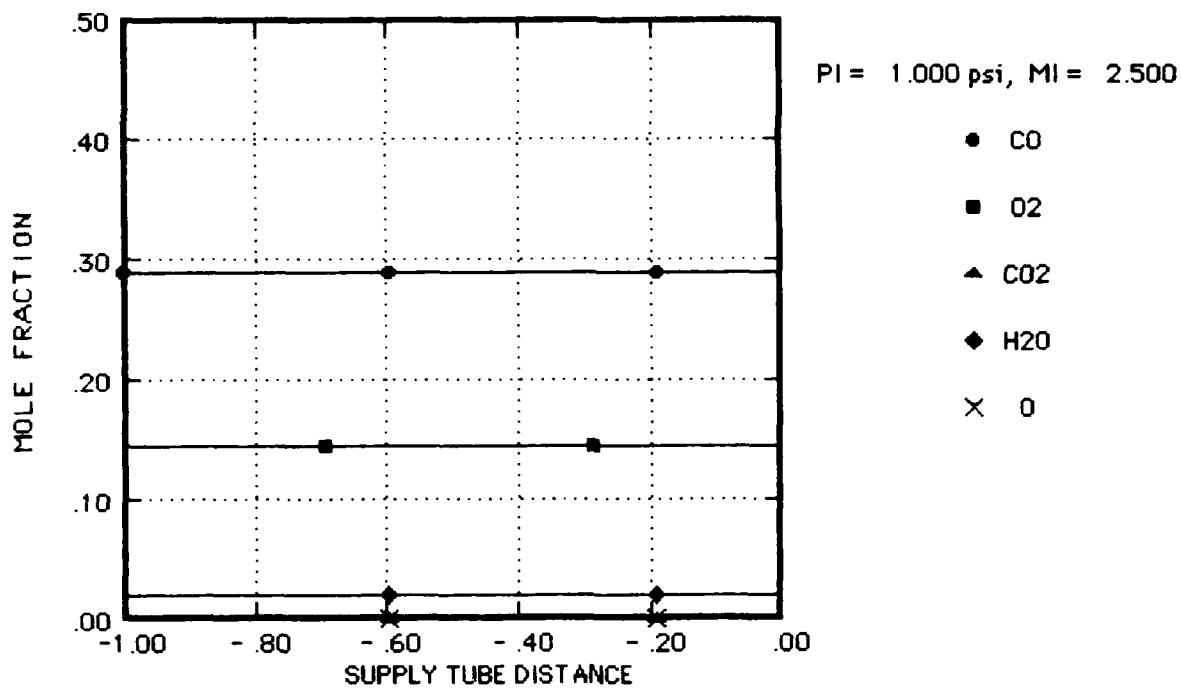
Figure 33. Effect of Peroxide on CO/Air Shock Tunnel Test Regimes Stoichiometric CO/Air at 1. psi Supply Tube Pressure 12. Inch Nose Dia. Test Model, Test Section Mach No. \approx 5.

As suggested earlier, the use of hydrogen and peroxide additives in the carbon monoxide-air mixture have the potential benefits of producing a more controllable and repeatable reaction and in the case of H₂O₂ of significantly increasing the reactivity of the mixture. The CO-Air reaction, for example, is sensitive to trace amounts of water vapor and adding hydrogen while reducing the unavoidable presence of water vapor will provide more control over the reaction. All of the reactive streamline simulations presented in Section 4 utilized 2% H₂O in the mixture since that represents a reasonable 80% humidity condition. Simulations using 2% H₂ instead of the water vapor result in negligible differences for selected test cases. On the other hand adding trace amounts of H₂O₂ to the CO-Air mixture provides a mechanism for reducing the shock intensity needed to achieve nonequilibrium shock layer conditions. The rapid H₂O₂ decomposition reaction can enhance the rate of radical buildup and as a result increase the overall rate of CO combustion.

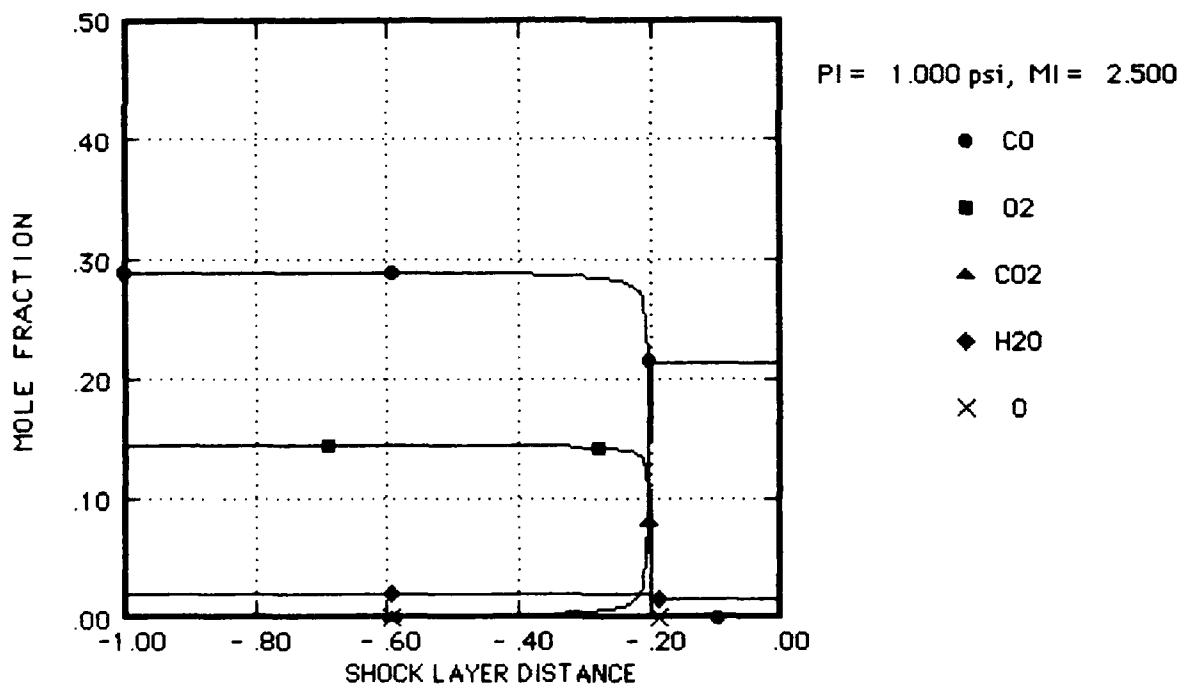
Figure 33 above presents results for the effect of small amounts of H₂O₂ on the reactivity of the supply tube and model shock layer for a stoichiometric CO-Air mixture with initial supply tube pressure of 1. psi and a model scale of 12 inches. The figure indicates that even trace amounts of peroxide (less than one part per million, ppm) significantly increases the reactivity of the CO-Air mixture and reduces the shock Mach number required to initiate

shock layer reactions ($.1 < \Lambda < 10$. curves on the figure). The degree of improvement in reactivity is not very sensitive to the amount of peroxide as long as some is present in the mixture. The most important result for the simulant gas test method is that the supply tube remains unreacted for at least a portion of the nonequilibrium regime, i.e. the curve for incipient supply tube reactivity is above (higher M_i) the $\Lambda = .1$ curve. These results still don't provide a robust simulant gas test, which would be provided if the curve of incipient supply gas reactivity were above the $\Lambda = 10$. curve as well, but they at least indicate a degree of potential for the technique.

The method is illustrated in Figure 34 which provides the reactive species distributions in the supply gas (34.a) and the model shock layer (34.b) for the following conditions: stoichiometric CO-Air with 100 ppm H_2O_2 , $P_i = 1$. psi, $M_i = 2.5$ and a 12 Inch nose diameter model. The distributions verify that the supply gas remains unreacted at these conditions while the model shock layer reacts at something approaching fully nonequilibrium rates. The shock Mach number could be increased to 2.6 say to simulate a more reactive shock layer while retaining a clean unreacted freestream, but any further increase to achieve near equilibrium conditions would result in a fully reacted freestream flow. Thus the approach is promising but does not attain the robustness needed for a successful simulant gas test.



a) Supply Tube, L = 70 ft



b) Model Shock Layer, D_N = 12 inch

Figure 34. CO/Air Reactive Species Distribution at Nonequilibrium CO Reaction Conditions: Stoichiometric CO/Air + 10^{-4} H₂O₂ Initial Pressure = 1. psi, Shock Mach Number = 2.5

8. CONCLUSIONS AND RECOMMENDATIONS

The feasibility of a proposed concept for a nonequilibrium air chemistry test, referred to as the "Simulant Gas" shock tunnel test, was investigated in the present report. The approach is based on the use of simulant gas mixtures in a shock tunnel operating in the nonreflected shock mode. Simulant gases were sought which would react at lower temperatures than oxygen and which have a relatively well defined "ignition" temperature thereby providing an unreacted freestream flow while reacting at representative rates in the shock layer of a test model placed in the test section of the shock tunnel. The feasibility of the simulant gas test concept has been evaluated by performing reactive flow similitude and reactive streamline flow analyses for a limited range of combustible gas mixtures. The method was illustrated by defining flight regimes (Mach Number, altitude) and baseline shock tunnel test regimes (shock Mach number, initial pressure) in air for which nonequilibrium oxygen dissociation is operative in the vehicle/model shock layer. Corresponding operating regimes were defined for various candidate simulant gases using results of analyses of both the shock tunnel flowfield and test model stagnation region flow. Carbon monoxide, peroxide and hydrogen gas mixtures in air, over a range of stoichiometries and additive combinations, were considered for operation in a large scale shock tunnel such as the Calspan 48 inch hypersonic shock tunnel.

The analyses indicated that the idealized concept of an "ignition temperature" is not very useful for anything more than general screening of reactive mixtures since the present concept is crucially dependent on the fluid particle residence times in the shock tunnel supply gas versus the model shock layer. This disparity of residence times results in an unfortunate precedence for supply gas reactivity over shock layer reactivity which cannot be overcome by the increased temperature (hence reaction rates) of the shock layer. Detailed reactive streamline analyses of both supply gas and model shock layer reactivity lead to the following conclusions:

- A simulant gas test using carbon monoxide, peroxide or hydrogen-air mixtures is not feasible since such mixtures react in the shock tunnel supply tube before a test model shock layer can achieve nonequilibrium reactive flow conditions. More promising but subsidiary results include:
 - a carbon monoxide air mixture with a small amount of peroxide can achieve a marginal test but it may not be practical due to the small domain of permissible operating conditions

- lean carbon monoxide air mixtures can induce oxygen dissociation at reduced supply gas intensities (shock Mach number) but with only marginal improvements over pure air
- conditions are described for a nonequilibrium oxygen dissociation test in air which minimizes freestream dissociation and maximizes test time.

Although the results of the study are overwhelmingly negative, it is believed that shock tunnel testing for air chemistry effects is not without benefit. In particular, the test in air, outlined above, which examines model shock layer response over a suite of test conditions which vary from near frozen to near equilibrium oxygen dissociation conditions, is believed to be a viable, though not completely ideal, test for air chemistry effects. It is also hoped that, at the very least, the present effort has engendered some interest in finite rate chemistry effects testing with both air and alternative gases—a long dormant area of aerodynamic investigation.

REFERENCES

1. Hansen, C.F., "Approximations for the Thermodynamic and Transport Properties of High-Temperature Air," NASA Technical Report R-50, November 1957.
2. Hansen, C.F., Heims, S.P., "A Review of the Thermodynamic, Transport, and Chemical Reaction Rate Properties of High-Temperature Air," NASA Technical Note 4359.
3. Bortner, M.H., "A Review of Rate Constants of Selected Reactions of Interest in Re-Entry Flow Fields in the Atmosphere," National Bureau of Standards Technical Note 484, May 1969.
4. Inouye, M., "Blunt Body Solutions for Spheres and Ellipsoids in Equilibrium Gas Mixtures," NASA Technical Note D-2780.
5. Stull, D.R., and H. Prophet, "JANAF Thermochemical Tables," Second Edition, NSRDS-NBS 37, June 1971.
6. Engleman, V., "Methane Combustion Reactions," Combustion and Flame, 1974.
7. Westbrook, C.K. and F.L. Dryer, "Simplified Reaction Mechanisms for Oxidation of Hydrocarbon Fuels in Flames," Combustion Science and Tech., Vol. 27, pp 31-43, 1981.

Appendix A

REACTIVE FLOW ANALYSIS ALONG BLUNTED CONE FLOW STREAMLINES

An analysis and solution method are presented in this appendix for determining non-equilibrium species distributions along flow streamlines in the hypersonic flowfield of blunted low angle cones. In reality, such a flowfield is highly dependent upon and coupled to the chemical make-up of the gas, however, in this analysis the streamline flow properties are assumed a priori known and the species conservation equations solved to determine the resulting specie distributions. This uncoupling of the chemistry and the dynamics of the flow is an adequate approximation since the dynamic flow properties (velocity, pressure) are but weakly dependent upon the local chemical constituents. Also, the intent of the analysis is not to calculate the overall non-equilibrium flow but to: i) delineate flight regimes in terms of air chemistry effects, i.e., determine flight conditions in which the flow may be considered frozen, in equilibrium or highly non-equilibrium; and, ii) to develop scaling parameters for non-equilibrium effects in "Simulant Gas" mixtures.

A schematic defining the relevant geometrical parameters is presented in Figure A1 above. The essential features of the model for oxygen dissociation in air include:

- Simplified air model: 21% O_2 and 79% N_2 at undissociated conditions.
- Considers oxygen dissociation/recombination with nitrogen as an inert specie

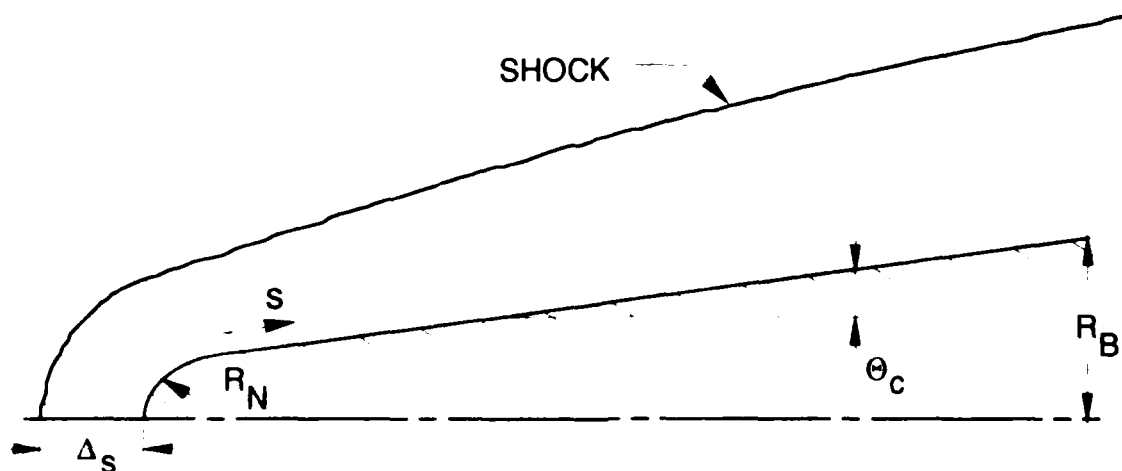
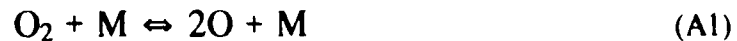


Figure A1. Blunted Cone Flow Schematic

- Neglects NO reactions.
- Uses an approximate model for streamline flow properties (velocity and pressure) developed for low angle (<15° semi-cone angle) blunted cones.

The restriction to oxygen dissociation is based on calculations which indicate that for flight velocities less than 18 Kft/sec, this is the only significant reaction. Independent equilibrium calculations for nitrogen dissociation, for example, indicate that it is less than 10% dissociated for velocities below 18 Kft/sec in this altitude regime. The neglect of NO reactions is based upon an estimate which indicates they have a negligible effect on the O₂ dissociation rate and on the energetics of the flow (See References 1 and 2. Finally, the focus on a single reaction step highlights and simplifies the similitude analysis for the definition of "Simulant Gas" shock tunnel tests and describes the essence of the model for later extension to general simulant gas mixtures.

Thus, consider an air model consisting of O₂, N₂, O and the third body dissociation reaction for oxygen given by:



where M can be O₂, N₂, or O. Then the overall reaction rate for O₂ can be written as:

$$\frac{dn_{\text{O}_2}}{dt} = \dot{\omega}_{\text{O}_2} = \sum_m (k_D^m n_{\text{O}_2} - k_R^m n_{\text{O}}^2) n_m \quad (\text{A2})$$

where n is the particle density with subscript denoting species; k_D^m, k_R^m are the dissociation, recombination reaction rate constants and the summation is over each species m = O₂, N₂, O. The rate constants are taken from a National Bureau of Standards survey by Bortner (1969) which for n in units of particles/ft³ can be written in the usual chemical kinetic formulation as:

$$\begin{aligned} k_D^{\text{O}_2} &= 4.838 \cdot 10^{-10} T^{-.83} e^{-59400./T} \\ k_R^{\text{O}_2} &= 2.37 \cdot 10^{-41} T^{-.33} \\ k_D^{\text{N}_2} &= 7.77 \cdot 10^{-8} T^{-1.7} e^{-59400./T} \\ k_R^{\text{N}_2} &= 3.74 \cdot 10^{-39} T^{-1.2} \\ k_D^{\text{O}} &= 5.29 \cdot 10^{-9} T^{-1} e^{-59400./T} \\ k_R^{\text{O}} &= 2.62 \cdot 10^{-40} T^{-1/2} \end{aligned} \quad (\text{A3})$$

where T is Temperature in °K and the units on k_D are $\text{ft}^3/(\text{particle sec})$ and units on k_R are $\text{ft}^6/(\text{particle}^2 \text{ sec})$.

The species conservation equation, neglecting specie diffusion can be written as:

$$\frac{Df_i}{Dt} = \frac{\partial f_i}{\partial t} + \vec{v} \cdot \text{grad } f_i = \frac{M_i W_i}{A_v \rho} \quad (\text{A4})$$

where f_i is the i^{th} species mass fraction, \vec{v} is velocity, M_i is the molecular weight of the i^{th} species, W_i is the reaction rate defined in Equation (A2), A_v is Avogadro's number and ρ is mean flow density. Now for $i = \text{O}_2$ and for flow along a streamline, (A4) can be written:

$$q \frac{d}{ds} \left(\frac{n_{\text{O}_2}}{\rho} \right) = -1 \sum_m (k_D^m n_{\text{O}_2} - k_R^m n_{\text{O}}^2) n_m \quad (\text{A5})$$

where the relation between mass fraction and number density has been used, i.e.:

$$\frac{n_i}{\rho} = \frac{A_v f_i}{M_i} \quad (\text{A6})$$

The conservation equation for n_{O} and n_{N_2} can be written immediately based on the reaction given in (A1), i.e.:

$$\frac{d}{ds} \left(\frac{n_{\text{O}}}{\rho} \right) = -2 \frac{d}{ds} \left(\frac{n_{\text{O}_2}}{\rho} \right) \quad (\text{A7})$$

and

$$\frac{d}{ds} \left(\frac{n_{\text{N}_2}}{\rho} \right) = 0$$

both of which are immediately integrable. Since the primary interest in the analysis is in the definition of scaling parameters, it is useful to non-dimensionalize the equations in the following manner:

$$n = \frac{n}{n_{\text{as}}}, \quad \bar{\rho} = \frac{\rho}{\rho_s} \quad (\text{A8})$$

$$\bar{q} = \frac{q}{U_\infty}, \quad \bar{s} = \frac{s}{R_N}$$

where $n_{as} = A_v \rho_s / M_a$ (with $M_a = 28.8$) is the number density of frozen air molecules at the stagnation conditions (subscript s), R_N is the nose radius and U_∞ is the freestream velocity. Thus, Equations (A5) and (A7) can be finally written as:

$$\frac{d}{ds} \left(\frac{\tilde{n}_{O_2}}{\rho} \right) = \frac{1}{\rho q} \sum_m \left(\Lambda_R^m \tilde{n}_O^2 - \Lambda_D^m \tilde{n}_{O_2} \right) \tilde{n}_m$$

$$\tilde{n}_O = -2 \tilde{n}_{O_2} + \frac{\rho}{\rho_i} \left[(\tilde{n}_O)_i + 2 (\tilde{n}_{O_2})_i \right] \quad (A9)$$

$$\tilde{n}_{N_2} = \frac{\rho}{\rho_i} (\tilde{n}_{N_2})_i$$

where the subscript i denotes the initial condition just behind the shock wave at which point the gas is assumed frozen; therefore:

$$(\tilde{n}_O)_i = 0, \quad (\tilde{n}_{O_2})_i = .21$$

$$(\tilde{n}_{N_2})_i = .79$$

and the non-dimensional reaction rates are:

$$\Lambda_R^m = \frac{R_N}{U_\infty} k_R^m n_{as}^2$$

$$m = O_2, N_2, O \quad (A10)$$

$$\Lambda_D^m = \frac{R_N}{U_\infty} k_D^m n_{as}$$

Given the flow properties ρ , q and temperature along any flow streamline, Equation (A9) can be integrated from the frozen conditions at the bowshock downstream along the length of the body, as indicated in Figure A1 earlier. The needed flow properties are approximated by joining empirical fits of Inouye⁴ for pressure and velocity distributions along the surface of a sphere to analytical fits for ideal gas cone flow relations. The joining is done somewhat arbitrarily using a smoothing function about the sphere-cone junction, but comparisons with numerical calculations indicate they are quite accurate for present purposes. The expressions used for the stagnation streamline are:

$$P(s) = \begin{cases} P_s & \text{for } s \leq 0 \\ P_s \{1 - 1.25 \sin^2(s) + .284 \sin^4(s)\} \\ -1/2 (.034 * P_s - P_c) \left[1 + \tanh \beta \left(s - \frac{\pi}{2} \right) \right] & \text{for } 0 \leq s \leq \frac{\pi}{2} \\ P_c + 1/2 (.034 * P_s - P_c) \left[1 + \tanh \beta \left(s - \frac{\pi}{2} \right) \right] & \text{for } s > \frac{\pi}{2} \end{cases} \quad (\text{A11})$$

$$q(s) = \begin{cases} \frac{dq}{ds} s + \left(\frac{1}{k} - \frac{dq}{ds} s_0 \right) \left(\frac{s}{s_0} \right)^2 & \text{for } s \leq 0 \\ \frac{dq}{ds} s + 1/2 \left(\frac{U_c}{U_\infty} - \frac{dq}{ds} \frac{\pi}{2} \right) \left[1 + \tanh \beta \left(s - \frac{\pi}{2} \right) \right] & \text{for } 0 \leq s \leq \frac{\pi}{2} \\ \frac{U_c}{U_\infty} - 1/2 \left(\frac{U_c}{U_\infty} - \frac{dq}{ds} \frac{\pi}{2} \right) \left[1 - \tanh \beta \left(s - \frac{\pi}{2} \right) \right] & \text{for } s > \frac{\pi}{2} \end{cases} \quad (\text{A12})$$

where

$$s_0 = - \frac{\Delta_s}{R_N} \quad (\text{A13})$$

$$\frac{dq}{ds} = \frac{1.187}{U_\infty} \frac{\sqrt{P_s/\rho_s}}{1 + .225/\sqrt{k}}$$

and where k is the shock density ratio, and subscript c denotes cone flow relations. The analytical fits to the cone flow relations valid for $\theta_c < 15^\circ$ and $M_\infty > 5$ are:

$$\frac{P_c - P_\infty}{1/2 \rho_\infty U_\infty^2} = .0003 \left\{ 1 - .06 \left[1 - \left(\frac{10}{M_\infty} \right)^{1.6} \right] \right\} \theta_c (\theta_c - 1)$$

and

$$M_c = \left\{ 1 - .918 + .0058 \theta_c - .053 \left[1 - \left(\frac{10}{M_\infty} \right)^{1.64} \right] \right\}^{-1} \quad (\text{A14})$$

Since the total enthalpy is constant along a streamline, the static enthalpy is immediately:

$$h = h_s - \frac{U_\infty^2}{2} \tilde{q}^2 \quad (\text{A15})$$

The other flow properties (T, ρ) can be determined by assuming a mixture of ideal gases ($\text{O}_2, \text{N}_2, \text{O}$) with the equation of state:

$$P = \rho \frac{R}{M_m} T \quad (\text{A16})$$

where the mixture molecular weight, M_m , is:

$$\frac{1}{M_m} = \sum_{\text{O}_2, \text{N}_2, \text{O}} \frac{f_i}{M_i}$$

The internal energy and enthalpy of the gas mixture are given by:

$$e = \sum_{\text{O}_2, \text{N}_2, \text{O}} f_i e_i \quad (\text{A17})$$

$$h = e + \frac{P}{\rho}$$

where specie internal energies, e_i , are determined from quadratic expressions as functions of temperature:

$$e_i(T) = e_{\text{O}_i} + a_i T + b_i T^2$$

The coefficients in the caloric equation of state are developed from a least squares fit of JANAF (Stull and Prophet, 1971) thermochemical data.

A computer code (STREAM) has been written which solves the equations formulated above for species distribution along a streamline. For a given geometry and flight condition (velocity, altitude) or Shock Tunnel Test condition (initial pressure and driver shock Mach Number), a Range Kutta Adams-Moulton integration procedure is used to integrate Equation (A9) along a flow streamline with flow properties as formulated above. The integration

begins at the shock with the frozen species concentration and ends at the end of the vehicle ($S_f = \pi/2 + (R_B/R_N - 1)/\sec\theta_c$) or as in most of the calculations in the present report, at the stagnation point of the spherical nose. Comparing the results to frozen or equilibrium species distribution (readily calculated) provides an assessment of the degree of disequilibrium in the flowfields. Such results can be used to map out regions of flight velocity and altitude for which non-equilibrium effects are important and regions in which the flow is essentially frozen or in equilibrium. The analysis is also used above to define a useful scaling parameter for assessing reactive flow similitude in test facilities.

This page intentionally left blank.

Appendix B

"SIMULANT GAS" REACTIVE MIXTURE CHEMISTRY ANALYSIS

The shock layer reactive streamline analysis presented in Appendix A can be readily generalized to gas mixtures other than air by appending additional specie conservation equations analogous to Equation (A4) (or (A9) in non-dimensional form) for oxygen. In addition to the numerical complexities, reaction steps and kinetic reaction rates must be defined. The objective of the analysis is the development of reactive gas mixtures which react in the shock layer of a model at significantly reduced flow temperatures compared to O₂ dissociation for example. A chemistry survey has been performed which focusses on simplified carbon-oxygen-hydrogen (C-O-H) species which may satisfy this objective. The results of the survey with the definition of a simplified reaction model are presented in this appendix.

The survey was guided by the above objective and the intuitive belief that relatively well understood reactive gases in air could provide ground test similitude to air chemistry in flight. The survey concentrated on carbon monoxide, CO, hydrogen, H₂, and peroxide, H₂O₂ with water vapor in air as being representative of reactive gases which could remain unreacted in a shock tunnel flow while reacting at representative rates in the shock layer of a model in the expanded test section flow. The list of reaction steps for the above reactive species is quite formidable, and impractical—if not intractable—for scoping calculations.

However, evaluation of the rates for the conditions of interest allows considerable abridgement of the list. A model to scope the effects of doping should consider at least two aspects of the chemistry: The generation of free radicals, and the resulting "combustion." The candidate additives all generate radicals at qualitatively faster rates than air chemistry does. There are order of magnitude differences in the ordering H₂O₂ > CO > H₂ > H₂O in the nominal experimental temperature range. Once a radical pool is created, it supports the "combustion" of the additives without depletion of the pool. This allows a considerable reduction in the size of the chemistry model for the range of conditions applicable to scoping this effect.

For the mixtures of interest, only a few processes produce significant quantities of radicals in the laboratory. From previous analyses, it is apparent that the radical generation rate can be approximated as:

$$\frac{d[R]}{dt} = 2 \times ([O_2] \{ k_1 [H_2O_2] + k_3 [C O] + k_4 [H_2] + k_5 [H_2O] \}) + 2 \times k_2 [H_2O_2] [M] \quad (B1)$$

where [] denotes molecular or molar concentrations of the respective specie. Once the radicals are generated, they equilibrate rapidly producing a distribution approximating thermodynamic equilibrium. Using a fit developed by Engleman (1974), the fractions of the principal radicals involved in combustion may be approximated as

$$f_H = f_{OOH} = \frac{1}{2 + K}, \quad f_{OH} = \frac{K}{2 + K} \quad (B2)$$

so that(B2)

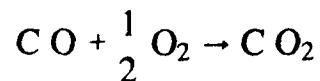
$$[H] = f_H R, \quad [OH] = f_{OH} R, \quad [OOH] = f_{OOH} R$$

are the concentrations of hydrogen, hydroxyl, and hydroperoxyl radicals respectively; and where

$$K = 10^{-1.36} T^{0.23} e^{\Delta p \left(\frac{19.05 \text{ kcal/mole}}{RT} \right)}$$

defines the temperature (T) dependent equilibrium constant for the radical mixture.

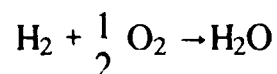
These radicals are directly responsible for air combustion through a number of reactions. For the materials under consideration, the dominant reactions can be isolated. Correctly accounting for the rates of these detailed reactions, models the rates of the combustion reaction. For the conditions occurring in the conceptual doped air stream, CO combustion



has the rate

$$\frac{d[C O]}{dt} = - [C O] \{ k_9 [OOH] + k_{10} [OH] \} + k_{12} [C O_2] \quad (B3)$$

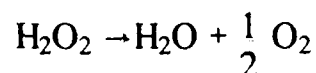
The H₂ combustion



has the rate

$$\frac{d[\text{H}_2]}{dt} = - [\text{H}_2] k_{11} [\text{OH}] \quad (\text{B4})$$

The contribution of H₂O₂



has the rate

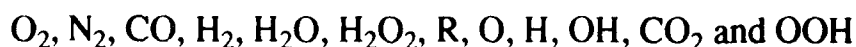
$$\frac{d[\text{H}_2\text{O}_2]}{dt} = - [\text{H}_2\text{O}_2] k_6 [\text{OH}] \quad (\text{B5})$$

The accompanying compilation in Table B1 provides temperature dependent fits for each of the rate constants to the form

$$k_i = 10^A T^B \exp\left(\frac{-E}{RT}\right) \quad (\text{B6})$$

with the recommended values for the constants given in the Table below.

The chemistry model has been tested for isothermal configurations and appears to have appropriate sensitivity to chemical concentrations and temperature. The model has also been implemented in the shock layer streamline analysis (STREAM code), which considers the reactive system consisting of:



in which N₂ is considered inert and R represents the totality of radicals consisting of H, OH and OOH. The model has been tested successfully against previous oxygen dissociation chemistry and against an alternative CO combustion formulation due to Westbrook (1981). In both cases the present model compares well in the range of non-equilibrium shock layer reaction conditions of interest to the "Simulant Gas" study.

Table B1. Kinetics Parameters for Simplified CO, H₂ & H₂O₂ Reaction
 (Units of moles, cm³ and seconds)

| i | A | B | E (Kcal/mole) |
|----|------|-----|------------------|
| 1 | 10.8 | 0.5 | 41.9 |
| 2 | 17.1 | 0.0 | 45.5 |
| 3 | 12.5 | 0.0 | 50.0 |
| 4 | 13.5 | 0.0 | 63.0 |
| 5 | 14.2 | 0.0 | 73.3 |
| 6 | 13.0 | 0.0 | 1.8 |
| 7 | 14.0 | 0.0 | 20.4 |
| 8 | 12.0 | 0.0 | 4.2 |
| 9 | 11.0 | 1.3 | 5.2 |
| 10 | 7.2 | 1.3 | 0.8 |
| 11 | 13.4 | 0.0 | 5.2 |
| 12 | 8.7 | 0.0 | 40.0 |